Memoirs of the School of Engineering, Nagoya University
Vol.44, No.1 (1992)

NONSTATIONARY VIBRATIONS OF A ROTATING SHAFT WITH NONLINEAR SPRING CHARACTERISTICS DURING ACCELERATION THROUGH CRITICAL SPEEDS

Yukio ISHIDA, Takashi IKEDA*, Toshio YAMAMOTO**
and Shin MURAKAMI***

Department of Electronic Mechanical Engineering

(Received June 2, 1992)

Abstract

Recently, there exist many rotating machineries which are operated above the major critical speeds. It is necessary for such a rotating shaft to pass resonance points under the rated speed with a small deflection safely at the start or end of its operation.

In this paper, nonstationary vibration characteristics of a rotating shaft with nonlinear spring characteristics are investigated concerning the following critical speeds: a major critical speed, the critical speeds of subharmonic oscillations of orders 1/2 and 1/3, and a critical speed of a summed-and-differential harmonic oscillation. The rotating speed is changed with a constant acceleration. Especially, the influences of the angular acceleration λ, the initial angular position Ψ_0 of a rotor unbalance, the initial rotating speed ω_s and the initial disturbance on the maximum amplitude are investigated.

Contents

* Associate Professor, Hiroshima University.
** Professor, Meijo University.
*** Research Associate, Nagoya Institute of Technology.

Chapter 1 General introduction

Rotating shafts are used in many kinds of machinery, such as turbines, machine tools, motors and generators. As the weight of these machineries become lighter and their operating speed becomes higher, various new kinds of vibration problem became to appear.

Every structures has natural frequencies and they vibrate with large amplitudes when a periodic external force with a frequency near one of these natural frequencies works. Such a phenomenon is called a resonance. In the fields of rotordynamics, such a resonance speed is called a critical speed. In the design of rotating machineries, it is necessary to separate its rated speed far from its critical speeds. If a rotating machinery is operated continuously near one of its critical speeds, it is feared that the machinery is destroyed due to vibration.

A centrifugal force due to unbalance causes a periodic external force in a rotating machine. Therefore, a resonance phenomenon appears when the rotating speed coincides with one of the natural frequencies. Such a rotating speed is a critical speed and it is also called a major critical speed. Generally, in a rotating machinery, there exist many major critical speeds corresponding to each mode of the system. It is not rare in modern machineries that the operating speed is located in the higher speed side of some of these major critical speeds. In such a case, the rotor passed multiple major critical speeds when it start or shut down the operation. For example, the rotors of aircraft gas-turbine engines are operated at a rotating speed above the second or third major critical speed. It is especially important for such a machinery whose rotating speed are changed frequently through critical speeds to pass safely with a small deflection of the shaft.

It is known that nonlinear spring characteristics may appear in a restoring force of a rotating shaft due to various causes, such as clearance in ball bearings, oil film in journal bearings, and nonlinear phenomena occur at various rotating speeds besides the major critical speeds. Such critical speeds are sometimes called a critical speed or a subcritical speed. It is also important to know nonstationary vibration characteristics during passage through such subcritical speeds.

Nonstationary vibration problems in a rotating shaft have already been studied by many researchers. These studies are classified as follows depending on the characters of the system and the conditions of acceleration: (a) a linear system and a nonlinear system, (b) a case of a constant acceleration and a case with mutual interaction between the driving torque and the rotor, (c) a symmetrical system with no directional difference in shaft stiffness or rotor inertia and a system such as an unsymmetrical rotor or an unsymmetrical shaft, and (d) a system with concentrated masses and a system with distributed mass.

We can find literature surveys on this field in the books by F.M. Dimentberg[1], I. Fernlund[2], V.O. Kononenko[3], R.M. Evan-Iwanowski[4]. In addition, R.M. Evan-Iwanowski[5],

Iwatsubo[6], Yanabe[7),8)], Matsuura[9] wrote survey articles on this topic. Including these reports and the studies thereafter, we summarize the researches by classifing them to three groups.

The first group of research studied a nonstationary vibration of a linear system when the rotor passes a major critical speed with a constant acceleration. The following researches have been made.

In the early stage of the research, very simplified models are discussed theoretically. F.M. Lewis[10], T. Poschl[11], J.G. Baker[12], Yamada et al.[13], A. Dornig[14], and R.L. Fearn et al.[15] discussed a nonstationary vibration problem in a one-degree-of-freedom system, which corresponds to a projection of the motion of a rotor which is mounted at the center of an elastic shaft. They obtained an exact solution or an approximate expression giving the maximum amplitude during the acceleration. Some of them used Fresnel integrals in their theoretical analysis. Shimoyama et al.[16] proposed a method which gives natural frequencies and the magnitude of eccentricity from the experimentally obtained time histories.

The most simple model which can represent a whirling motion is a two-degree-of-freedom system in which one disc is mounted at the center of a symmetrical shaft. F.M. Dimentberg[1] and I. Fernlund[2] obtained amplitude variation curves by a Fresnel integral and a numerical integration, respectively. A.S. Qazi et al.[17] studied by an analogue computer. Yanabe et al.[18)-20)] investigated variations of an amplitude and a phase angle by a numerical integration and derived an approximated expression.

In a case in which the position of a rotor is not at the center of a shaft or a case in which a rotor is mounted at the overhung of a shaft, the deflection and the inclination of the rotor couple each other and the gyroscopic moment works due to the inclination of the rotor. Such a system with four degrees of freedom system are analyzed by Yu.A. Mitropol'skii[21] and Yanabe et al.[22]. The former used the asymptotic method and the latter used a numerical integration.

In addition to these researches, phenomena in other types of systems with a symmetrical rotor and a symmetrical shaft are also studied. Nonami et al.[23),24)] studied a system with an internal damping. I. Koretysski[25] and Nonami et al.[26] studied a rotor system with elastic supports. Yanabe[27] and Nonami[28),29)] investigated a system with distributed mass. Yanabe[30),31)] investigated a nonstationary vibration when a rotor passes two critical speeds successively. G.D. McCann et al.[32] investigated a case of twisting motion. Iwata et al.[33] reported about supression of nonstationary vibration by controlling a supporting condition.

In an unsymmetrical rotor system with a difference in moment of inertia and an unsymmetrical shaft system with a difference in stiffness, an unstable region exists in the neighborhood of the major critical speed. In this region, no stable stationary solution exists. About the nonstationary oscillation when the rotor passes such an unstable region, Aiba et al.[34),35)] studies a system with a gyroscopic moment by the Runge-Kutta method, Kodera[36] studied a system with distributed mass by an integral equation, and Ota et al.[37] performed experiments on an unsymmetrical shaft and compared it with the result of a numerical simulation.

The second group investigated phenomena in systems which have the mutual interaction between a driving source and a rotor motion. Concerning the nonstationary oscillations of a rotor when it passes through a major critical speed, the following researches are performed:

V.O. Kononenko[3] analyzed by the asymptotic method taking the energy of the driving source into account. Matsuura[38)-44)] studied a system in which an unbalance is comparatively large and the driving torque is small. He discussed the nonstationary characteristics using various estimation functions. Tsuchiya[45] studied by the method of multiple scale. R.Gasch and et al.[46] discussed a vibration of a symmetrical shaft with distributed mass.

About an unsymmetrical shaft and an unsymmetrical rotor systems, Kawai et al.[47] and Iwatsubo et al.[48] investigated a case of concentrated mass and Kodera[49] studied a case of

distributed mass.

The third group studied nonstationary vibrations of nonlinear systems and the following researches are made:

Yu.A.Mitropol'skii[21] obtained an amplitude variation curve during passage through a major critical speed by the asymptotic method which was proposed by himself. By the same procedure, R.M.Evan-Iwanowski[4] and B.N.Agrawal et al.[50] obtained an amplitude variation curve during passage through a critical speed of a summed-and-differential harmonic oscillation. However, these researches showed only some representative amplitude variation curves and the nonstationary characteristics are not discussed in detail from the physical point of view.

As mentioned above, researches on nonlinear systems are very few comparing to those on linear systems. However, a nonlinear system has more kinds of critical speed than a linear system, and in addition, the shape or resonance curves in nonlinear system is more complex. Therefore, it is necessary to investigate nonstationary phenomena in detail, especially from physical point of view.

In this paper, nonstationary vibrations of a rotating shaft with nonlinear spring characteristics during acceleration through various kinds of critical speed are investigated. The treated system is a concentrated mass system constituted by a disc and an elastic shaft. The rotating speed is changed at a constant rate. A major critical speed, subharmonic oscillations of order 1/2 and 1/3, and summed-and-differential harmonic oscillations are investigated. Especially, the influence of the angular acceleration λ, the initial angular position Ψ_0 of a rotor unbalance, the initial rotating speed ω_s and the initial disturbance on the maximum amplitude are investigated.

Chapter 2 Equations of motion and nonlinear components

2. 1. *Introduction*

In this chapter, equations of motion of a system in which a disk is mounted on an elastic shaft with a circular cross section is derived. Then, under the condition that the rotating speed of the shaft changes with a constant acceleration, equations of motion for a deflection motion and an inclination motion of a rotor which is mounted at the center of the shaft are derived. In this case, a deflection motion and an inclination motion does not couple each other and each of them can be expressed by a equation of motion of two degrees of freedom. In the theoretical analyses in the next and the later sections, such equations of motion of two degrees of freedom are used for simplicity.

Nonlinear spring characteristics which are expressed by the power series up to the third order are considered. These characteristics are transformed to the polar coordinate expression proposed by Yamamoto et al.[51].

2. 2. *Derivation of equations of motion*

A vertical rotating shaft system in which a disc is mounted on an elastic shaft is considered. The coordinates are taken as shown in Fig. 2.1[52]. The coordinate O–xyz is a rectangular coordinate system whose z-axis coincides with the bearing center line. Let the geometrical center of the rotor be M and it is assumed that the center S of the shaft coincides with this point M. Let the coordinate system whose X-, Y- and Z-axes are paralell to the x-, y- and z-axes, respectively, and whose origin coincides with the geometrical center M be M–XYZ. The Z_0-axis is taken in the tangential direction of the elastic line of the shaft, and the Z_1-axis

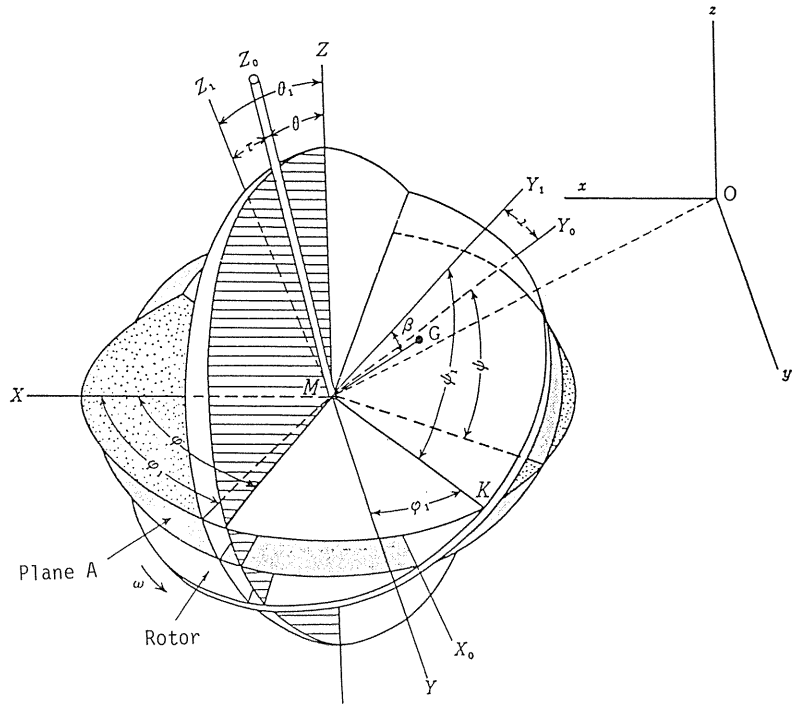

Fig. 2.1. Coordinate systems

is taken in the direction of the polar moment of inertia of the rotor. The angle τ between these two axes represents a dynamic unbalance of the rotor. The plane A contains the point M and is perpendicular to the elastic line or Z_0-axis. Let the line of intersection of the plane A and the rotor be X_0-axis and X_1-axis, and let the lines perpendicular to them and on the plane A and on the rotor be Y_0-axis and Y_1-axis. Then, the coordinate systems $M-X_0Y_0Z_0$ and $M-X_1Y_1Z_1$ are defined. The line of intersection of the plane containing the dynamic unbalance τ and the disc is Y_1-axis. The center of gravity G is located at the angle β in the direction toward the X_1-axis. The magnitude MG is the static unbalance e. Let the angle between the Z-axis and Z_1-axis be θ_1, the angles between the Y-axis and MK which is the line of intersection of XY plane and the disc be φ_1, and the angle between the Y_1-axis and MK be ψ_1.

As Eulerian angles representing the angular position of the rotor, the angles θ_1, φ_1 and ψ_1 are adopted. The angular velocities in the MK, MZ and MZ_1 directions are represented by $\dot{\theta}_1$, $\dot{\varphi}_1$ and $\dot{\psi}_1$, respectively. Here, we transform these angular velocities to those in the MX, MY and MZ-directions. The directions MK, MZ and MZ_1 have the following direction cosines for the coordinate system $M-X_1Y_1Z_1$.

	MX_1	MY_1	MZ_1
MK ($\dot{\theta}_1$-direction)	$\sin\psi_1$	$\cos\psi_1$	0
MZ ($\dot{\varphi}_1$-direction)	$-\sin\theta_1\cos\psi_1$	$\sin\theta_1\sin\psi_1$	$\cos\theta_1$
MZ_1 ($\dot{\psi}_1$-direction)	0	0	1

Therefore, the components of the angular velocity in the directions of the principal momentum of inertia of the rotor MX_1, MY_1 and MZ_1 are expressed as follows:

$$\begin{aligned} MX_1 &: \omega_{X1} = \dot{\theta}_1\sin\psi_1 - \dot{\varphi}_1\sin\theta_1\cos\psi_1 \\ MY_1 &: \omega_{Y1} = \dot{\theta}_1\cos\psi_1 + \dot{\varphi}_1\sin\theta_1\sin\psi_1 \\ MZ_1 &: \omega_{Z1} = \dot{\varphi}_1\cos\theta_1 + \dot{\psi}_1. \end{aligned} \tag{2.1}$$

The angular moments L_{X1}, L_{Y1}, L_{Z1} in each directions are given by

$$L_{X1} = I\omega_{X1}\,, \quad L_{Y1} = I\omega_{Y1}\,, \quad L_{Z1} = I_p\omega_{Z1}. \tag{2.2}$$

The variations of the angular momentum per unit time, H_{X1}, H_{Y1} and H_{Z1}, are obtained from Eqs. (2.1) and (2.2) as

$$\begin{aligned} H_{X1} &= I\dot{\omega}_{X1} - (I - I_p)\omega_{Y1}\omega_{Z1} \\ H_{Y1} &= I\dot{\omega}_{Y1} - (I_p - I)\omega_{Z1}\omega_{X1} \\ H_{Z1} &= I_p\dot{\omega}_{Z1}. \end{aligned} \tag{2.3}$$

By substituting Eq. (2.1) into (2.3), we get

$$\begin{aligned} H_{X1} &= I\frac{d}{dt}(\dot{\theta}_1\sin\psi_1 - \dot{\varphi}_1\sin\theta_1\cos\psi_1) \\ &\quad - (I - I_p)\,(\dot{\theta}_1\cos\psi_1 + \dot{\varphi}_1\sin\theta_1\sin\psi_1)\,(\dot{\varphi}_1\cos\theta_1 + \dot{\psi}_1) \\ H_{Y1} &= I\frac{d}{dt}(\dot{\theta}_1\cos\psi_1 + \dot{\varphi}_1\sin\theta_1\sin\psi_1) \\ &\quad - (I_p - I)\,(\dot{\theta}_1\sin\psi_1 + \dot{\varphi}_1\sin\theta_1\cos\psi_1)\,(\dot{\varphi}_1\cos\theta_1 + \dot{\psi}_1) \\ H_{Z1} &= I_p\frac{d}{dt}(\dot{\varphi}_1\cos\theta_1 + \dot{\psi}_1) \end{aligned} \tag{2.4}$$

Next, we obtain the variations of the angular momentum per unit time in the direction of the stationary coordinates x, y and z. We represent these quantities by H_x, H_y and H_z. For the transformation from H_{X1}, H_{Y1} and H_{Z1} to H_x, H_y and H_z, the direction cosines of MX_1, MY_1 and MZ_1 for the x-, y- and z-axis are obtained as follows:

	MX_1	MY_1	MZ_1
x	$l_1' = \cos\theta_1\cos\varphi_1\cos\psi_1 - \sin\varphi_1\sin\psi_1$	$l_2' = -\cos\theta_1\cos\varphi_1\sin\psi_1 - \sin\varphi_1\cos\psi_1$	$l_3' = \sin\theta_1\cos\varphi_1$
y	$m_1' = \cos\theta_1\sin\varphi_1\cos\psi_1 + \cos\varphi_1\sin\psi_1$	$m_2' = -\cos\theta_1\sin\varphi_1\sin\psi_1 + \cos\varphi_1\cos\psi_1$	$m_3' = \sin\theta_1\sin\varphi_1$
z	$n_1' = -\sin\theta_1\cos\psi_1$	$n_2' = \sin\theta_1\sin\psi_1$	$n_3' = \cos\theta_1$

Therefore,

$$\begin{aligned} H_x &= l_1' H_{X1} + l_2' H_{Y1} + l_3' H_{Z1} \\ H_y &= m_1' H_{X1} + m_2' H_{Y1} + m_3' H_{Z1} \\ H_z &= n_1' H_{X1} + n_2' H_{Y1} + n_3' H_{Z1}. \end{aligned} \tag{2.5}$$

By substituting Eq. (2.4) into this equation, we get the following expressions.

$$\begin{aligned} H_x &= I(-\ddot{\theta}_1 S_{\varphi 1} - \ddot{\varphi}_1 C_{\theta 1} C_{\varphi 1} S_{\theta 1} - 2\dot{\theta}_1\dot{\varphi}_1 C_{\theta 1}^2 C_{\varphi 1} + \dot{\varphi}_1^2 S_{\varphi 1} S_{\theta 1} C_{\theta 1}) \\ &\quad + I_p\{\dot{\theta}_1\dot{\varphi}_1(C_{\theta 1}^2 C_{\varphi 1} - S_{\theta 1}^2 C_{\varphi 1}) - \dot{\varphi}_1^2(S_{\varphi 1} C_{\theta 1} S_{\theta 1}) \\ &\qquad + \dot{\theta}_1\dot{\psi}_1(C_{\theta 1} C_{\varphi 1}) - \dot{\varphi}_1\dot{\psi}_1(S_{\varphi 1} S_{\theta 1}) \\ &\qquad + \ddot{\varphi}_1(S_{\theta 1} C_{\varphi 1} C_{\theta 1}) + \ddot{\psi}_1(S_{\theta 1} C_{\varphi 1})\} \\ H_y &= I(\ddot{\theta}_1 C_{\varphi 1} - \ddot{\varphi}_1 C_{\theta 1} S_{\varphi 1} S_{\theta 1} - 2\dot{\theta}_1\dot{\varphi}_1 C_{\theta 1}^2 S_{\varphi 1} - \dot{\varphi}_1^2 C_{\varphi 1} S_{\theta 1} C_{\theta 1}) \\ &\quad + I_p\{\dot{\theta}_1\dot{\varphi}_1(C_{\theta 1}^2 S_{\varphi 1} - S_{\theta 1}^2 S_{\varphi 1}) + \dot{\varphi}_1^2(C_{\varphi 1} S_{\theta 1} C_{\theta 1}) \\ &\qquad + \dot{\theta}_1\dot{\psi}_1(C_{\theta 1} S_{\varphi 1}) + \dot{\varphi}_1\dot{\psi}_1(C_{\varphi 1} S_{\theta 1}) \\ &\qquad + \ddot{\varphi}_1(S_{\theta 1} S_{\varphi 1} C_{\theta 1}) + \ddot{\psi}_1(S_{\theta 1} S_{\varphi 1})\} \\ H_z &= I(\ddot{\varphi}_1 S_{\theta 1}^2 + 2\dot{\theta}_1\dot{\varphi}_1 S_{\theta 1} C_{\theta 1}) \\ &\quad + I_p(-2\dot{\theta}_1\dot{\varphi}_1 S_{\theta 1} C_{\theta 1} - \dot{\theta}_1\dot{\psi}_1 S_{\theta 1} + \ddot{\varphi}_1 C_{\theta 1}^2 + \ddot{\psi} C_{\theta 1}) \end{aligned} \tag{2.6}$$

where the symbols $C_{\theta 1} = \cos\theta_1$, $S_{\theta 1} = \sin\theta_1$, $C_{\varphi 1} = \cos\varphi_1$ and $S_{\varphi 1} = \sin\varphi_1$ are used. The quantity θ_1 is small in practical machineries, and we represent this by $\theta_1 = O(\varepsilon)$. This means that the magnitude of θ_1 is the same order as a small parameter ε. Let the projections of the angle θ_1 to XZ and YZ planes be θ_{1x} and θ_{1y}, respectively. They are expressed within the accuracy of $O(\varepsilon)$ as follows:

$$\theta_{1x} = \theta_1 \cos\varphi_1 , \quad \theta_{1y} = \theta_1 \sin\varphi_1 \tag{2.7}$$

After substituting these expressions into Eq. (2.6), we get the following expressions within the same accuracy.

$$\begin{aligned} H_x &= -I\ddot{\theta}_{1y} + I_p \frac{d}{dt}(\dot{\Theta}_1 \theta_{1x}) \\ H_y &= I\ddot{\theta}_{1x} + I_p \frac{d}{dt}(\dot{\Theta}_1 \theta_{1y}) \\ H_z &= I_p \ddot{\Theta}_1 \end{aligned} \tag{2.8}$$

where $\Theta_1 = \varphi_1 + \psi_1$.

Next, we consider the moments which work on the rotor. In the stationary coordinate system O$-xyz$, let the deflections of the geometric center be M (which coincides with the center of the shaft cross section S) be x and y, the projections of the inclination angle θ of Z_0-axis on the xz and yz planes be θ_x and θ_y, respectively. The moments around x-, y- and z-axis, M_{tx}, M_{ty} and M_{tz} respectively, are expressed as follows:

$$M_{tx} = \gamma y + \delta\theta_y \quad M_{ty} = -\gamma x - \delta\theta_x \quad M_{tz} = T \tag{2.9}$$

where α, γ and δ are the spring constants, and T is the torque in the z-axis. This torque T is a summation of a driving torque and the torque made by the restoring force. By substituting Eqs. (2.8) and (2.9) into

$$H_x = M_{tx} , \quad H_y = M_{ty} , \quad H_z = M_{tz} \tag{2.10}$$

we obtain the equations of motion for the inclination oscillation. For the deflection motion, we use the following equations.

$$m\ddot{x}_G = P_x , \quad m\ddot{y}_G = P_y \tag{2.11}$$

$$P_x = -(\alpha x + \gamma\theta_x) , \quad P_y = -(\alpha y + \gamma\theta_y) \tag{2.12}$$

Finally, we get the following equations of motion:

$$\begin{aligned} &m\ddot{x}_G + \alpha x + \gamma\theta_x = 0 \\ &m\ddot{y}_G + \alpha y + \gamma\theta_y = 0 \\ &I\ddot{\theta}_{1x} + I_p \frac{d}{dt}(\dot{\Theta}_1 \theta_{1y}) + \gamma x + \delta\theta_x = 0 \\ &I\ddot{\theta}_{1y} - I_p \frac{d}{dt}(\dot{\Theta}_1 \theta_{1x}) + \gamma y + \delta\theta_y = 0 \\ &I_p \ddot{\Theta}_1 = T \end{aligned} \tag{2.13}$$

As many variables in various kinds of coordinate systems are contained in this equation, we restrict them to x, y, θ_x and θ_x in one coordinate. We can know that the relation $\Theta_1 \fallingdotseq \Theta$ holds approximately between the variables $\Theta_1 = \varphi_1 + \psi_1$ and $\Theta = \varphi + \psi$. From Fig. 2.1, we get the following relationship

$$x_G \fallingdotseq x - e\sin(\Theta - \beta)\,, \quad y_G \fallingdotseq y - e\cos(\Theta - \beta). \tag{2.14}$$

Next, we derive the relationships between the angles θ_1, θ and τ. It is assumed that these angles are small quantities of $O(\varepsilon)$. Considering the relationships $\theta_1\cos\varphi_1 = \theta_{1x}$ and $\theta_1\sin\varphi_1 = \theta_{1y}$, we get the following relations within the accuracy of $O(\varepsilon^2)$.

$$\begin{aligned}
\theta_{1x} &= -\{-\sin\Theta + (1/2)\,\theta^2\cos\varphi\,\sin\psi\}\,\sin\tau + \theta_x\cos\tau \\
\theta_{1y} &= -\{\cos\Theta + (1/2)\,\theta^2\,\sin\varphi\sin\psi\}\,\sin\tau + \theta_y\cos\tau
\end{aligned} \tag{2.15}$$

Within the accuracy of $O(\varepsilon)$, these relationships becomes

$$\theta_{1x} = \sin\Theta\,\sin\tau + \theta_x\cos\tau \quad \theta_{1y} = -\cos\Theta\,\sin\tau + \theta_y\cos\tau. \tag{2.16}$$

Substituting Eqs. (2.14) and (2.16) into (2.13), we get the following equations of motion expressed by x, y, θ_x and θ_y.

$$\begin{aligned}
&m\{\ddot{x} - e\ddot{\Theta}\cos(\Theta - \beta) + e\dot{\Theta}^2\sin(\Theta - \beta)\} + \alpha x + \gamma\theta_x = 0 \\
&m\{\ddot{y} - e\ddot{\Theta}\sin(\Theta - \beta) - e\dot{\Theta}^2\cos(\Theta - \beta)\} + \alpha y + \gamma\theta_y = 0 \\
&I\{\ddot{\Theta}\cos\Theta\sin\tau - \dot{\Theta}^2\sin\Theta\sin\tau + \ddot{\theta}_x\cos\tau\} \\
&\quad + I_p\{\ddot{\Theta}(-\cos\Theta\sin\tau + \theta_y\cos\tau) + \dot{\Theta}(\dot{\Theta}\sin\Theta\sin\tau + \dot{\theta}_y\cos\tau)\} \\
&\quad + \gamma x + \delta\theta_x = 0 \\
&I\{\ddot{\Theta}\sin\Theta\sin\tau + \dot{\Theta}^2\cos\Theta\sin\tau + \ddot{\theta}_y\cos\tau\} \\
&\quad - I_p\{\ddot{\Theta}(\sin\Theta\sin\tau + \theta_x\cos\tau) + \dot{\Theta}(\dot{\Theta}\cos\Theta\sin\tau + \dot{\theta}_x\cos\tau)\} \\
&\quad + \gamma x + \delta\theta_x = 0 \\
&I_p\ddot{\Theta} = T
\end{aligned} \tag{2.17}$$

This equation is changed into the following form using the approximate relationships $\sin\tau \fallingdotseq \tau$ and $\cos\tau \fallingdotseq 1$.

$$\begin{aligned}
&m\ddot{x} + \alpha x + \gamma\theta_x = me\ddot{\Theta}\cos(\Theta - \beta) - me\dot{\Theta}^2\sin(\Theta - \beta) \\
&m\ddot{y} + \alpha y + \gamma\theta_y = me\ddot{\Theta}\sin(\Theta - \beta) + me\dot{\Theta}^2\cos(\Theta - \beta) \\
&I\ddot{\theta}_x + I_p\ddot{\Theta}\,\theta_y + I_p\dot{\Theta}\,\dot{\theta}_y + \gamma x + \delta\theta_x = (I - I_p)\tau(\dot{\Theta}^2\sin\Theta - \ddot{\Theta}\cos\Theta)
\end{aligned} \tag{2.18}$$

$$I\ddot{\theta}_y - I_p\ddot{\Theta}\,\theta_x - I_p\dot{\Theta}\,\dot{\theta}_x + \gamma y + \delta\theta_y = (I - I_p)\tau(-\dot{\Theta}^2\cos\Theta - \ddot{\Theta}\sin\Theta)$$
$$I_p\ddot{\Theta} = T$$

When an external torque T is given, this equation contains five unknown quantities x, y, θ_x, θ_y, and Θ. If we give some condition to the acceleration, the quantity Θ is determined as a function of time and this system becomes a four-degree-of-freedom system.

2. 3. Equations of motion of a two degrees of freedom system

For simplicity, hereafter, we treat a system in which a rotor is mounted at the center of an elastic shaft and the rotating speed is changed at a constant rate. In such a case, a deflection and an inclination does not couple each other and $\gamma = 0$ holds. Therefore, we can treat the first and second equations and the third and fourth equations in Eq. (2.18) independently.

Concerning a deflection oscillation, we get the following equations of motion of a two degrees of freedom system after the damping terms and the nonlinear terms are added.

$$\begin{aligned} m\ddot{x} + c\dot{x} + \alpha x + N_x &= me\dot{\Theta}^2\sin\Theta - me\ddot{\Theta}\cos\Theta \\ m\ddot{y} + c\dot{y} + \alpha y + N_y &= -me\dot{\Theta}^2\cos\Theta - me\ddot{\Theta}\sin\Theta \end{aligned} \tag{2.19}$$

where c is damping coefficient and N_x and N_y represent the second and the third power terms in restoring forces. As the angle β has no means now, we put $\beta = \pi$.

From the condition of a constant acceleration, we get

$$\ddot{\Theta} = \lambda\,, \quad \dot{\Theta} = \lambda t + \omega_s\,, \quad \Theta = (1/2)\lambda t^2 + \omega_s t + \Theta_0 \tag{2.20}$$

where λ is an angular acceleration, ω_s is an initial angular velocity and Θ_0 is an initial angular position. If the angular position of the dynamic unbalance τ is measured from the x-axis in xy-plane and represented by Ψ, then the relationship

$$\Theta = \Psi + \pi/2 \tag{2.21}$$

holds. By this notion, we can express Eq. (2.29) as follows.

$$\begin{aligned} m\ddot{x} + c\dot{x} + \alpha x + N_x &= me\dot{\Psi}^2\cos\Psi + me\ddot{\Psi}\sin\Psi \\ m\ddot{y} + c\dot{y} + \alpha y + N_y &= me\dot{\Psi}^2\sin\Psi - me\ddot{\Psi}\cos\Psi \end{aligned} \tag{2.22}$$

By adopting a representative length $e_{st} = mg/\alpha$ (g: the acceleration of gravity), we define the following dimensionless quantities:

$$\begin{aligned} &x' = x/e_{st}\,, \quad y' = y/e_{st}\,, \quad e' = e/e_{st}\,, \quad c' = c/\sqrt{m\alpha}\,, \\ &t' = t\sqrt{\alpha/m}\,, \quad N_{\theta x}' = N_{\theta x}/(\alpha e_{st})\,, \quad N_{\theta y}' = N_{\theta y}/(\alpha e_{st}) \end{aligned} \tag{2.23}$$

Using these quantities, we obtain the equations of motion in dimensionless form:

$$\begin{aligned} &\ddot{x} + c\dot{x} + x + N_x = e\dot{\Psi}^2\cos\Psi + e\ddot{\Psi}\sin\Psi \\ &\ddot{y} + c\dot{y} + y + N_y = e\dot{\Psi}^2\sin\Psi - e\ddot{\Psi}\cos\Psi \end{aligned} \tag{2.24}$$

where the primes in the dimensionless quantities are omitted.

Concerning an inclination oscillation, we get the following equations of motion of a two degrees of freedom system.

$$\begin{aligned} &I\ddot{\theta}_x + I_p\ddot{\Theta}\theta_y + I_p\dot{\Theta}\dot{\theta}_y + c\dot{\theta}_x + \delta\theta_x + N_{\theta x} = (I - I_p)\tau(\dot{\Theta}^2\sin\Theta - \ddot{\Theta}\cos\Theta) \\ &I\ddot{\theta}_y - I_p\ddot{\Theta}\theta_x - I_p\dot{\Theta}\dot{\theta}_x + c\dot{\theta}_y + \delta\theta_y + N_{\theta y} = (I - I_p)\tau(-\dot{\Theta}^2\cos\Theta - \ddot{\Theta}\sin\Theta) \end{aligned} \tag{2.25}$$

By considering the condition (2.20), we get

$$\begin{aligned} &I\ddot{\theta}_x + I_p\ddot{\Psi}\theta_y + I_p\dot{\Psi}\dot{\theta}_y + c\dot{\theta}_x + \delta\theta_x + N_{\theta x} = (I - I_p)\tau(\dot{\Psi}^2\cos\Psi + \ddot{\Psi}\sin\Psi) \\ &I\ddot{\theta}_y - I_p\ddot{\Psi}\theta_x - I_p\dot{\Psi}\dot{\theta}_x + c\dot{\theta}_y + \delta\theta_y + N_{\theta y} = (I - I_p)\tau(\dot{\Psi}^2\sin\Psi - \ddot{\Psi}\cos\Psi) \end{aligned} \tag{2.26}$$

By adopting a representative angle τ_0, we define the following dimensionless quantities.

$$\begin{aligned} &\theta_x' = \theta_x/\tau_0\,, \quad \theta_y' = \theta_y/\tau_0\,, \quad \tau' = \tau/\tau_0\,, \quad i_p = I_p/I\,, \quad c' = c/\sqrt{\delta I}\,, \\ &t' = t\sqrt{\delta/I}\,, \quad N_{\theta x}' = N_{\theta x}/(\delta\tau_0)\,, \quad N_{\theta y}' = N_{\theta y}/(\delta\tau_0) \end{aligned} \tag{2.27}$$

By these dimensionless quantities, the equations of motion are expressed as follows:

$$\begin{aligned} &\ddot{\theta}_x + i_p\ddot{\Psi}\theta_y + i_p\dot{\Psi}\dot{\theta}_y + c\dot{\theta}_x + \theta_x + N_{\theta x} = (1 - i_p)\tau(\dot{\Psi}^2\cos\Psi + \ddot{\Psi}\sin\Psi) \\ &\ddot{\theta}_y - i_p\ddot{\Psi}\theta_x - i_p\dot{\Psi}\dot{\theta}_x + c\dot{\theta}_y + \theta_y + N_{\theta y} = (1 - i_p)\tau(\dot{\Psi}^2\sin\Psi - \ddot{\Psi}\cos\Psi) \end{aligned} \tag{2.28}$$

where the primes in the dimensionless quantities are omitted.

2. 4. Nonlinear terms

The nonlinear terms N_x, N_y and $N_{\theta x}$, $N_{\theta y}$ have the same form. In order to avoid repetition, we consider the latter here. The results for the former are obtained by replacing the variables from θ_x and θ_y to x and y.

The nonlinear terms are expressed as the sum of the terms up to the third power of the coordinates θ_x and θ_y. The corresponding potential energy V is expressed as follows:

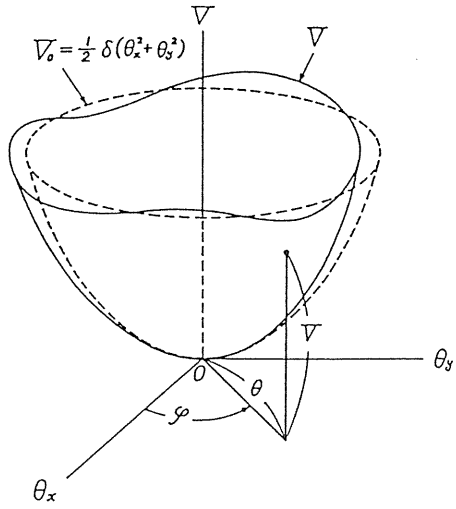

Fig. 2.2. The distribution of the potential energy

$$V = V_0 + V_N$$
$$= \frac{1}{2}(\theta_x^2 + \theta_y^2) \sum_{\substack{i,j=0 \\ (i+j=3)}}^{3} \varepsilon_{ij}\theta_x^i\theta_y^j + \sum_{\substack{i,j=0 \\ (i+j=4)}}^{4} \beta_{ij}\theta_x^i\theta_y^j \tag{2.29}$$

where V_0 and V_N are the components corresponding to the linear and the nonlinear terms in the restoring forces, respectively. The nonlinear terms $N_{\theta x}$ and $N_{\theta y}$ are derived from the potential energy V_N by differentiating partially.

$$N_{\theta x} = \frac{\partial V_N}{\partial \theta_x}$$
$$= (3\varepsilon_{30}\theta_x^2 + 2\varepsilon_{21}\theta_x\theta_y + \varepsilon_{12}\theta_y^2)$$
$$+ (4\beta_{40}\theta_x^3 + 3\beta_{31}\theta_x^2\theta_y + 2\beta_{22}\theta_x\theta_y^2 + \beta_{13}\theta_y^3)$$
$$N_{\theta y} = \frac{\partial V_N}{\partial \theta_y}$$
$$= (\varepsilon_{21}\theta_x^2 + 2\varepsilon_{12}\theta_x\theta_y + 3\varepsilon_{03}\theta_y^2)$$
$$+ (\beta_{31}\theta_x^3 + 2\beta_{22}\theta_x^2\theta_y + 3\beta_{13}\theta_x\theta_y^2 + 4\beta_{04}\theta_y^3) \tag{2.30}$$

The distribution of the potential energy V is shown in Fig. 2.2. The potential energy V_0 corresponding to linear spring characteristics is represented by a rotated paraboloid shown by broken lines.

The potential enregy V given by Eq. (2.29) deviates from the surface V_0 irregularly due to nonlinearity. However, this nonlinearity is divided into the regular components in the polar coordinate expression. By substituting the transformation

$$\theta_x = \theta\cos\varphi\,, \quad \theta_y = \theta\sin\varphi \tag{2.31}$$

into Eq. (2.29), we obtain the following expression.

$$\begin{aligned} V &= V_0 + (\varepsilon_C^{(1)}\cos\varphi + \varepsilon_S^{(1)}\sin\varphi + \varepsilon_C^{(3)}\cos 3\varphi + \varepsilon_S^{(3)}\sin 3\varphi)\theta^3 \\ &\quad + (\beta^{(0)} + \beta_C^{(2)}\cos 2\varphi + \beta_S^{(2)}\sin 2\varphi + \beta_C^{(4)}\cos 4\varphi + \beta_S^{(4)}\sin 4\varphi)\theta^4 \\ &= V_0 + \{\varepsilon^{(1)}\cos(\varphi - \varphi_1) + \varepsilon^{(3)}\cos 3(\varphi - \varphi_3)\}\,\theta^3 \\ &\quad + \{\beta^{(0)} + \beta^{(2)}\cos 2(\varphi - \varphi_2) + \beta^{(4)}\cos 4(\varphi - \varphi_4)\}\,\theta^4 \end{aligned} \tag{2.32}$$

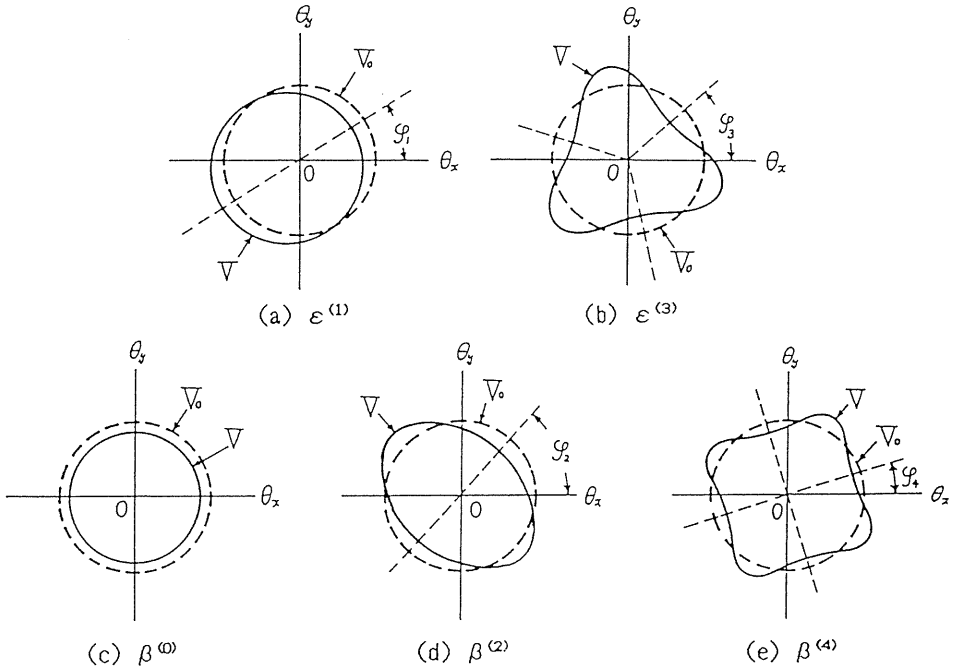

Fig. 2.3. Equipotential lines of each nonlinear component

The following relationships hold between the coefficients in Eq. (2.29) and that in Eq. (2.32).

$$\varepsilon_C^{(1)} = \frac{1}{4}(3\varepsilon_{30} + \varepsilon_{12}), \quad \varepsilon_S^{(1)} = \frac{1}{4}(\varepsilon_{21} + 3\varepsilon_{03}), \quad \varepsilon^{(1)} = \sqrt{\varepsilon_C^{(1)2} + \varepsilon_S^{(1)2}}$$

$$\varepsilon_C^{(3)} = \frac{1}{4}(\varepsilon_{30} + \varepsilon_{12}), \quad \varepsilon_S^{(3)} = \frac{1}{4}(\varepsilon_{21} + \varepsilon_{03}), \quad \varepsilon^{(3)} = \sqrt{\varepsilon_C^{(3)2} + \varepsilon_S^{(3)2}}$$

$$\beta^{(0)} = \frac{1}{8}(3\beta_{40} + \beta_{22} + 3\beta_{04}), \quad \beta_C^{(2)} = \frac{1}{2}(\beta_{40} - \beta_{04}),$$

$$\beta_S^{(2)} = \frac{1}{2}(\beta_{31} + \beta_{13}), \quad \beta^{(2)} = \sqrt{\beta_C^{(2)2} + \beta_S^{(2)2}}, \quad \beta_C^{(4)} = \frac{1}{8}(\beta_{40} - \beta_{22} + \beta_{04}),$$

$$\beta_S^{(4)} = \frac{1}{8}(\beta_{31} - \beta_{13}), \quad \beta^{(4)} = \sqrt{\beta_C^{(4)2} + \beta_S^{(4)2}} \tag{2.33}$$

$$\varphi_1 = \tan^{-1}(\varepsilon_S^{(1)}/\varepsilon_C^{(1)}), \quad 3\varphi_2 = \tan^{-1}(\varepsilon_S^{(3)}/\varepsilon_C^{(3)}),$$

$$2\varphi_2 = \tan^{-1}(\beta_S^{(2)}/\beta_C^{(2)}), \quad 4\varphi_4 = \tan^{-1}(\varepsilon_S^{(4)}/\varepsilon_C^{(4)}),$$

From Eq. (2.32), we know that the potential energy V_N is devided into the components whose magnitude change n times ($n = 0, 1, 2, 3, 4$) while the direction φ changes 2π with keeping θ constant. Figure 2.3 shows the cross sections of the curved surface V with a plane parallel to the $\theta_x\theta_y$-plane. Each figure shows the case that $\varepsilon^{(1)}$, $\varepsilon^{(3)}$, $\beta^{(0)}$, $\beta^{(2)}$ and $\beta^{(4)}$ exists, respectively. The superscripted number n of the coefficient represent the number of times of periodic variation in the magnitude of the term. We denote the nonlinear component, which is represented by such terms, by the symbol $N(n)$.

Chapter 3 A major critical speed[53)]

3. 1. Introduction

As mentioned in chapter 1, almost all the previous papers treated a major critical speed of a linear system. If the restoring force has nonlinear spring characteristics, resonance curves incline and becomes a hard or a soft spring type.

In this chapter, a nonstationary phenomenon during passage through a major critical speed with a constant acceleration is discussed for a rotating shaft system with nonlinear spring characteristics. In the experimental apparatus, the nonlinearity is caused by ball bearings. A theoretical analysis is carried out in a two-degree-of-freedom system, with paying attention to the nonlinear components represented by polar coordinates. The deflection motion of an elastic shaft is considered. The result is also compared with the phenomena in linear systems.

3. 2. Equations of motion

The experimental apparatus to be described later is a four-degree-of-freedom system whose deflection and inclination of the rotor couple each other. However, in the theoretical analysis, for simplicity, we deal with only a deflection oscillation in the case where the rotor is mounted in the middle of the shaft and the deflection and the inclination do not couple each

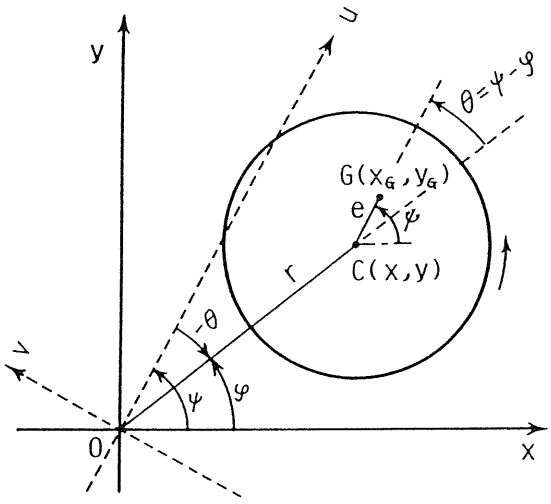

Fig. 3.1. Coordinate systems

other. Coordinate systems are shown in Fig. 3.1. Let the driving torque T_1 and using the dimensionless quantities $T_1' = mT_1/(\alpha I_p)$ and $K = me_{st}/I_p$ in addition to Eq. (2.23), we obtain the equation of motion from the result of the previous chapter as follows:

$$\begin{aligned} &\ddot{x} + c\dot{x} + x + N_x = e\dot{\Psi}^2\cos\Psi + e\ddot{\Psi}\sin\Psi \\ &\ddot{y} + c\dot{y} + y + N_y = e\dot{\Psi}^2\sin\Psi - e\ddot{\Psi}\cos\Psi \\ &\ddot{\Psi} = T_1 - Ke(x\sin\Psi - y\cos\Psi) \end{aligned} \tag{3.1}$$

where the primes of the dimensionless quantities are omitted.

3. 3. Steady-state solutions and resonance curves

In this chapter, we investigate the amplitude when the rotating speed $\dot{\Psi}(=\omega)$ is kept constant. Denoting a natural frequency by p, we obtain the frequency equation as follows.

$$1 - p^2 = 0 \tag{3.2}$$

This equation has two roots $p = \pm 1$. The positive root $p = +1$ represents a forward precessional motion and the negative root $p = -1$ represents a backward one. When the rotating speed ω nearly equals the natural frequency $p = +1$, a resonance phenomenon occurs. The steady-state solution has the following form with an accuracy of $O(\varepsilon^0)$.

$$x = R_0\cos(\omega t + \beta_0), \quad y = R_0\sin(\omega t + \beta_0) \tag{3.3}$$

The resonance curves are given by the following equations with an accuracy of $O(\varepsilon)$.

$$[(-\sigma + 4\beta^{(0)}R_0^2)^2 + c^2\omega^2]R_0^2 = e^2\omega^2$$
$$\tan\beta_0 = \frac{-c\omega}{-\sigma + 4\beta^{(0)}R_0^2} \tag{3.4}$$

where $\sigma = \omega^2 - 1$. The stability criteria can be obtained in the same manner as in the previous paper[54] and are given as follows.

$$(\sigma + 12\beta^{(0)}R_0^2)(\sigma + 4\beta^{(0)}R_0^2) + c^2\omega^2 > 0 \tag{3.5}$$

As only $\beta^{(0)}$ among the various coefficients in Eq. (5) is contained in Eqs. (3.4) and (3.5), we find that only component $N(0)$ has an influence on this steady-state oscillation with an accuracy of $O(\varepsilon)$. Figure 3.2 shows an influence of component $N(0)$ (the coefficient $\beta^{(0)}$) on the

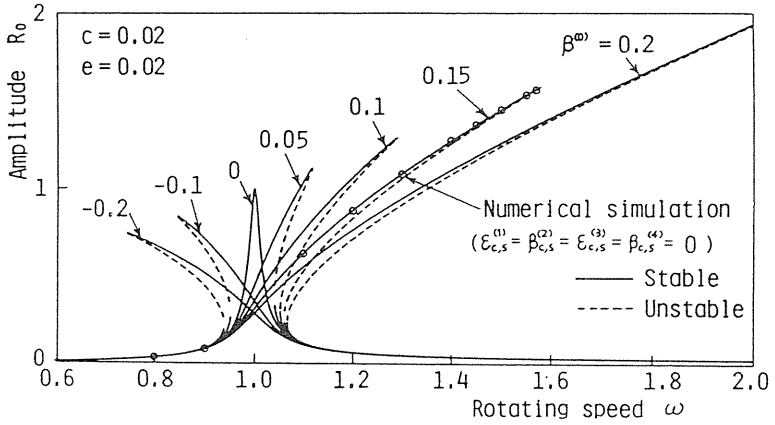

Fig. 3.2. Influence of component $N(0)$ on the resonance curve

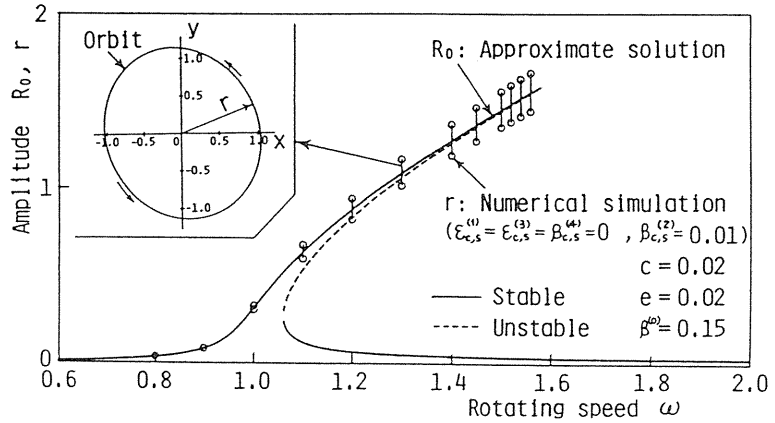

Fig. 3.3. Influence of component $N(2)$ on the resonance curve

resonance curve. We see from this figure that the coefficient $\beta^{(0)}$ determines the inclination of the resonance curve. It is also seen that the maximum amplitude of the resonance curve increases as $\beta^{(0)}$ becomes large. Therefore, even if the magnitude of the unbalance e is constant, it becomes dangerous to operate a rotating machine when component $N(0)$ starts to increase. In addition, it is imagined that passing through the critical speed in a nonlinear system is more difficult than in a linear system.

The symbol ○ in the figure represents an amplitude obtained from the numerical simulation performed to check the accuracy of the approximate solution (3.4). In these simulations, the coefficients of nonlinear terms, except $\beta^{(0)}$, are set at zero. The results agree well with the approximate solutions.

In the approximate solution (3.4), obtained with an accuracy of $O(\varepsilon)$, only $\beta^{(0)}$ is contained. However, the components $N(1) \sim N(4)$ influence the phenomena with an accuracy of $O(\varepsilon^2)$. These components are derived from the directional difference of the potential distribution shown in Fig. 2.3. Therefore, the orbit of the whirling motion in the neighborhood of the major critical speed deviates slightly from a circle. As an example, Fig. 3.3, we show an orbit and the fluctuation in the amplitude (the maximum and the minimum shaft deflection) in the case where the coefficient $\beta_c^{(2)}$ and $\beta_s^{(2)}$, belonging to component $N(2)$, coexists with $N(0)$. In this case, the orbit is an ellips and the deflection r changes twice periodically while the shaft whirls once.

3. 4. The case where the rotor passes through the critical speed with a constant acceleration

3. 4. 1. Transformation of the equations of motion

When a rotor passes through a resonance point with a constant acceleration λ, and with an initial conditions $\dot{\Psi} = \omega_0$, $\Psi = \Psi_0$ at $t = 0$, the angle Ψ is given as

$$\psi = \frac{1}{2}\lambda t^2 + \omega_0 t + \psi_0 \tag{3.6}$$

For this case, the first and second equations in the equations of motion (3.1) can be solved independently of the third equation. For convenience's sake, we transform the first and second equations in Eq. (3.1) into polar coordinates by Eq. (2.31). Then we obtain the following equation.

$$\begin{aligned} \ddot{r} &= -(1-\dot{\varphi}^2)r - c\dot{r} - (N_x\cos\varphi + N_y\sin\varphi) + e\dot{\Psi}^2\cos\theta + e\ddot{\Psi}\sin\theta \\ \ddot{\varphi} &= -c\dot{\varphi} - \{2\dot{r}\dot{\varphi} + (-N_x\sin\varphi + N_y\cos\varphi) - e\dot{\Psi}^2\sin\theta + e\ddot{\Psi}\cos\theta\}/r \end{aligned} \tag{3.7}$$

where $\theta = \Psi - \varphi$. The complete form of the nonlinear terms are given as follows:

$$\begin{aligned} N_xC + N_yS = {} & 3r^2\{(\varepsilon_C^{(1)} + \varepsilon_C^{(3)})C^3 + (\varepsilon_S^{(1)} + 3\varepsilon_S^{(3)})C^2S \\ & + (\varepsilon_C^{(1)} - 3\varepsilon_C^{(3)})CS^2 + (\varepsilon_S^{(1)} - \varepsilon_S^{(3)})S^3\} \\ & + 4r^3\{(\beta^{(0)} + \beta_C^{(2)} + \beta_C^{(4)})C^4 + 2(\beta_S^{(2)} + 2\beta_S^{(4)})C^3S \\ & + 2(\beta^{(0)} - 3\beta_C^{(4)})C^2S^2 + 2(\beta_S^{(2)} - 2\beta_S^{(4)})CS^3 \\ & + (\beta^{(0)} - \beta_C^{(2)} + \beta_C^{(4)})S^4\} \end{aligned} \tag{3.8}$$

$$
\begin{aligned}
-N_x S + N_y C = r^2 \{ & (\varepsilon_S^{(1)} + 3\varepsilon_S^{(3)}) C^3 - (\varepsilon_C^{(1)} + 9\varepsilon_C^{(3)}) C^2 S \\
& + (\varepsilon_S^{(1)} - 9\varepsilon_S^{(3)}) C S^2 - (\varepsilon_C^{(1)} - 3\varepsilon_C^{(3)}) S^3 \} \\
& + 2r^3 \{ (\beta_S^{(2)} + 2\beta_S^{(4)}) C^4 - 2(\beta_C^{(2)} + 4\beta_C^{(4)}) C^3 S \\
& - 12\beta_S^{(4)} C^2 S^2 - 2(\beta_C^{(2)} - 4\beta_C^{(4)}) C S^3 - (\beta_S^{(2)} - 2\beta_S^{(4)}) S^4 \}
\end{aligned}
$$

Here the abbrebiated forms $C = \cos\varphi$ and $S = \sin\varphi$ are used.

3. 4. 2. Results of numerical calculation

We investigate Eq. (3.7) numerically by the Runge-Kutta-Gill method. The state at the instant when $\varphi = 0$ in a steady-state oscillation with a constant angular velocity $\dot{\Psi} = \omega_0$ is chosen as the initial condition. Therefore, $\Psi_0 = -\beta_0$ holds. As it is thought that the components $N(1) \sim N(4)$ are small in the experimental apparatus[55] only the component $\beta^{(0)}$, which belongs to component $N(0)$, is considered here.

3. 4. 2. 1. General features

A representative example of a nonstationary oscillation obtained by accelerating the shaft speed ($\lambda > 0$) is shown in Fig. 3.4. Both the changes in the amplitude r (Fig. 3.4(a)) and in the angular velocity of the whirling motion $\dot{\varphi}$ (Fig. 3.4(b)) are similar to those in a linear system[16]. The curve for $\dot{\varphi}$ shows a characteristic change, which can be explained as follows. Figures 3.4(c) and 3.4(d) show trajectories observed in a coordinate system O—uv rotating with the same speed as that of the rotor. The following relationships hold.

$$
u = r\cos(\varphi - \Psi) = r\cos(-\theta), \quad v = r\sin(\varphi - \Psi) = r\sin(-\theta) \tag{3.9}
$$

As seen from this equation, $-\theta = \varphi - \Psi$ and $-\dot{\theta} = \dot{\varphi} - \dot{\Psi}$ present an angular position of the deflection r and angular velocity of the whirling motion of the shaft respectively, in the rotating rectangular coordinate system.

In the steady-state oscillation ($\dot{\Psi} = \omega =$ constant), the rotor is at rest on the uv-plane and the position vector $\overline{OC}$ in Fig. 3.1 has a constant length $r = R_0$ and a constant angular position $-\theta = \beta_0$. If the angular velocity ω is changed quasi-statically, the end of this vector traces the curve L_1. In Fig. 3.4(c), ω_A and ω_B are rotating speeds corresponding to points A and B on Fig. 3.4(a), respectively.

When the rotating speed is accelerated from $\omega_0 = 0.8$, for example, the geometrical center C, which starts from point a, moves along the curve L_1. Then, once its amplitude becomes large very rapidly, it converges to point b, which corresponds to the steady-state solution for $\dot{\Psi} = \infty$ along the spiral trajectory L_2. Since the rotating speed $\dot{\Psi}$ increases linearly, we know from the relation $-\dot{\Psi} = -\dot{\theta}$ that the variation of $\dot{\varphi}$ in Fig. 3.4(b) corresponds directly to the variation of $-\dot{\theta}$. The variation of $-\dot{\theta}$, that is, the angular velocity of whirling motion in the uv-plane, can be determined from Figs. 3.4(c) and 3.4(d). The center of the spiral deviates from the origin O. Therefore, when the origin O is inside the trajectory (that is, when $\dot{\Psi}$ is less than about 1.75 in Fig. 3.4(d)), the sign of $-\dot{\theta}$ does not change, although its magnitude varies. This situation corresponds to the range from ① to ② in Fig. 3.4(b). In this case, the degree of variation of the angular velocity during one whirling motion depends on the degree of deviation of the center of the spiral from point O. In Fig. 3.4(d), this varia-

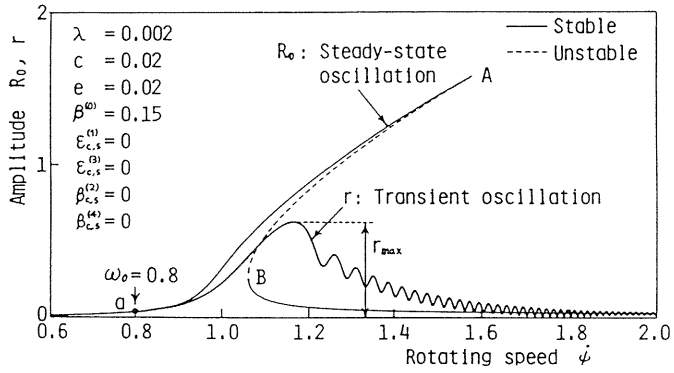

(a) Change in the amplitude r

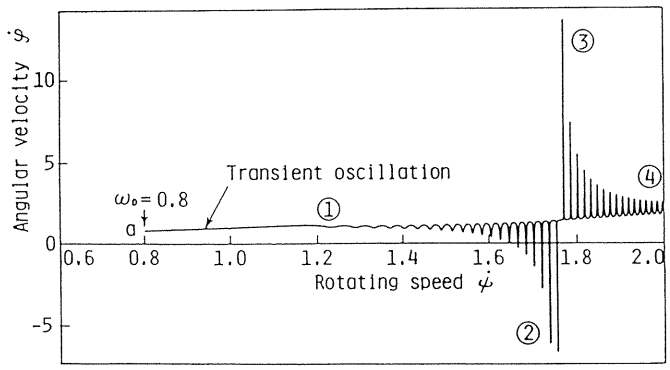

(b) Change in the angular velocity of whirling motion $\dot{\varphi}$

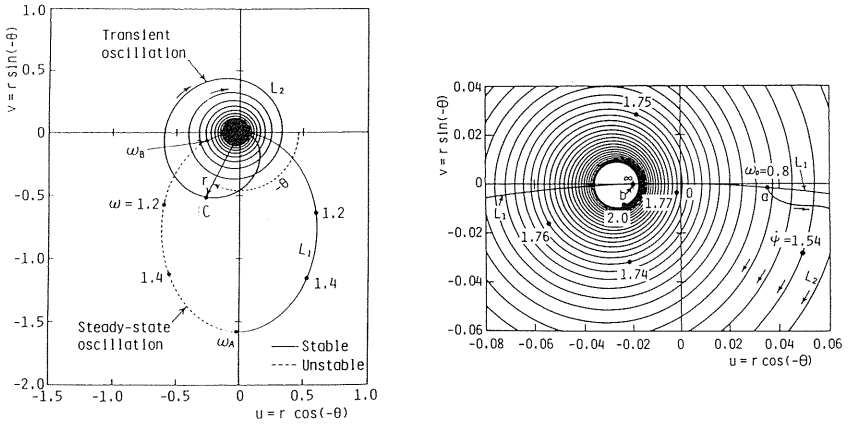

(c) Trajectories of the rotor (d) An enlarged figure of (c)

Fig. 3.4. Changes in the amplitude r and in the angular velocity of the whirling motion $\dot{\varphi}$ and trajectories of the rotor during acceleration

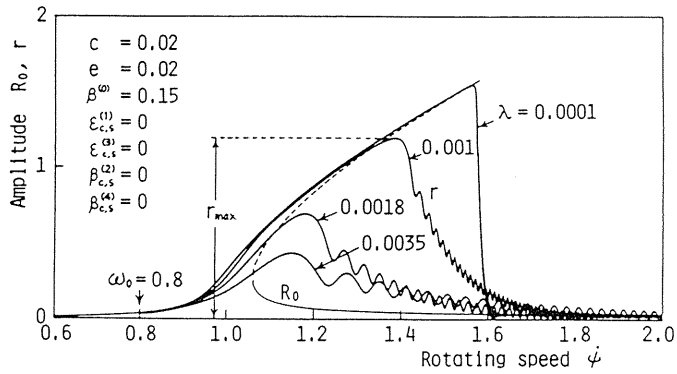

(a) The case when unbalance e is small

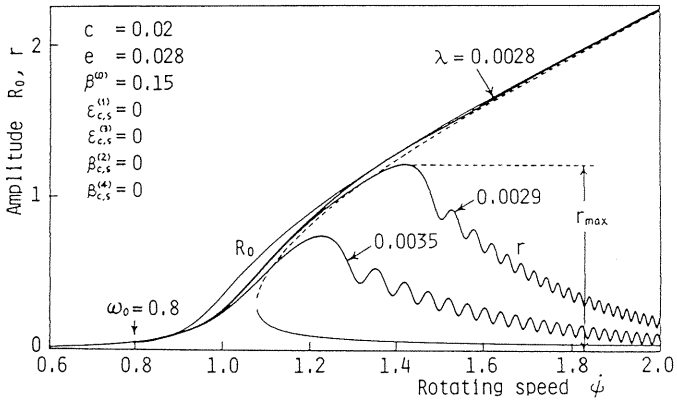

(b) The case when unbalance e is large

Fig. 3.5. We show an influence of the angular acceleration λ on the change in amplitude r

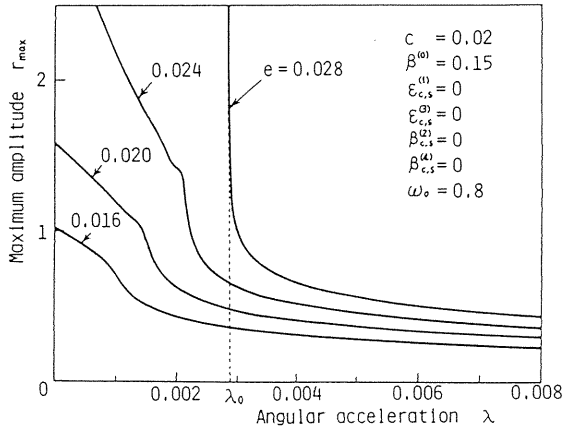

Fig. 3.6. Influence of the magnitude of the unbalance e on the r_{max}-λ curve (nonlinear system)

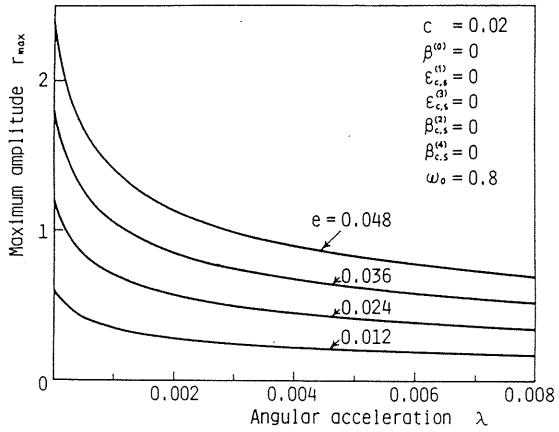

Fig. 3.7. Influence of the magnitude of the unbalance e on the r_{max}-λ curve (a linear system)

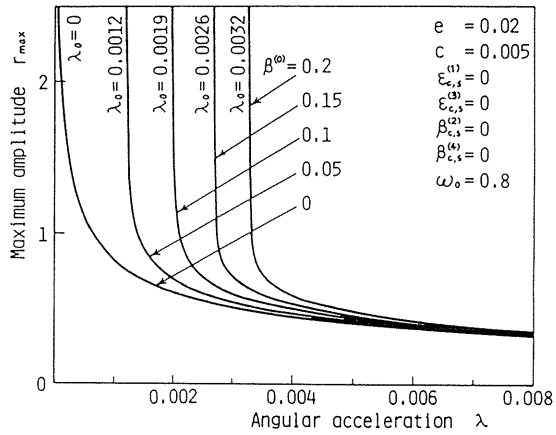

Fig. 3.8. Influence of the coefficient of nonlinear term $\beta^{(0)}$ on the r_{max}-λ curve

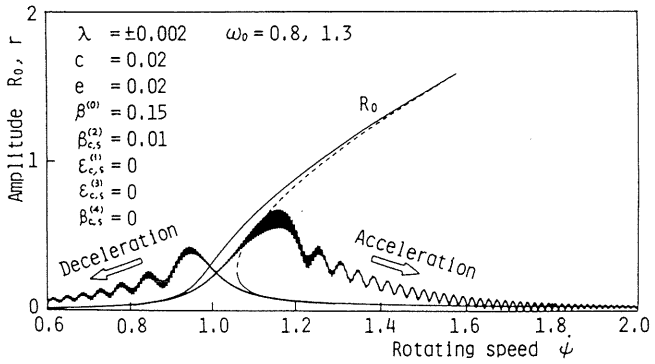

Fig. 3.9. Influence of the nonlinear component $N(2)$ on the wave of the nonstationary oscillation

tion is not so large when $\dot{\Psi} = 1.54$ but it becomes very large when $\dot{\Psi} = 1.74$. When $\dot{\Psi} = 1.77$, for example, the origin O is located at the right side and outside of the spiral. Therefore in the vicinity of this rotating speed, the direction of rotation of the position vector $\overline{OC}$ is different on the right and left sides of the trajectories. Namely, the sign of the quantity $-\dot{\theta}$ changes during one cycle of whirling motion. The rapid change from ② to ③ in Fig. 3.4(b) corresponds to the change which is observed when the origin O shifts from the inside to the outside of the trajectory in the uv-plane at about $\dot{\Psi} = 1.75$ in Fig. 3.4(d).

3. 4. 2. 2. Influences of angular acceleration λ

In Fig. 3.5, we show an influence of the angular acceleration λ on the nonstationary oscillation. The magnitude of unbalance in Fig. 3.5(a) is different from that of Fig. 3.5(b). We discuss Fig. 3.5(b) as an example where the peak of the resonance curve expands too much to be observed experimentally. When λ is small, in Fig. 3.5(a), the amplitude slowly traces the resonance curve and then jumps to the resonance curve of smaller amplitude at about $\dot{\Psi} = 1.58$, where the resonance curve of larger amplitude disappears. Although the feature that the maximum amplitude r_{max} decreases as λ increases is similar to that of a linear system, the rate of decrement is considerably smaller than the case of a linear system (Figs. 3.6 and 3.7). The difference between the linear system and the nonlinear system appears markedly when the maximum amplitude of the resonance curve is large. In Fig. 3.5(b), the amplitude r increases along the resonance curve without jumping to that of smaller amplitude when the angular acceleration is smaller than 0.0028. As λ increases, the maximum amplitude r_{max} decreases abruptly at about $\lambda = 0.0028 \sim 0.0029$. The existence of such a critical acceleration $\lambda = \lambda_0$ is one of the features of the nonlinear system. Therefore, in Fig. 3.5(b), an acceleration larger than this critical value λ_0 is necessary to pass safely through the critical speed with a small amplitude. In the nonlinear system, whether or not it is possible to pass through the critical speed depends on the magnitude of this critical value λ_0.

In Fig. 3.6, the maximum amplitude r_{max} is shown as a function of the angular acceleration λ for various magnitudes of unbalance. When $\lambda = 0$, r_{max} corresponds to the maximum amplitude R_{max} of the resonance curve of steady-state oscillation. The curve r_{max} shows a characteristic change. In the case where R_{max} is small, as in the case of $e = 0.020$, r_{max} first decreases linearly, then decreases abruptly at a certain value, and becomes almost constant as the angular acceleration λ increases. In the case where R_{max} is large, as in the case of $e = 0.028$, r_{max} decreases abruptly at $\lambda = \lambda_0$ and then the rate of decrement becomes small as λ increases. The change in the latter case is shown clearly in Fig. 3.5(b).

For comparison, we show a similar figure for a linear system in Fig. 3.7. In such a case, r_{max} decreases rapidly at small values of λ and then decreases gradually. There exists no critical value corresponding to λ_0. From the comparison of Figs. 3.6 and 3.7, it is concluded that it is easier to pass through the critical speed in a linear system than in a nonlinear system.

3. 4. 2. 3. Influences of the nonlinear component N(0)

In Fig. 3.8, we show λ_0 for various values of $\beta^{(0)}$. The value λ_0 increases with $\beta^{(0)}$ and it becomes more difficult to pass through the critical speed as $N(0)$ increases.

From Figs. 3.2 and 3.8, the following is concluded. As the component $N(0)$ increases, (a) the resonance curve inclines more intensely, (b) the maximum amplitude R_{max} of the resonance curve increases, (c) the minimum angular acceleration λ_0 necessary to separate from the resonance curve with larger amplitude becomes larger, and then (d) it becomes more difficult to pass through the critical speed.

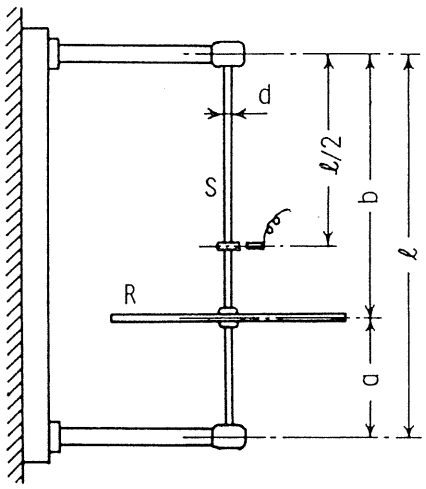

Fig. 3.10. Experimental apparatus

3. 4. 2. 4. Influences of the other nonlinear components N(n)

Similar to the case of a steady-state oscillation, the shaft deflection r changes due to component $N(n)$ ($n = 1 \sim 4$) and the nonstationary waves representing the amplitude change shown in Figs. 3.4 and 3.5 have vibratory components of higher order. For example, in the case of where $N(0)$ and $N(2)$ coexist, as in Fig. 3.3, the change in amplitude becomes that shown in Fig. 3.9. These components of higher order are caused by the distortion of the spiral trajectory shown in Fig. 3.4 to the elliptic shape due to $N(2)$.

3. 5. Experimental apparatus and experimental method

An experimental apparatus is shown in Fig. 3.10. A disc R was mounted at the position $a:b = 1:4$ on an elastic shaft S with a circular cross section. The upper end of the shaft was simply supported by a self-aligning double-row ball bearing (#1200). The lower end was simply supported by a self-alining double-row ball bearing (#1204) or fixed-supported by a single-row deep-groove ball bearing (#6204). However, in the case of the latter, the restoring force of the shaft had nonlinear spring characteristics due to the angular clearance of the bearing. The dimensions of the rotor were as follows: the diameter is 481.3 mm, the thickness is 5.55 mm, the polar moment of inertia $I_p = 0.228\,\mathrm{kg \cdot m^2}$, and the diametral moment of inertia $I = 0.114\,\mathrm{kg \cdot m^2}$. The dimensions of the shaft were as follows: the length $l = 700$ mm and the diameter $d = 12$ mm.

A small disc was mounted at the middle of the shaft and its deflection, x and y, were measured in two directions perpendicular to each other. The mass of this disc was negligible. By processing the detected signals in an electronic circuit, we obtained the value $r = \sqrt{x^2 + y^2}$. This signal r was sent to a personal computer. The rotating speed was detected by a rotary encorder attached to the shaft. The pulse from the rotary encorder, whose frequency was proportional to the rotating speed, was transformed (D/A-transformation) into a voltage signal and then it was also sent to a personal computer. In the personal computer, the voltages, which were proportional to the amplitude r, and the rotating speed were sampled. On the CRT of the personal computer, the amplitude change was shown in coordinates whose ordi-

nate and abscissa represented the amplitude r and rotating speed $\dot{\Psi}$, respectively. The result was recorded by an X-Y plotter. In the following figures, the ordinate represents the shaft deflection (mm) which was obtained after calibration.

3. 6. Experimental results

3. 6. 1. Angular acceleration

In Fig. 3.11, changes in angular velocity $\dot{\Psi}$ for various angular acceleration are shown. It is ascertained that the rotor was accelerated with a constant angular acceleration.

3. 6. 2. Experimental results in a nonlinear system

We performed experiments in a nonlinear system with a single-row deep groove ball bearing. The amplitude change is shown in Fig. 3.12. The sampling frequency f_s shown in the figure was decided from the angular acceleration and the memory size of the personal computer. In every experiment, the acceleration, the acceleration was started from a rotating speed below 800 rpm and the deceleration from that over 2000 rpm. The sampling of the data was begun at a different rotating speed. The edge of the resonance curve represents the starting point of data sampling. A detail of the resonance curve is shown in Fig. 3.12(b). From this enlarged figure, we see that these curves have a component whose amplitude changes twise during one cycle of whirling motion. The following possible reasons are given for the occurrence of this component: the existence of the above-mentioned component $N(2)$, the directional difference of fit between a bearing pedestal and bearing, the difference between output voltages from sensors in the x- and y-directions due to small differences in installation conditions, and so on. In assembling this experimental apparatus, great care was taken to ensure that the upper and lower bearing centers coincided. Therefore, isotropic nonlinear components $N(0)$ should be large and the other components $N(1) \sim N(4)$ small[55].

Figure 3.12(a) shows the amplitude change in the case of acceleration $\lambda = \pm 3.91$ rpm/s. These are small accelerations and the amplitude curve almost coincides with the resonance curve of the steady-state oscillation except when jumpings occurred.

As shown in Fig. 3.12, a hysteresis phenomenon due to the inclination of the resonance curve is observed. Although the angular acceleration are very different among each case in

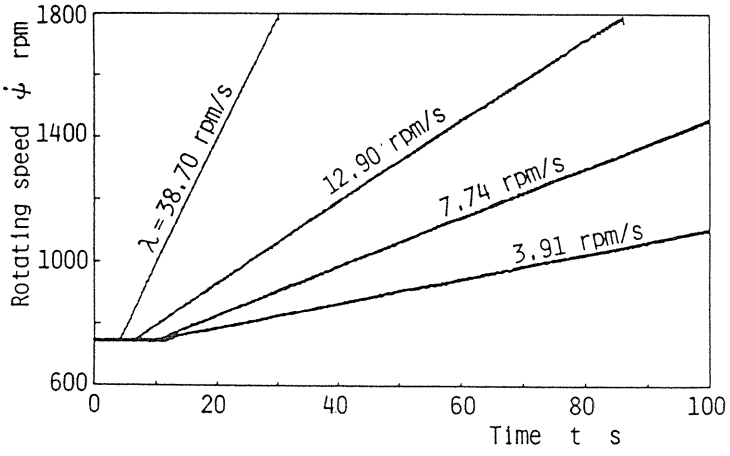

Fig. 3.11. Changes in angular velocity $\dot{\Psi}$

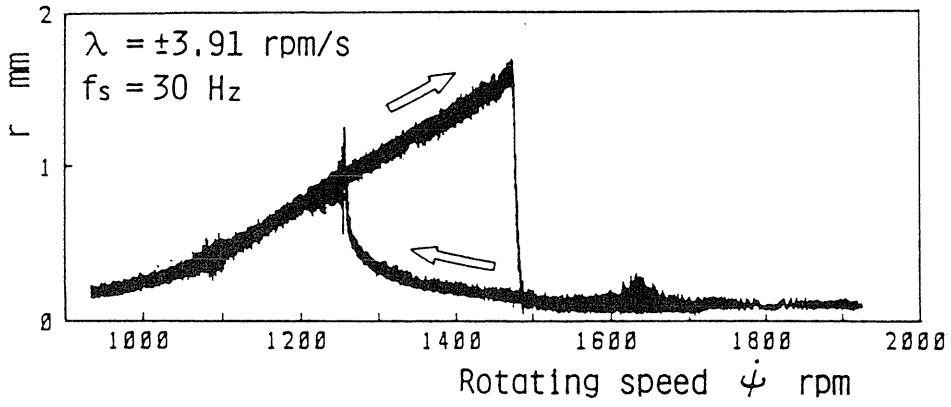

(a)

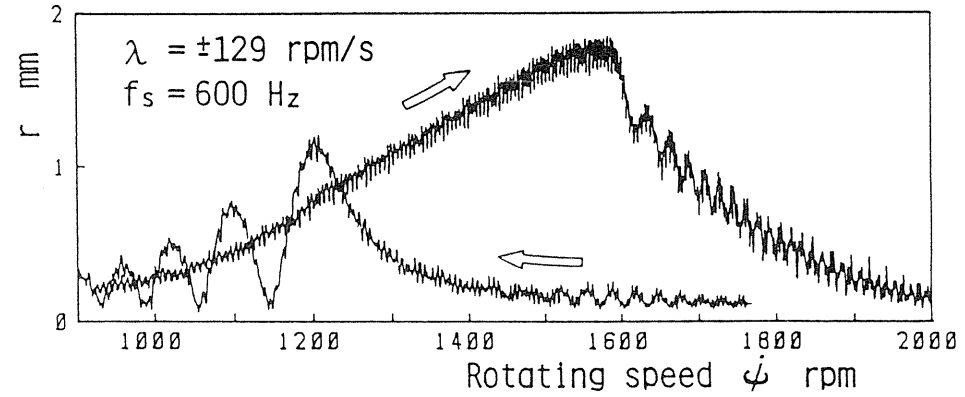

(b)

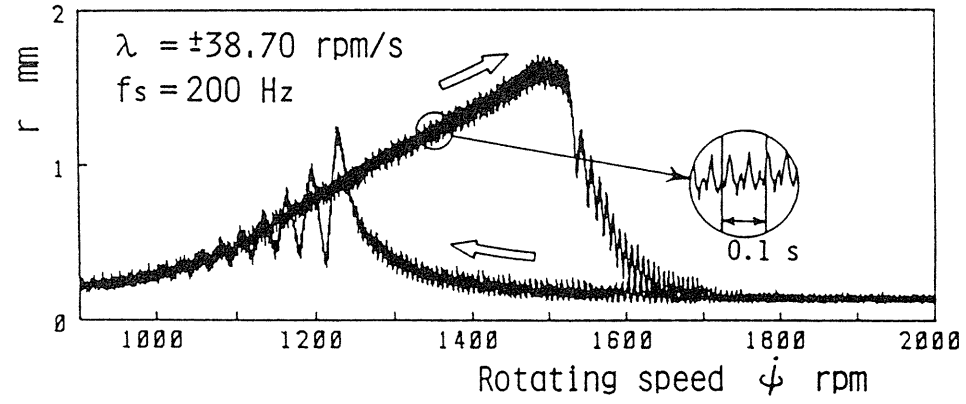

(c)

Fig. 3.12. Amplitude change during the passage through the major critical speed (a nonlinear system)

Fig. 3.12, the amplitude changes along the resonance curve and the maximum amplitudes during the acceleration are almost the same.

The variation of the maximum amplitude r_{max} is shown as a function of angular acceleration $\lambda(>0)$ in Fig. 3.13. For comparison, the results in a linear system with self-aligning double-row ball bearings are shown. There exists a remarkable difference between these two systems. Namely, r_{max} decreases rapidly in the range of small angular acceleration in the linear system, but it does not change in the experimental range in the nonlinear system. In this experimental apparatus, because the magnitude of the nonlinear component $N(0)$ could not be measured quantitatively, the angular acceleration λ_0 shown in Fig. 3.6 is undefined. However, it is thought that the angular acceleration range of Fig. 3.13 lies below such a critical value. The angular acceleration $\lambda = 200$ rpm/s corresponds to $\lambda \fallingdotseq 0.0013$ in a dimensionless form.

Figure 3.14 shows a result for the case in which the unbalance was large and the maximum amplitude of the resonance curve exceeded the measureable range. In such cases, it is almost impossible to pass through the critical speed within the acceleration shown in Fig. 3.13. In Fig. 3.14, the experiment was stopped when the shaft touched the guard ring prepared to limit the amplitude for safety.

3. 6. 3. Results in a linear system

Experimental results in a linear system are shown in Fig. 3.15. When the angular acceleration is changed from $\lambda = 3.91$ to 77.4 rpm/s, the maximum amplitude r_{max} in accelerating the rotating speed decreases considerably. For the same absolute value of acceleration, the maximum amplitude obtained in the process of increasing the rotating speed is larger than that in the process of decreasing. The change of r_{max} with λ is shown in Fig. 3.13. The magnitude of r_{max} decreases rapidly in the small range of angular acceleration. This behavior is qualitatively similar to that of the numerical result shown in Fig. 3.13. It is also concluded from Fig. 3.13 that the amplitude decreases more easily in the linear system than in

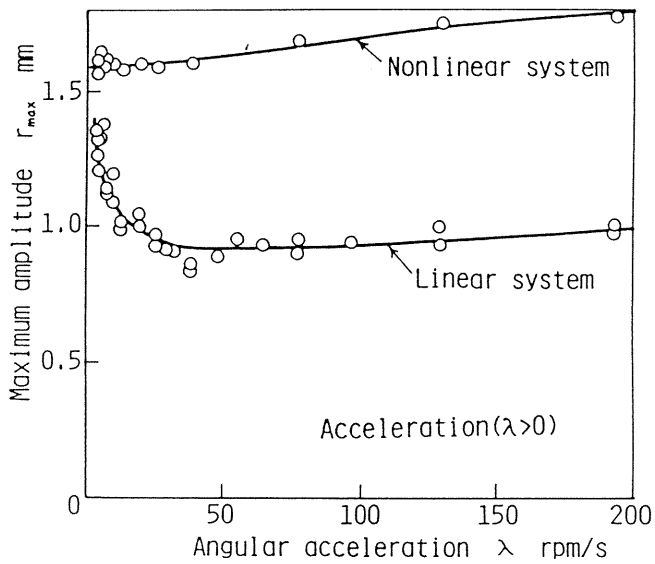

Fig. 3.13. Changes in the maximum amplitude r_{max} for angular acceleration λ

the nonlinear system, and that it is easier to pass through the critical speed in the linear system than in the nonlinear system.

3. 7. Conclusions

(1) In the nonlinear system, due to the change of the resonance curve of the steady-state oscillation into the hard or soft spring type, a hysteresis phenomenon appears in a nonstationary oscillation.

(2) In the nonlinear system, the maximum amplitude r_{max} shows a characteristic change when the angular acceleration λ increases. In the case of increasing the rotating speed in a system with a resonance curve of a hard spring type, the maximum amplitude shows the following changes. When the maximum amplitude of the steady-state oscillation is compara-

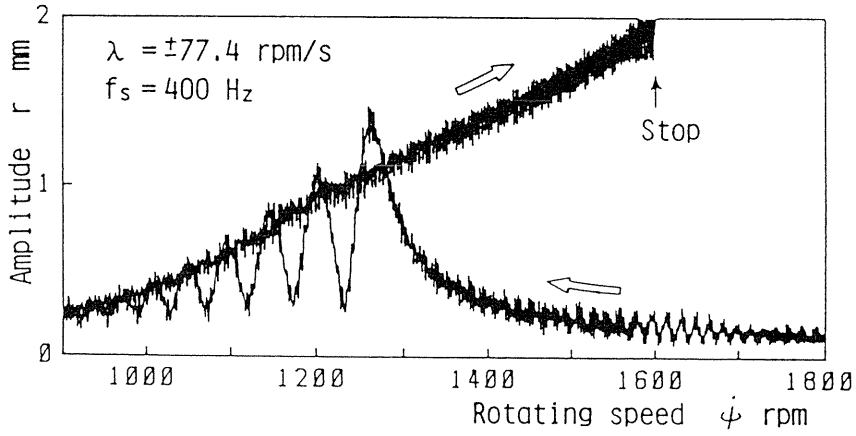

Fig. 3.14. Amplitude change during the passage through the major critical speed (comparatively large unbalance, nonlinear system)

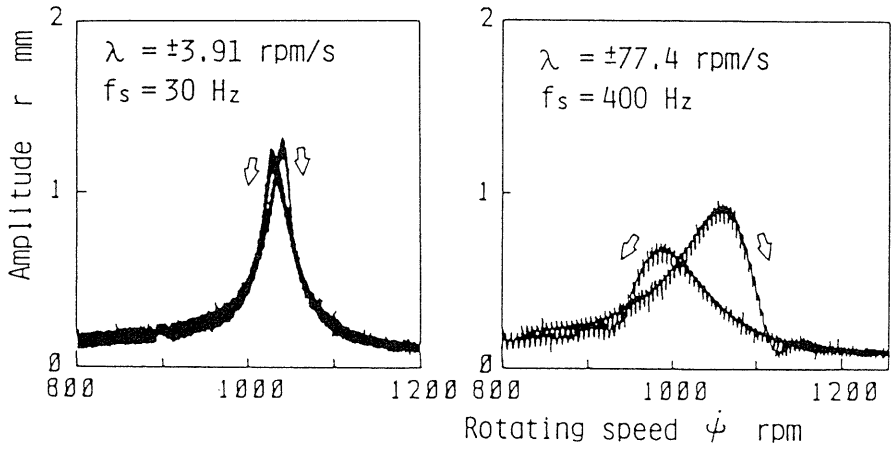

Fig. 3.15. Amplitude change during the passage through the major critical speed (a linear system)

tively small, the maximum amplitude decreases abruptly at a certain value of λ after previously decreasing linearly in the range of small angular acceleration, and then it gradually begins to decrease further. When the maximum amplitude of the steady-state oscillation is considerably large, the rotor cannot pass through the critical speed with an angular acceleration smaller than a critical value λ_0. In this case, r_{max} decreases abruptly at this value λ_0, and then decreases gradually. This critical value λ_0 depends on the magnitude of the nonlinear component $N(0)$.

(3) As the nonlinear component $N(0)$ increases, the inclination of the resonance curve of the steady-state oscillation becomes stronger and, at the same time, its maximum amplitude increases. A larger angular acceleration is necessary to depress the maximum amplitude in the transition.

(4) When a nonlinear component $N(n)$ $(n = 1 \sim 4)$ exists, the radious of the trajectory changes n times while the rotor whirls once in the passage through the critical speed.

(5) In the experiments on the nonlinear system, where the shaft was supported by a single-row deep groove ball bearing, the maximum amplitude r_{max} was almost constant for various values of acceleration. However, in the experiments on the linear system, where the shaft was supported by a self-aligning double-row ball bearings, the maximum amplitude decreases rapidly in the range of small angular acceleration and then became almost constant.

(6) In general, it is more difficult to pass through the critical speed with a small amplitude in the nonlinear system than in the linear system.

Chapter 4 A critical speed of a 1/2-order subharmonic oscillation[56]

4. 1. Introduction

The majority of the reports on the nonstationary oscillations of rotating shaft systems during acceleration through critical speeds discussed problems about a major critical speed of a linear system. Nonlinear systems have the following characteristics that differ from linear systems: (a) in addition to a harmonic oscillation at the major critical speed, various kinds of oscillations, such as subharmonic oscillations and summed-and-differential harmonic oscillations, appear at resonance points called subcritical speeds, (b) resonance curves at these resonance points incline.

In this chapter, we shall investigate a nonstationary oscillation when a rotor passes the critical speed of a 1/2-order subharmonic oscillation of a forward precession mode in the case of constant deceleration. In particular, we shall discuss the effects of an angular acceleration and initial conditions, such as an angular velocity and an angular position of the shaft at the start, on the maximum amplitude of the nonstationary oscillation. The result is also compared with the result on the major critical speed in the previous chapter.

The asymptotic method has been generally used in the study of nonstationary oscillations. However, we use digital data processing techniques such as the fast Fourier transformation in the analysis of data obtained in numerical simulations and experiments.

4. 2. Equations of motion

The experimental apparatus used in this chapter is a four-degree-of-freedom system where a deflection and an inclination of the rotor couple each other. But, for simplicity, we use a two-degree-or-freedom model representing an inclination oscillation. This system is realized by a rotor system where a rotor is mounted at the center of the shaft and its deflection and inclination do not couple. Figure 4.1 shows a rotor model and coordinate systems.

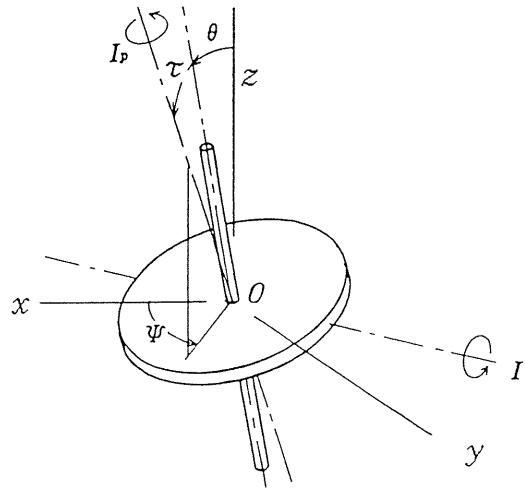

Fig. 4.1. A rotor model and coordinate systems

The equations of motion of this system is given by Eq. (2.28), that is,

$$\begin{aligned}
&\ddot{\theta}_x + i_p\ddot{\Psi}\theta_y + i_p\dot{\Psi}\dot{\theta}_y + c\dot{\theta}_x + \theta_x + N_{\theta x} = (1 - i_p)\tau(\dot{\Psi}^2\cos\Psi + \ddot{\Psi}\sin\Psi) \\
&\ddot{\theta}_y - i_p\ddot{\Psi}\theta_x - i_p\dot{\Psi}\dot{\theta}_x + c\dot{\theta}_y + \theta_y + N_{\theta y} = (1 - i_p)\tau(\dot{\Psi}^2\sin\Psi - \ddot{\Psi}\cos\Psi)
\end{aligned} \tag{4.1}$$

4. 3. Steady-state response

Firstly, we discuss the response in the case where the rotating speed $\dot{\Psi}$ is constant. This constant rotating speed is represented by ω. In this case, the angle Ψ in Eq. (4.1) is given as follows:

$$\ddot{\Psi} = 0, \quad \dot{\Psi} = \omega, \quad \Psi = \omega t + \Psi_0 \tag{4.2}$$

The natural frequency p of this system is obtained from the following frequency equation:

$$G(p) \equiv 1 + i_p\omega p - p^2 = 0 \tag{4.3}$$

Two roots of this equation is denoted by $p_f(>0)$ and $p_b(<0)$. A $p-\omega$ diagram for the case $i_p = 0.25$ is shown in Fig. 4.2. In this figure, the abscissa of intersection A of curve p_f and straight line $p = \omega$ is the major critical speed, and that of intersection B is the critical speed of the 1/2-order subharmonic oscillation in the forward precessional mode. We can write an approximate solution within an accuracy of $O(\varepsilon)$ as follows[57]

$$\begin{aligned}
\theta_x &= R\cos\theta_f + P\cos\theta_\omega + \varepsilon(a\cos\theta_f + b\sin\theta_f) \\
\theta_y &= R\sin\theta_f + P\sin\theta_\omega + \varepsilon(a'\sin\theta_f + b'\cos\theta_f)
\end{aligned} \tag{4.4}$$

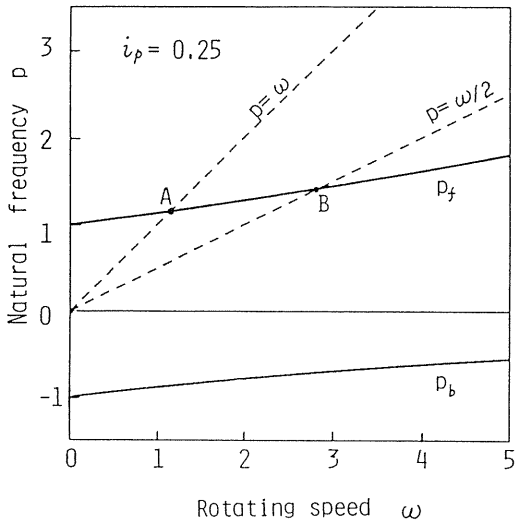

Fig. 4.2. $p - \omega$ diagram

where $\theta_f = \Psi/2 + \delta_f = (1/2)\omega t + \Psi_0/2 + \delta_f$ and $\theta_\omega = \Psi + \beta = \omega t + \Psi_0 + \beta$. In these equations, the terms multiplied by ε are compensation terms of order $O(\varepsilon)$. The steady-state solution $R = R_0$, $\delta_f = \delta_{f0}$ can be obtained by the same method as in the previous paper[58] as follows:

$$R_0 = 0 \tag{4.5a}$$

or

$$\begin{aligned} &\{G_1 + 4\beta^{(0)}(R_0^2 + 2P^2)\}^2 + \{(1/2)c\omega\}^2 = (2\varepsilon^{(1)}P)^2 \quad \text{(i)} \\ &2\delta_{f0} = -\tan^{-1}\frac{(1/2)c\omega}{G_1 + 4\beta^{(0)}(R_0^2 + 2P^2)} + \varphi_1 \quad \text{(ii)} \end{aligned} \tag{4.5b}$$

where $P = -(1 - i_p)\tau\omega^2/G(\omega)$, $G_1 = G(1/2 \cdot \omega)$. The stability criteria for the solution $R_0 = 0$ of Eq. (4.5a) is given as

$$(G_1 + 8\beta^{(0)}P^2)^2 - \{(1/2)c\omega\}^2 + (2\varepsilon^{(1)}P)^2 > 0 \tag{4.6}$$

and that for $R_1 \neq 0$ of Eq. (4.6) is given as

$$\beta^{(0)}\{G_1 + 4\beta^{(0)}(R_0^2 + 2P^2)\} > 0 \tag{4.7}$$

4. 4. Nonstationary response during Acceleration through the critical speed

We discuss a nonstationary phenomenon during acceleration through a critical speed of a subharmonic oscillation of order 1/2 of a forward whirling mode with a constant acceleration. In this case, the following relations hold:

$$\ddot{\Psi} = \lambda\,, \quad \dot{\Psi} = \lambda t + \omega_s\,, \quad \Psi = \frac{1}{2}\lambda t^2 + \omega_s t + \Psi_0 \tag{4.8}$$

4. 4. 1. Method of analysis

The main theoretical method used in the discussions of nonstationary phenomena was the asymptotic method. But as shown in the book by Evan-Iwanowski[59], its first order solution contains comparatively large error. In addition, the state that the subharmonic oscillation is not appearing cannot be used as an initial condition. Because of such reasons, we adopted the following method which is different from the asymptotic method used widely. First, the relation given by Eq. (4.8) is substituted into Eq. (3.1) and then the equations of motion is integrated numerically by Runge-Kutta-Verner method. The obtained time histories are treated using digital signal processing technique in the obtained time history, we cannot determine the amplitude variation of nonstationary subharmonic oscillation directly from the numerical data. Therefore we use the following data processing procedure which enables us to distinguish a desired component from others.

First, numerical data of the time history on the inclinations θ_x and θ_y, obtained by numerical integration, are transformed from the time domain into the frequency domain by fast Fourier transform (FFT). From the spectrum distribution, those spectrum components related to the subharmonic oscillation are separated from others by filtering and then transformed inversely into the time domain again. Then the time history becomes a simple one containing only a subharmonic component. In the whirling motion of rotating machinery, not only the frequency but also the direction of precession is important. In the ordinary FFT method which treats only real numbers, it is impossible to separate a forward component and a backward component if they have the same frequency. In order to discuss and clarify the nonstationary characteristics, it is necessary to separate the forward component from the backward component. For this purpose, we used the following data processing procedure. In the theory of fast Fourier transformation, there exists a transformation between complex numbers and complex spectrum. In order to use this complex-FFT, we defined a complex coordinate system in the whirling plane or $\theta_x\theta_y$-plane. The θ_x- and θ_y-axes are taken as the real and imaginary axes, respectively. We produce complex discrete data Z_k from real sampled data X_k and Y_k in the θ_x and θ_y directions as follows:

$$Z_k = X_k + iY_k\,, \quad \mathrm{k} = 1, 2, ..., \mathrm{N} \tag{4.9}$$

where i is the imaginary unit. The complex-FFT is defined by the following expression:

$$C_j = \frac{1}{N}\sum_{\mathrm{k}=0}^{\mathrm{N}-1} Z_k W^{\mathrm{jk}}\,, \quad \mathrm{j} = 0, 1, ..., \mathrm{N}-1 \tag{4.10}$$

where $W = exp(-2\pi i/N)$. The quantity C_j is a complex number which represents jth order amplitude spectrum of time series data which repeat periodically at intervals of N data. Such a spectrum is periodic with the period N. In the range of $-N/2 \sim N/2$, a positive frequency corresponds to a forward whirling motion and a negative frequency corresponds to a backward whirling motion. In the case of the steady state oscillation, each spectrum C_j corresponds to the amplitude of oscillation. However, because the amplitude of the subharmonic component varies in the nonstationary process, the quantity C_j does not represent the amplitude of the oscillation component directly. Therefore, after removal of the positive spectra C_j

corresponding to the 1/2-order subharmonic oscillation of the forward precession mode (this processis called filtering), they are transformed inversely from the frequency domain to the time domain. In this inverse complex-FFT process, the following equation is used.

$$Z_k = \sum_{k=0}^{N-1} C_k W^{-jk}, \quad k = 0, 1, ..., N-1 \tag{4.11}$$

In this data processing, a Blackmann-Harris time window is used for the purpose of eliminating leakage error. After a time history is again obtained from the filtered spectrum by the inverse FFT, it is divided by the same time window to compensate its multiplication to the original time history. As such a time window is close to zero at both edges, some quantitative error is included in the neighborhoods of the start and the end of the finally obtained time series. Figure 4.3(a) shows a variation of the amplitude $\sqrt{\theta_x^2 + \theta_y^2}$ before data processing, Fig. 4.3(b) shows the amplitude spectrum distribution obtained by complex-FFT, and Fig. 4.3(c) shows the amplitude variation curve after data processing.

4. 4. 2. Maximum amplitude during acceleration through the critical speed

Figure 4.4 shows a resonance curve of a steady-state solution R_0 obtained from Eq. (4.5) and amplitude variation curves of nonstationary oscillations during acceleration with various angular acceleration λ. A positive value is given to $\beta^{(0)}$ so as to make the resonance curve a hard-spring type which is qualitatively the same shape as that obtained in the experiments mentioned later. Concerning the resonance curve R_0, a solid line represents a stable solution and a broken line represents an unstable solution. In Fig. 4.4, the stability is not distinguished for the solution of zero amplitude. However, it is unstable between two intersection points which are the cross points between the resonance curves $R_0 \neq 0$ and $R_0 = 0$ ($\dot{\Psi}$-axis), and it is stable outside of them. The nonstationary responses during acceleration through the critical speed of 1/2-order subharmonic oscillation are classified into two groups. One is the case (for example, when $\lambda = 0.00037$) where r' increases along the stable resonance curve, and the other is the case (for example, when $\lambda = 0.00038$) where the rotor can pass the critical speed with a comparatively small amplitude. In the former case, the amplitude will increase unlimitedly as long as the stable resonance curve exists. In the latter case, although the amplitude starts growing toward the stable resonance curve R_0 in the beginning, it soon decreases toward the stable resonance curve of zero amplitude. Therefore, we call the former a nonpassable case and the latter a passable case. In a passable case, we can define the maximum amplitude during acceleration as shown in Fig. 4.4 and we can represent it by r'_{max}. In a nonpassable case, we represent $r'_{max} = \infty$ for convenience. The following parameters are considered to influence the maximum amplitude: the angular acceleration λ, the initial rotating speed ω_s from which the acceleration starts, and the initial angular position Ψ_0 if the unbalance at ω_s. In the following, we shall discuss the influences of these parameters. The values of i_p, c, τ, $\beta^{(0)}$ and $\varepsilon^{(1)}$ in the following numerical calculation are the same as those in Fig. 4.4.

Initial rotating speed ω_s influences the maximum amplitude. However, for simplicity and to decrease the amount of calculation, we fix this value at a certain rotating speed which is relatively close to the critical speed in the following numerical analysis. Figure 4.5(a) shows a relation between the angular acceleration λ and the maximum amplitude r'_{max} in the case of acceleration ($\lambda > 0$) for $\Psi_0 = 120°$ and 180°. The symbols ● and ▲ are the values obtained by simulations and the curves were drawn by connecting these data. From this figure, we see that r'_{max} depends markedly on λ, and the rotor cannot always pass the critical speed with an angular acceleration below a certain value of λ. In addition, it is noteworthy that, unlike the case of the major critical speed reported previously[53], r'_{max} does not decrease monoto-

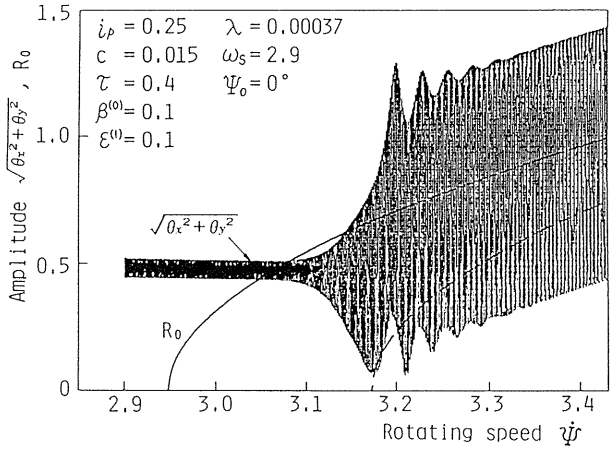

(a) Amplitude $\sqrt{\theta_x^2 + \theta_y^2}$ obtained by Runge-Kutta method

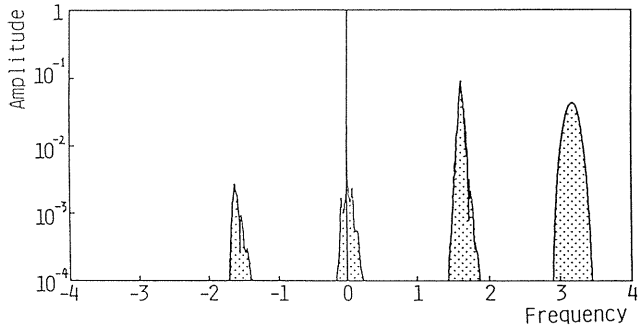

(b) Spectrum distribution obtained by complex-FFT

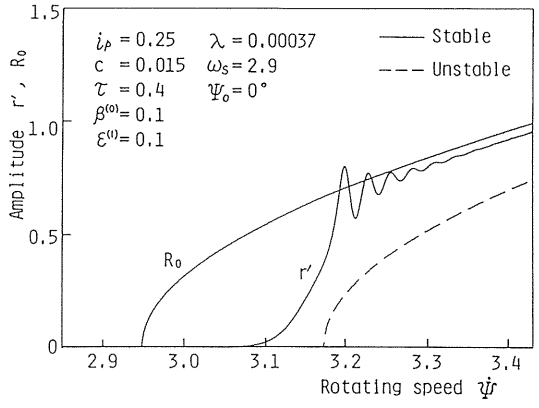

(c) Amplitude variation curve of subharmonic oscillation after data processing

Fig. 4.3. Flow of data processing

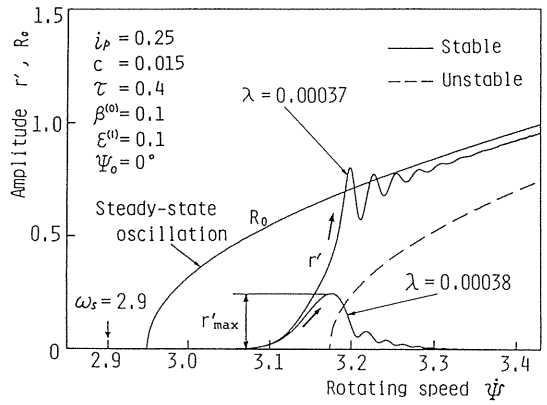

Fig. 4.4. Amplitude variation curve during acceleration through a critical speed

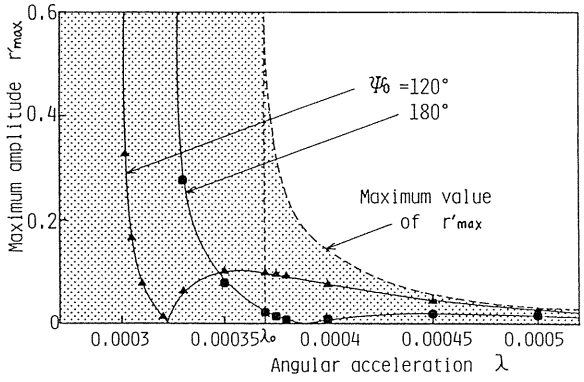

(a) Influence of angular acceleration λ

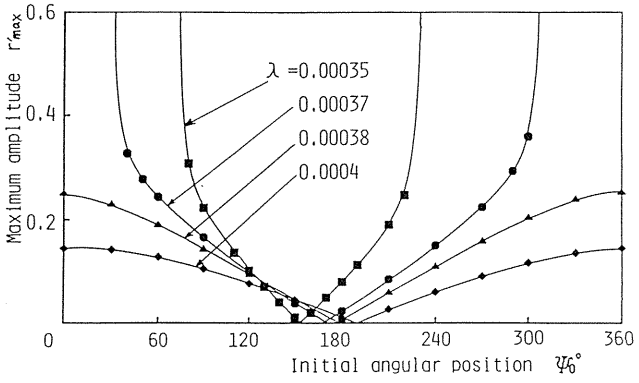

(b) Influence of initial angular position Ψ_0

Fig. 4.5. Variations of maximum amplitude (acceleration)

nously as λ increases and the rotor can pass the critical speed without the occurrence of subharmonic oscillation at a certain value of λ. From this figure, we see that r'_{max} also depends on Ψ_0. Therefore, we show the influence of Ψ_0 on r'_{max} in Fig. 4.5(b) where λ is treated as a parameter. The r'_{max} varies markedly depending on Ψ_0. For angular acceleration beyond a certain value, the maximum amplitude does not become infinite and the rotor can always pass the critical speed with finite amplitude for any value of Ψ_0 (for example, the cases in which λ = 0.00038, 0.0004). For small angular acceleration, a range of Ψ_0 exists where the critical speed cannot be passed with finite amplitude and this range expands as λ becomes small (for example, when λ = 0.00035, 0.00037). For example, in the case of λ = 0.00035, the rotor cannot pass in the range of $\Psi_0 = 0° \sim 71°$ and $230° \sim 360°$. Because r'_{max} varies depending on Ψ_0, we show the maximum value of the maximum amplitude r'_{max} by a broken line in Fig. 4.5(a). As shown in Fig. 4.5(b), the curve representing r'_{max} touches the Ψ_0-axis at a certain value of Ψ_0. In the case of acceleration, r'_{max} takes a value in the shaded zone. We represent the value of angular acceleration to which this broken line approaches asymptotically by λ_0. If we accelerate the rotor at a rate beyond this critical value, the rotor can always pass the critical speed with finite amplitude.

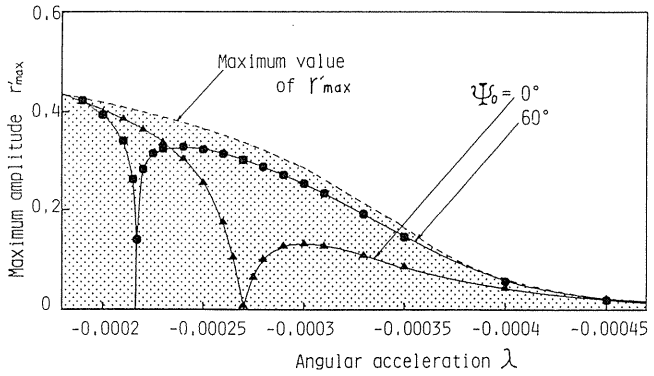

(a) Influence of angular acceleration λ

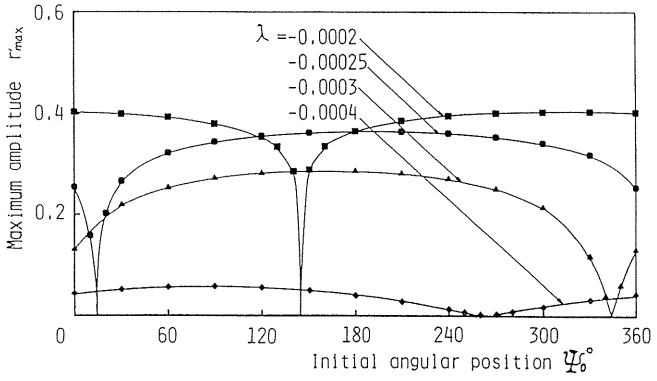

(b) Influence of initial angular position Ψ_0

Fig. 4.6. Variations of maximum amplitude (deceleration)

Figure 4.6(a) and 4.6(b) show the influence of λ and Ψ_0, respectively, in the case of deceleration. When the resonance is a hard-spring type, the rotor can always pass the critical speed with finite amplitude with any value of λ. As the absolute value of the angular acceleration increases, the maximum value of r'_{max} decreases. Although the maximum amplitude r'_{max} also depends on the initial angular position Ψ_0 in this case, the character of this dependence is different from the case of acceleration. Namely, unlike that shown in Fig. 4.5(b), the maximum amplitude is almost constant except for a narrow zone near a certain value of Ψ_0.

4. 4. 3. Trajectory during acceleration on the coordinates rotating with an angular velocity (1/2)$\dot{\Psi}$

We shall explain why the initial angular position Ψ_0 influences the maximum amplitude r'_{max}. After extracting a component of subharmonic oscillation, we observe the oscillation on the coordinate system $O-uv$ rotating with the angular velocity $(1/2)\dot{\Psi}$. As mentioned above, the inclination θ_x, θ_y contains various kinds of components. We express the inclination corresponding to the 1/2-order subharmonic oscillation by θ_{x1} and θ_{y1}. The transformation from θ_{x1} and θ_{y1} to the rotating coordinates u and v is given by

$$\begin{aligned} u &= \theta_{x1}\cos(\Psi/2) + \theta_{y1}\sin(\Psi/2) \\ v &= -\theta_{x1}\sin(\Psi/2) + \theta_{y1}\cos(\Psi/2) \end{aligned} \tag{4.12}$$

When the rotor is rotating with a constant angular velocity $\dot{\Psi} = \omega$, we can transform Eq. (4.12) to $u = R\cos\delta_f$, $v = R\sin\delta_f$.

Figure 4.7 shows an example of trajectories on the uv-plane. Those are the trajectories for the initial angular position $\Psi_0 = 0°$ and 60° in the case of constant angular acceleration $\lambda = 0.00037$. The arrows on the trajectories represent the direction of movement of the solution (the representative point). As can be seen from Fig. 4.5(b), the case $\Psi_0 = 0°$ corresponds to a non-passable case and the case $\Psi_0 = 60°$ corresponds to a passable case.

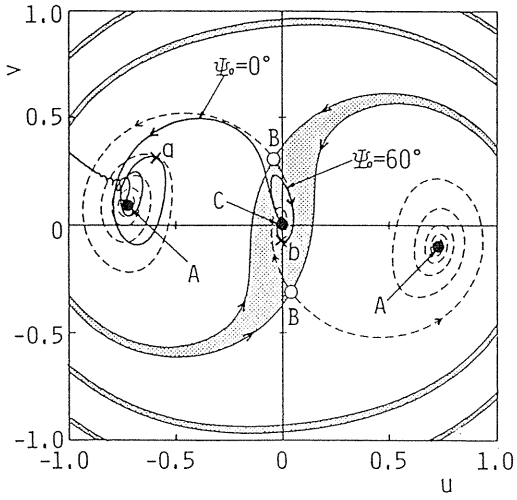

Fig. 4.7. Trajectories on the uv-plane and separatrices

Here, we discuss the case that the shaft is rotating with the constant rotating speed $\dot{\Psi} = 3.22$ corresponding to the symbol × (points a and b) on the trajectories in Fig. 4.7. When $\dot{\Psi}$ $(=\omega)$ is constant, the stationary solution of 1/2-order subharmonic oscillation is represented by a fixed point called a singular point in the uv-plane. The symbol ● and ○ in Fig. 4.7 represent a stable and an unstable solution at $\omega = 3.22$, respectively. Points A (a spiral point), B (saddle point) and C (a spiral point) represent a stable solution $R_0 \fallingdotseq 0.730$, an unstable solution $R_0 \fallingdotseq 0.310$, and a stable solution $R_0 = 0$, respectively. In addition, among the trajectories, which start from various initial values, those which pass unstable stationary solution B are shown. The trajectory in the shaded zone converges to stable solution C corresponding to the solution with zero amplitude, and that in the other zone converges to stable solution A corresponding to the stable solution with nonzero amplitude. The boundary lines between these zones are separatrices. The zone in which the initial position exists determines the stable solution to which the trajectory converges.

Next, we discuss the case where the rotating speed changes with a constant angular acceleration $\ddot{\Psi} = \lambda$. At every rotating speed, the solution (the representative point) moves toward the point corresponding to the stable stationary solution of that instant at every rotating speed. For example, when the stability of the stationary solution of zero amplitude changes from stable to unstable during the acceleration, the representative point departs from the origin and then moves toward the stable solution with a finite amplitude (refer Fig. 4.4). If the rotating speed increases further, the solution of zero amplitude changes to a stable one again and the shaded zone shown in Fig. 4.7 appears. This shaded zone expands as the rotating speed increases. In the case $\Psi_0 = 0°$, as the angular velocity $\dot{\Psi}$ increases, the representative point moves toward the stable singular point with a finite amplitude without entering this shaded zone. Conversely, in the case of $\Psi_0 = 60°$, although the amplitude increases initially, it decreases toward the origin after the representative point enters the shaded zone. As explained above, whether the representative point enters the shaded zone or not depends on the growing speed of the trajectory, and this growing speed varies depending on Ψ_0.

The reason for the difference in this growing speed is as follows. If the rotor traces an orbit containing only a harmonic component precisely when the rotating speed enters the resonance region of subharmonic oscillation, that is, the region where the stationary solution of zero amplitude is unstable, initial values given to the subharmonic oscillation component are zero on the uv-plane. Therefore, in such a case, the representative point continues to stay on the unstable saddle point if no other disturbance works, and no 1/2-order subharmonic oscillation occurs. However, in reality, the amplitude and the phase of the solution of the harmonic component change step by step as a function of the rotating speed, and the rotor always follows this harmonic component. The rotor lags slightly behind the position corresponding to the steady-state solution and it enters the resonance region in such a condition. This small discrepancy causes a small disturbance in the subharmonic oscillation. It is considered that the direction of this disturbance varies depending on the initial angular position Ψ_0.

From such a consideration, we compared trajectories which start from various angular positions at the constant rotating speed $\omega = 3.10$. At this rotating speed, the origin corresponding to the zero-amplitude steady-state solution is an unstable singular point on the uv-plane. The initial position, which corresponds to an initial disturbance, is selected at various angular positions α but at the same distance from the origin. The result is shown in Fig. 4.8. In this figure, the symbol ● represents the initial position and the symbol ○ is marked at the same time interval on the trajectories. The origin is a saddle point. Therefore, if the representative point is exactly on the origin, it continues to stay there, and the nearer the representative point is to the origin, the slower it moves. For example, when the initial position is near

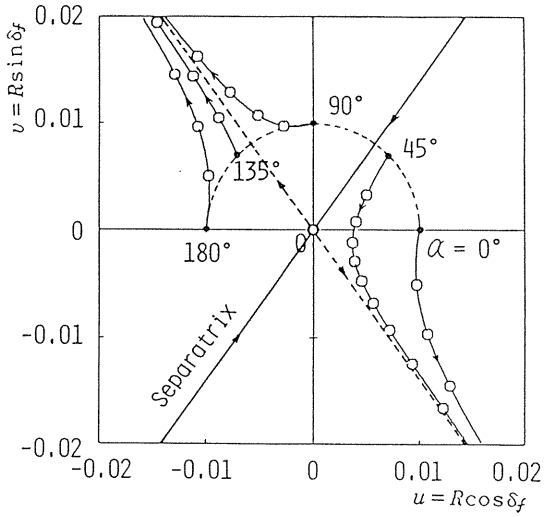

Fig. 4.8. Variation of trajectory due to initial position (a case of constant rotating speed)

the separatrix whose direction is toward the origin as in the case of $\alpha = 45°$, the representative point approaches the origin once, and then leaves it, moving toward a stable singular point corresponding to a resonance curve of finite amplitude. Conversely, in the case of $\alpha = 135°$, it moves toward a stable singular point without approaching the origin. Therefore, it is understood that the amplitude grows slowly in the former case because it takes long time in movement near the origin, and the amplitude grows rapidly in the latter case.

The same situation appears in the case of constant acceleration. As mentioned above, the direction and magnitude of the initial disturbance given at the entrance of the resonance region of subharmonic oscillation depends on the initial angular position Ψ_0. Therefore, it is understood that a large difference appears in the growing speed of the amplitude depending on the initial angular position Ψ_0.

4. 5. Experimental apparatus and experimental results

4. 5. 1. Experimental apparatus

The experimental apparatus and the measurement system are shown in Fig. 4.9. The constitution of this experimental apparatus is the same as that used in the previous chapter, but its dimension was changed in order to have a critical speed in a rotating speed range convenient for experiments. The dimensions of the rotor were as follows: the diameter was 400 mm, the thickness was 7.9 mm, the mass was 7.90 kg. The dimensions of the shaft were as follows: the diameter was 12 mm, the length was 700 mm. The rotor was mounted at a position 175 mm above the lower end.

The measurement system is different from that used in the previous paper. The deflections of the rotor were measured by detecting disk edge displacement in the x- and y-directions. The rotating speed was detected by a rotary encorder attached to the upper end of the shaft. The outputs of these sensors were amplified by operation amplifier circuits and sent to a personal computer through an A/D-converter. This A/D converter had a distinguishable minimum deflection of 0.002 mm.

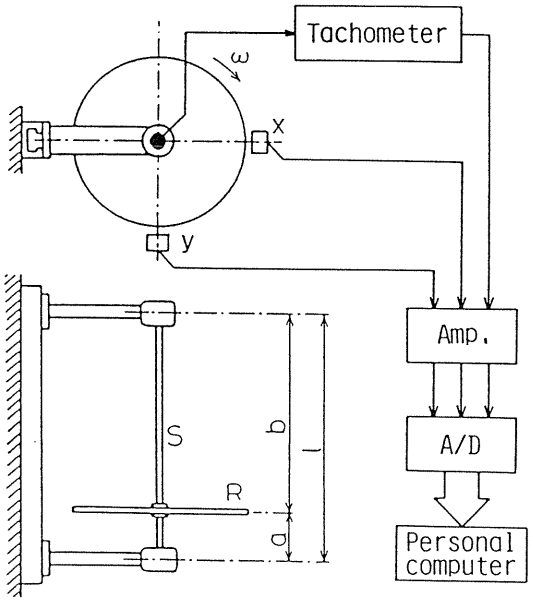

Fig. 4.9. Experimental apparatus and measurement system

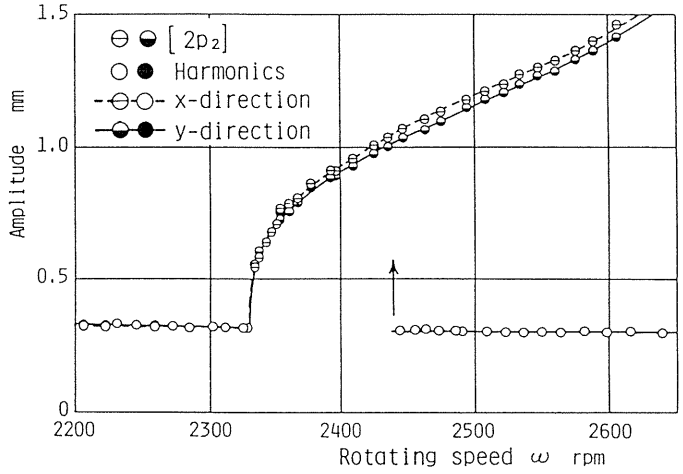

Fig. 4.10. Resonance curve of the subharmonic oscillation in an experiment

4. 5. 2. Experimental results

A resonance curve of the 1/2-order subharmonic oscillation which appeared in the neighborhood of $\omega \fallingdotseq 2p_2$ is shown in Fig. 4.10. The abscissa represents rotating speed (rpm) and the ordinate represents total amplitude (mm), that is, the summation of the amplitude of

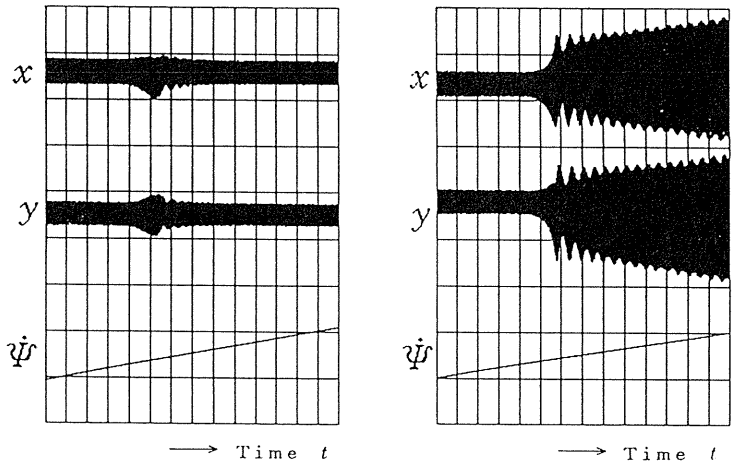

Fig. 4.11. Experimental results of time histories and of angular velocity $\dot{\Psi}$

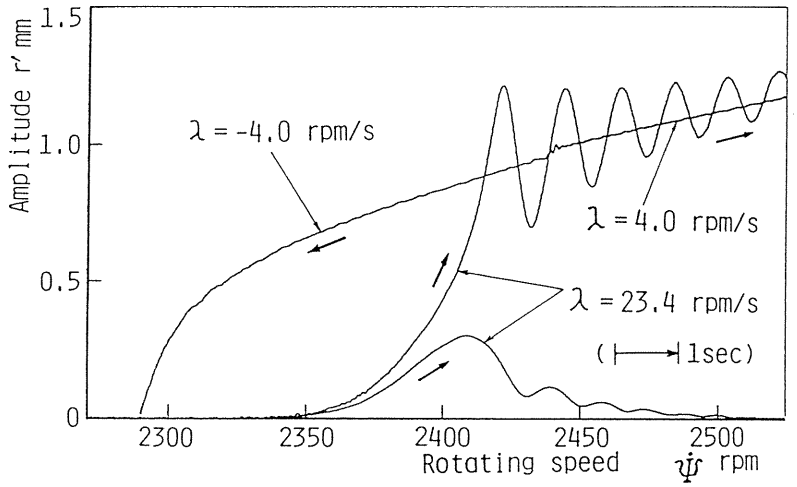

Fig. 4.12. Amplitude variations of subharmonic oscillation during acceleration in experiments

a harmonic oscillation and that of a subharmonic oscillation. The symbols ○ ⊖, and ●, ⊖ represent amplitudes in the x- and y-directions, respectively. The arrow indicates a jump phenomenon where the amplitude changes discontinuously. The shape of this resonance curve is a hard-spring type and it agrees well with that obtained in the theoretical analysis.

In our experiments, it was impossible to set the angular position Ψ_0 as we desired and also impossible to measure it at the start of acceleration, so the initial angular position was random. We observed nonstationary responses by performing experiments many times under the same conditions of assembly, acceleration and initial angular velocity.

Figure 4.11 shows experimental results of time histories in the x- and y-directions and of angular velocity $\dot{\Psi}$. These were digital quantities sampled by the computerized measurement

system. The angular acceleration of Fig. 4.11(a) was $\lambda = 22.8$ rpm/s and that of Fig. 4.11(b) was 19.4 rpm/s. The initial angular velocity was $\omega_s = 2100$ rpm and the sampling frequency was 300 Hz in both cases. In this figure, there are 512 data between the scale lines of the abscissa. It is seen from the envelopes of time histories that Fig. 4.11(a) is a passable case and Fig. 4.11(b) is a non-passable case. It is ascertained from the curve $\dot{\Psi}$ that the shaft was accelerated with a constant angular acceleration.

With the same procedure as that adopted in the numerical analysis, we extracted the component of the 1/2-order subharmonic oscillation from such waves as those shown in Fig. 4.11. The amplitude variation curves obtained by such data processing are shown in Fig. 4.12. From the same angular acceleration $\lambda = 23.4$ rpm/s, a passable case and non-passable case are shown. In addition, in order to show approximately a stable resonance curve of a steady-state oscillation, we measured the amplitude change during very slow acceleration. The value $\lambda = \pm 4.0$ rpm/s was the smallest acceleration that this apparatus could give. In this case, the initial angular velocity was $\omega_s \fallingdotseq 2450$ rpm, and this was the rotating speed where a subharmonic oscillation occurred with a large amplitude and the shaft was accelerated and decelerated from this rotating speed. In this figure, different types of nonstationary responses were obtained with the same angular acceleration $\lambda = 23.4$ rpm/s. This difference in the amplitude variation curve was due to the difference in the initial angular posi-

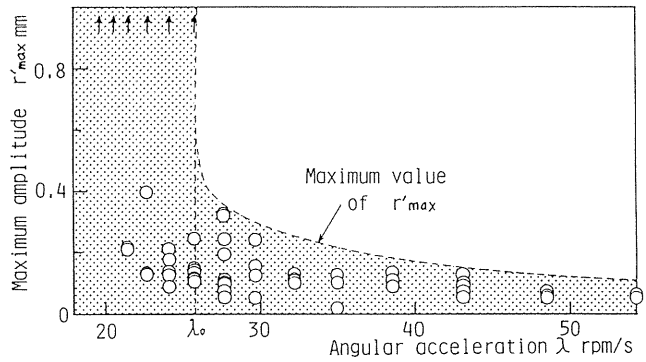

(a) Acceleration

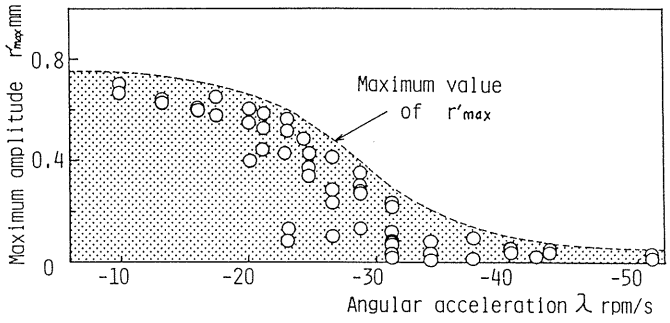

(b) Deceleration

Fig. 4.13. Influence of the angular acceleration on the maximum amplitude in experiments

tion Ψ_0 given in experiments. It is seen that the experimental results in Fig. 4.12 are explained well by the theoretical results in Fig. 4.5 where r'_{max} varies remarkably depending on the angular position Ψ_0 of the unbalance even with the same angular acceleration.

Figure 4.13(a) shows the relationship between the angular acceleration λ and the maximum amplitude r'_{max} in the case of acceleration. In this figure, the arrow indicates a nonpassable case, namely the case that the amplitude increased along the resonance curve. The broken line is an envelope of maximum amplitudes r'_{max}, that is, it shows maximum values of r'_{max}. We denote the value of λ which this envelope approaches by λ_0. From this figure, it is seen that, even at the same angular acceleration, the maximum amplitude varies within a certain value. When the angular acceleration was less than $\lambda_0 \fallingdotseq 26$ rpm/s, both a passable case and non-passable case appeared. In experiments, as the angular acceleration became small, the probability of a non-passable case became large. This experimental result agree qualitatively with the theoretical result in Fig. 4.5. Figure 4.13(b) shows the relationship between the angular acceleration λ and the maximum amplitude r'_{max} when the rotor was decelerated from $\omega_s = 2600$ rpm. The broken line is the envelope of r'_{max}. It is seen from this figure that the system was passable at any value of angular acceleration in the case of deceleration. The maximum amplitude also varies depending on the initial angular position Ψ_0 in this case. This experimental result agrees well with the theoretical result shown in Fig. 4.6(a).

4. 6. Conclusions

A. From the theoretical discussions:

(1) Unlike the case of a major critical speed, the maximum amplitude r'_{max} during acceleration or deceleration through the critical speed of the 1/2-order subharmonic oscillation depends not only on the angular acceleration $\ddot{\Psi} = \lambda$ but also on the angular position Ψ_0 of the unbalance at the start of acceleration.

(2) In order to pass the critical speed with finite amplitude in the case of acceleration ($\lambda > 0$), an angular acceleration larger than the critical value λ_0 is necessary. If the rotor is accelerated with an angular acceleration smaller than this critical value, the amplitude increases along the resonance curve and the rotor cannot pass the critical speed for a certain range of Ψ_0. The smaller the angular acceleration becomes, the wider this range of Ψ_0 becomes.

(3) In the case of deceleration ($\lambda < 0$), the rotor can always pass the critical speed with any value of angular acceleration. As the absolute value of angular acceleration increases, the maximum value of the maximum amplitude r'_{max} decreases. The maximum amplitude is almost constant for Ψ_0 except near a certain value of Ψ_0.

(4) The maximum amplitude depends on the initial angular position Ψ_0 because the initial disturbance caused when the rotating speed enters the resonance region varies depending on Ψ_0, and the speed of amplitude growth is different depending on the relative position of the representative point to the origin (a saddle point) on the $u\upsilon$-plane.

B. From the experimental discussions:

(1) With the same angular acceleration, the maximum amplitude during acceleration or deceleration through the critical speed varied remarkably within a certain value. In some cases, the rotor could pass the critical speed without any subharmonic oscillation appearing.

(2) In the case of acceleration, the range of variation of the maximum amplitude during acceleration expands as the angular acceleration λ decreases. In some cases, when the acceleration is less than a critical value λ_0, the rotor could not pass the critical speed.

(3) In the case of deceleration, the rotor could always pass the critical speed with finite amplitude.

Chapter 5 Critical speed of a summed-and-differential harmonic oscillation[60]

5. 1. *Introduction*

Concerning nonstationary oscillations during acceleration through critical speeds of summed-and-differential harmonic oscillations, Evan-Iwanowski[5] and Agrawal and Evan-Iwanowski[50] obtained nonstationary solutions by the asymptotic method. However, the main purpose of their studies was the theoretical determination of approximate nonstationary response curves. In addition, the obtained solutions in their analyses give amplitude variation curves only in the cases that the acceleration was started from a condition that a summed-and-differential harmonic oscillation was appearing in its resonance region. Their results give no solution about the case that a rotor is accelerated from a rotating speed where a summed-and-differential harmonic oscillation does not appear.

In this chapter, a nonstationary oscillation when a rotor passes a critical speed of a summed-and-differential harmonic oscillation with constant acceleration or deceleration is discussed. Among various kinds of summed-and-differential harmonic oscillations, one due to the same asymmetrical nonlinear spring characteristics as the 1/2-order subharmonic oscillation treated in the previous chapter is investigated. In this kind of oscillation, two vibration components, whose frequencies are nearly equal to the natural frequencies respectively, occur in addition to the harmonic component $[+\omega]$ when the rotating speed approaches a value which is equal to the difference of the two natural frequencies. It is known that the shape of the resonance curve of this steady-state oscillation is similar to that of the 1/2-order subharmonic oscillation[51]. However, as the number of vibration components differs, the characteristics of nonstationary oscillation may differ from those of the subharmonic oscillation. In this research, influences of angular acceleration and initial conditions (for example, an rotating speed and an angular position of unbalance) on the maximum amplitude of the nonstationary oscillation are investigated. In addition, the result is compared with those of the major critical speed and the subharmonic oscillation of order 1/2.

5. 2. *Equation of motion and steady-state oscillations*

Similar to the case of chapter 4, an inclination motion of the rotor is discussed in the following theoretical analysis. The equation of motion is the same as Eq. (4.1) and given by

$$\begin{aligned}
&\ddot{\theta}_x + i_p\ddot{\Psi}\theta_y + i_p\dot{\Psi}\dot{\theta}_y + c\dot{\theta}_x + \theta_x + N_{\theta x} = (1 - i_p)\tau(\dot{\Psi}^2\cos\Psi + \ddot{\Psi}\sin\Psi)\\
&\ddot{\theta}_y - i_p\ddot{\Psi}\theta_x - i_p\dot{\Psi}\dot{\theta}_x + c\dot{\theta}_y + \theta_y + N_{\theta y} = (1 - i_p)\tau(\dot{\Psi}^2\sin\Psi - \ddot{\Psi}\cos\Psi)
\end{aligned} \tag{5.1}$$

Here, we discuss the steady-state response under the condition of constant rotating speed ($\ddot{\Psi} = \omega$). In this case, the relations

$$\Psi = \omega t + \Psi_0\,, \quad \dot{\Psi} = \omega\,, \quad \ddot{\Psi} = 0 \tag{5.2}$$

hold, where Ψ_0 is the initial angular position of τ at $t = 0$. The frequency equation of this system is $G(p) \equiv 1 + i_p\omega p - p^2 = 0$. We represent two roots of this equation by $p_f(>0)$ and $p_b(<0)$. They represent natural frequencies of forward and backward whirling modes, respectively. The change of natural frequency p with the rotating speed ω for $i_p = 0.25$ is shown in Fig. 5.1. In this figure, let the point of intersection of curve $p_f - p_b$ and straight line

$p = \omega$ be A, its abscissa be ω_0, and the natural frequencies at $\omega = \omega_0$ be p_{f0} and p_{b0}. In the neighborhood of ω_0, stationary oscillations whose frequencies are near the natural frequencies p_f, p_b appear in addition to the harmonic oscillation $[+\omega]$. This kind of oscillation is called the summed-and-differential harmonic oscillation of $[p_f - p_b]$ type[55]. We represent their total phases by θ_ω, θ_f, θ_b. The frequencies $\dot{\theta}_f$, $\dot{\theta}_b$ can be expressed approximately within an accuracy of

$$\begin{aligned} \dot{\theta}_f &\fallingdotseq (p_{f0}/\omega_0)\omega = (p_{f0}/\omega_0)\dot{\Psi} \quad (\equiv \omega_f) \\ \dot{\theta}_b &\fallingdotseq (p_{b0}/\omega_0)\omega = (p_{b0}/\omega_0)\dot{\Psi} \quad (\equiv \omega_b) \end{aligned} \tag{5.3}$$

With reference to these equations, the total phases θ_f, θ_b are written as follows:

$$\begin{aligned} \theta_f &= (p_{f0}/\omega_0)\Psi + \delta_f = \omega_f t + (p_{f0}/\omega_0)\Psi_0 + \delta_f \\ \theta_b &= (p_{b0}/\omega_0)\Psi + \delta_b = \omega_b t + (p_{b0}/\omega_0)\Psi_0 + \delta_b \end{aligned} \tag{5.4}$$

From the comparison of Eqs. (5.3) and (5.4), we find that the quantities $\dot{\theta}_f - \omega_f$, $\dot{\theta}_b - \omega_b$, which are the differences between the correct frequency and the approximate frequency, are $\dot{\delta}_f$, $\dot{\delta}_b$. The values δ_f, δ_b change slowly because $\dot{\delta}_f$ and $\dot{\delta}_b$ are small quantities of order $O(\varepsilon)$. The total phase angle of the harmonic oscillation component is given as follows:

$$\theta_\omega = \Psi + \beta = \omega t + \Psi_0 + \beta \tag{5.5}$$

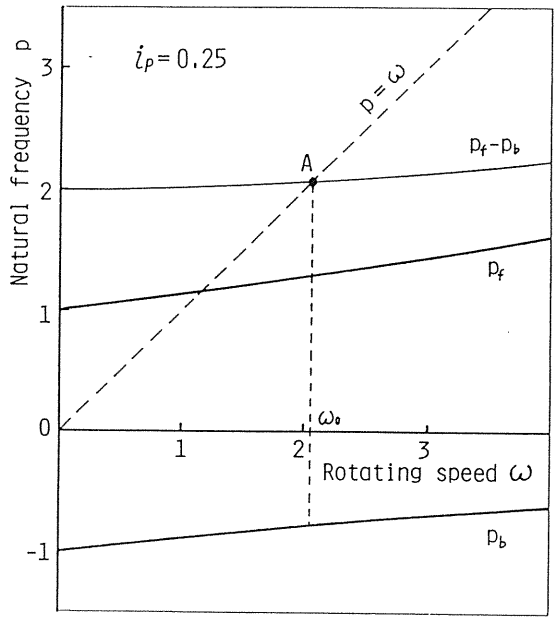

Fig. 5.1. Natural frequency p as a function of the rotating speed ω

where β is the phase difference between this harmonic component and the angular position Ψ of the unbalance τ. Therefore, the solution of summed-and-differential harmonic oscillation is expressed, within an accuracy of $O(\varepsilon)$[57], as follows:

$$\begin{aligned}\theta_x &= R_f\cos\theta_f + R_b\cos\theta_b + P\cos\theta_\omega \\ &\quad + \varepsilon(a_f\cos\theta_f + b_f\sin\theta_f + a_b\cos\theta_b + b_b\sin\theta_b) \\ \theta_x &= R_f\sin\theta_f + R_b\sin\theta_b + P\sin\theta_\omega \\ &\quad + \varepsilon(a'_f\sin\theta_f + b'_f\cos\theta_f + a'_b\sin\theta_b + b'_b\cos\theta_b)\end{aligned} \tag{5.6}$$

Substituting this into Eq. (5.1) and supposing that the amplitudes R_f, R_b, a_f, etc., are quantities which vary slowly with time, we obtain the following equations within the order $O(\varepsilon)$ by the harmonic balance method.

$$\dot{R}_f = (1/A_f)\,(-c\omega_f R_f - 2\varepsilon^{(1)}R_b P\sin\psi) \tag{a}$$

$$\dot{R}_b = (1/A_b)\,(-c\omega_b R_b + 2\varepsilon^{(1)}R_f P\sin\psi) \tag{b}$$

$$\begin{aligned}\dot{\psi} &= (1/A_f)\,\{G_f + 4\beta^{(0)}(R_f^2 + 2R_b^2 + 2P^2) - 2\varepsilon^{(1)}P(R_b/R_f)\cos\psi\} \\ &\quad -(1/A_b)\,\{G_b + 4\beta^{(0)}(2R_f^2 + R_b^2 + 2P^2) - 2\varepsilon^{(1)}P(R_f/R_b)\cos\psi\}\end{aligned} \tag{c}$$

(5.7)

where

$$\begin{aligned}&A_f = (2\omega_f - i_p\omega)\,, \quad A_b = (2\omega_b - i_p\omega)\,, \quad G_f = G(\omega_f)\,, \quad G_b = G(\omega_b)\,, \\ &\psi = \delta_f - \delta_b\,, \quad P = -(1 - i_p)\tau\omega^2/G(\omega),\end{aligned} \tag{5.8}$$

The steady-state solutions $R_f = R_{f0}$, $R_b = R_{b0}$, $\psi = \psi_0$ can be obtained by $\dot{R}_f = 0$, $\dot{R}_b = 0$, $\dot{\psi} = 0$. The stability of these stationary solutions can be ascertained by the same procedure as that in the previous paper[57].

5. 3. Nonstationary response during acceleration through the critical speed

5. 3. 1. Process of analysis

The rotor is accelerated with a constant acceleration. Let the acceleration be $\lambda(=\ddot{\Psi})$, the initial rotating speed ω_s, and the initial angular position of the dynamic unbalance τ of the rotor be Ψ_0 (refer Fig. 4.1).

$$\Psi = (1/2)\lambda t^2 + \omega_s t + \Psi_0 \tag{5.9}$$

This condition is inserted into Eq. (5.2). The nonstationary time histories observed in θ_x, θ_y directions are calculated by the Runge-Kutta-Verner method. The rotor is accelerated from a certain rotating speed which is outside of the resonance region where the summed-and-differential oscillation occurs. At this initial rotating speed, only a harmonic oscillation appears. In the nonstationary time history, a component whose frequency is near the rotating speed $\dot{\Psi}$

and two components whose frequencies are near p_f and p_b coexist. Therefore, the radius of rotor inclination $\sqrt{\theta_x^2 + \theta_y^2}$ becomes very complex as shown in Fig. 5.2(a). These data on θ_x, θ_y are processed by the complex FFT in the same way as the previous chapter. A obtained spectrum is shown in Fig. 5.2(b). We extracted the spectrum component near the frequency p_f and p_b by filtering, and obtain the amplitude variation curve shown in Fig. 5.2 by transforming them into the time domain by inverse FFT. In the case of Fig. 5.2, data were sampled at an interval corresponding to 1/20 of the period at ω_s, and 2^{14} data were processed by FFT.

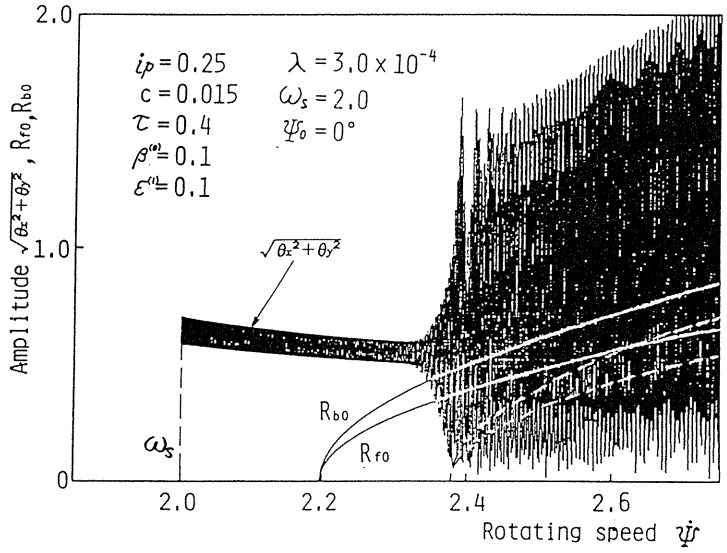

(a) Radius variation obtained by a numerical integration and the amplitudes of the steady-state resonance curve

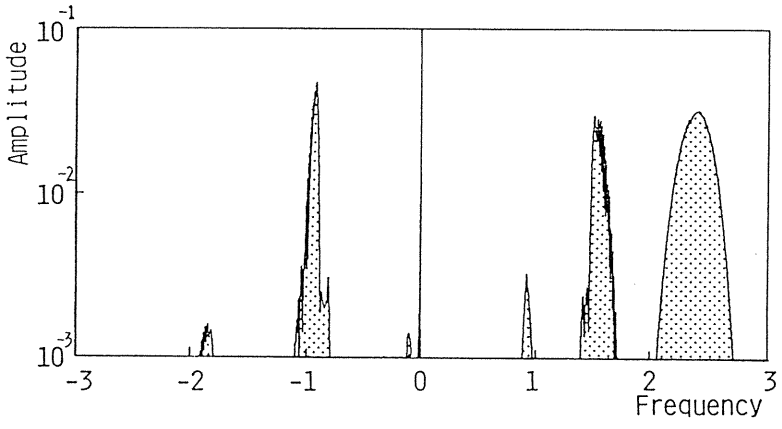

(b) Spectrum is shown

Fig. 5.2. Signal processing by the comples-FFT (Numerical analysis)

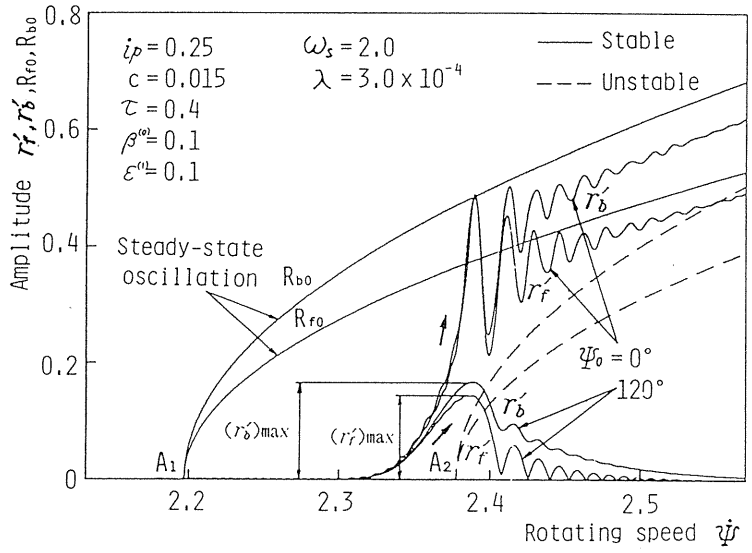

Fig. 5.3. Amplitude variations during acceleration through a critical speed for two different initial angular positions Ψ_0 (acceleration)

Therefore the sampled range varied according to λ. For example, in the case of $\lambda = 3.0 \times 10^{-4}$ in Figs. 5.2 and 5.3, the sampled range was $\dot{\Psi} \fallingdotseq 2.0 \sim 2.77$. In this case, the frequency ranges $-1.1 \sim -0.75$ and $1.3 \sim 1.8$ were extracted.

5. 3. 2. Maximum amplitude during acceleration through the critical speed

Figure 5.3 shows resonance curves of steady-state solutions R_{f0}, R_{b0} calculated in section 5.2 and amplitude variation curves r'_f, r'_b of nonstationary oscillations during acceleration for two initial angular positions Ψ_0. In the resonance curves, a solid line represents a stable solution and a broken line represents an unstable solution. (In Fig. 5.2(a), the resonance curves which overlap the amplitude variation curve $\sqrt{\theta_x^2 + \theta_y^2}$ are denoted by white lines.) In Fig. 5.3, the stability of the trivial solution is not distinguished. However, it is unstable between A_1 and A_2 which are the intersections of the resonance curves with the $\dot{\Psi}$-axis, and it is stable outside of them. Similar to the case of the 1/2-order subharmonic oscillation, the nonstationary responses during acceleration through the critical speed of summed-and-differential harmonic oscillation are classified into two groups. One is the case (for example, $\Psi_0 = 0°$) where the amplitudes increase along the stable resonance curve, and the other is the case (for example, $\Psi_0 = 120°$) where the rotor can pass the critical speed with a small amplitude. We call the former non-passable case and the latter a passable case.

The amplitudes start to increase with a delay after the rotating speed enters the unstable zone of the trivial solution through point A_1. (This phenomenon is called penetration.) The amplitudes r'_f and r'_b of components whose frequencies are nearly equal to p_f and p_b, respectively, increase almost with the same velocity. In a non-passable case, the amplitude converge to the stationary resonance curves varying periodically after taking the maximum values almost at the same time. The discrepancies between the amplitude variation curves and resonance curves are due to an error in the approximate solutions of the resonance curve. In a

passable case, however, after their amplitudes takes the maximum values $(r'_f)_{max}$, $(r'_b)_{max}$, they converge to the trivial solution. In a non-passable case, althogh it drops down when it reaches the end of the stable resonance curve with a very large finite amplitude, we use symbols $(r'_f)_{max} = \infty$, $(r'_b)_{max} = \infty$ for convenience. Because as mentioned above, we thought that the difference between a very large amplitude and infinity is not so important from a practical point of view.

Next, we investigate the influence of the following three parameters on the maximum amplitude $(r'_b)_{max}$: the angular acceleration λ, the initial rotating speed ω_s, and the initial angular position Ψ_0 of the unbalance τ. Treatment of $(r'_f)_{max}$ is avoided due to its similarity to $(r'_b)_{max}$. Figure 5.4(a) shows relations between the maximum amplitude $(r'_b)_{max}$ and the angular acceleration $\lambda(\lambda > 0)$ for various values of Ψ_0. The initial rotating speed is set at $\omega_s = 2.0$. The full line and the dash-dotted line show the cases of $\Psi_0 = 120°$ and 180°, respectively. The broken lines represent the maximum and minimum values of amplitude variation curves obtained when the parameter Ψ_0 changed from $0° \sim 360°$ with the interval of 30°. Thus, $(r'_b)_{max}$ exists within the shaded zone, bounded by the broken lines. These broken lines take several maxima and minima, becoming infinite for some ranges of small λ. At the angular acceleration λ corresponding to an infinite upper bound of $(r'_b)_{max}$, the rotor cannot pass the critical speed with finite amplitude for some values of initial angular position Ψ_0. The maximum value of angular acceleration of such non-passable case is denoted by λ_1. At λ for which upper bound on $(r'_b)_{max}$ is finite, the rotor can always pass the critical speed for any value of Ψ_0. In the case of 1/2-order subharmonic oscillation in the previous chapter, the upper bound of the maximum amplitude τ'_{max} decreases monotonously with the angular acceleration λ, and the range of λ is divided into two by a critical value λ_0. Namely, if λ is larger than λ_0, it can pass for any value of Ψ_0 with finite amplitude, and if λ is less than λ_0, it cannot pass for some values of Ψ_0. But in the case of summed-and-differential harmonic oscillation treated here, there exist several passable (finite-bounded) sub-ranges (for example, $\lambda \fallingdotseq 2.91 \sim 2.98$, $2.79 \sim 2.83$ in Fig. 5.4(a)) under a non-passable sub-ranges (for example, $\lambda \fallingdotseq 2.98 \sim 3.03$).

Next, Fig. 5.4(b) shows the influence of the angular acceleration λ on the maximum amplitude $(r'_b)_{max}$. The initial rotating speed ω_s is treated as a parameter. The initial angular position is fixed at $\Psi_0 = 180°$. It is found from this figure that the curve varies remarkably when ω_s deviates by only $\pm 0.1\,\%$ from the value 2.0. Nevertheless, these differences among the variation curves do not necessarily imply a variation of the angular acceleration λ_1 which is the maximum angular acceleration in a non-passable case. If the figure corresponding to Fig. 5.4(a) is drawn for various values of ω_s, we know that the value of λ_1 does not differ greatly even if the initial rotating speed ω_s changes. In the experimental apparatus mentioned later, the error in the adjustment of the rotating speed is about $\pm 0.1\,\%$. Therefore, when we draw an experimental diagram corresponding to Fig. 5.4(a), the unshaded zones in the angular acceleration range below λ_1 disappear due to the slight adjustment error in the initial rotating speed ω_s. In order to compare with the experimental results, we must consider Figs. 5.4(a) and 5.4(b) combined. If the envelope of these curves is drawn, the upper bound of the maximum amplitude $(r'_b)_{max}$ decreases monotonously for λ, similar to the case of the 1/2-order subharmonic oscillation, and we can determine the critical value $\lambda_0(\lambda_0 \geqq \lambda_1)$ above which the rotor can always pass the critical speed with finite amplitude.

The influence of Ψ_0 on the maximum amplitude $(r'_b)_{max}$ is shown in Fig. 5.4(c), where the angular acceleration λ is treated as a parameter and the initial rotating speed is fixed at $\omega_s = 2.0$. The following cases are shown: $\lambda = 2.94 \times 10^{-4}$ in a passable sub-range between non-passable ranges in Fig. 5.4(a); $\lambda = 3.00 \times 10^{-4}$ in a nonpassable range; and $\lambda = 3.16 \times 10^{-4}$ in a passable range. In the case of subharmonic oscillation, all of these curves are in contact

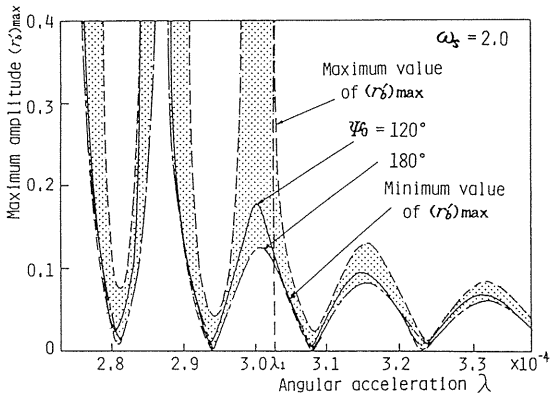

(a) Influence of the angular acceleration λ and the initial angular position Ψ_0

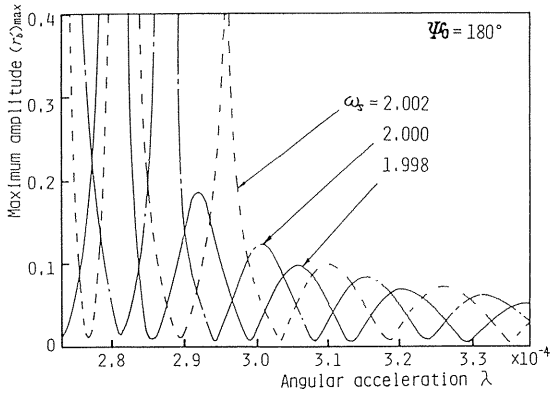

(b) Influence of the angular acceleration λ and the initial angular rotating speed ω_s

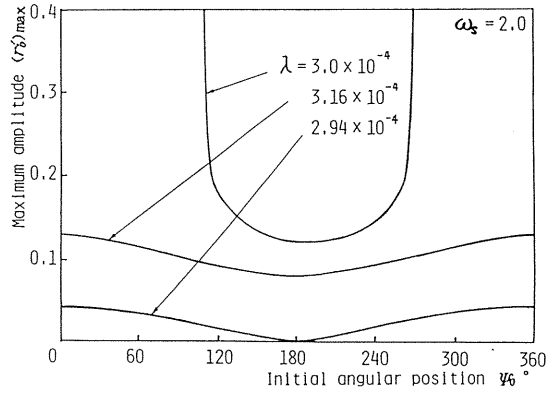

(c) Influence of the initial angular position Ψ_0 and angular acceleration λ

Fig. 5.4. Variations of the maximum amplitude (acceleration)

with the abscissa (Ψ_0-axis) and there always exists a value of Ψ_0 for which the maximum amplitude r'max is nearly zero. This means that the lower bound of r'max is always zero in the case of 1/2-order subharmonic oscillation. However, in the case of summed-and-differential harmonic oscillation, for most of the λ's these curves do not make contact with the abscissa, and therefore $(r'_b)_{max}$ does not become zero for any value of Ψ_0 (for example, $\lambda = 3.00 \times 10^{-4}$, $\lambda = 3.16 \times 10^{-4}$ in Fig. 5.4(c)).

In Fig. 5.5, $(r'_b)_{max}$ is plotted as a function of λ for the case of deceleration ($\lambda < 0$), with Ψ_0 as a parameter, and with the initial rotating speed fixed at $\omega_s = 2.55$. The curves for $\Psi_0 = 90°$ is represented by a solid line, while for other values of Ψ_0 the curve shifts vertically within the band shaped zone, bounded by the dashed lines. This is different from the 1/2-order subharmonic oscillation case, where the corresponding shaded zone has the abscissa ($(r'_b)_{max} = 0$) as a bound.

5. 4. Phase space and trajectories

5. 4. 1. Phase space with a constant rotating speed

As shown in Eq. (5.7), the stationary oscillation of summed-and-differential harmonic oscillation is determined by three quantities, that is, amplitudes R_f, R_b and phase difference ψ. Although we showed the ratio of these amplitudes is constant in the stationary solution, that does not hold in the nonstationary solution. Therefore, the nonstationary solution is represented by a point in the three-dimensional space called phase space. We can represent its position by the cylindrical coordinates R_f (radius), R_b (height), and ψ (angle). Between such cylindrical coordinates and rectangular coordinates (x, y, z), the following relations hold:

$$x = R_f \cos\psi\,, \quad y = R_f \sin\psi\,, \quad z = R_b \tag{5.10}$$

The trajectories in this phase space, which represent time histories of R_f, R_b and ψ, can be obtained by integrating Eq. (5.7) numerically. As $R_b > 0$, the trajectories exist above the xy-

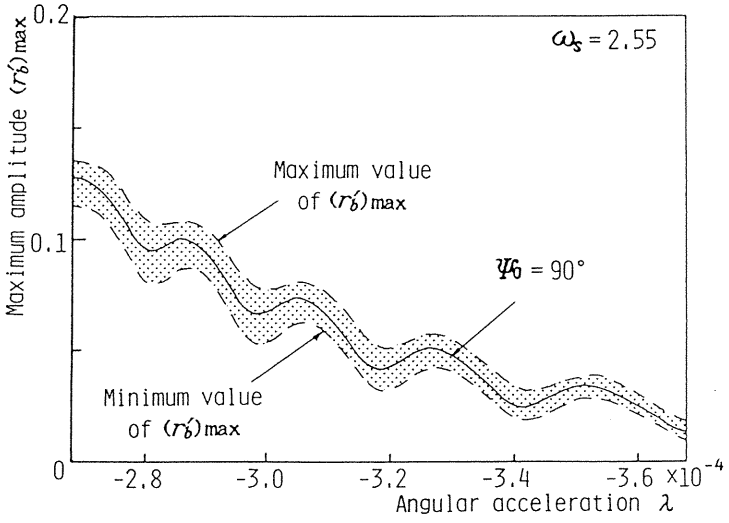

Fig. 5.5. Variations of the maximum amplitude with respect to the angular acceleration λ (deceleration)

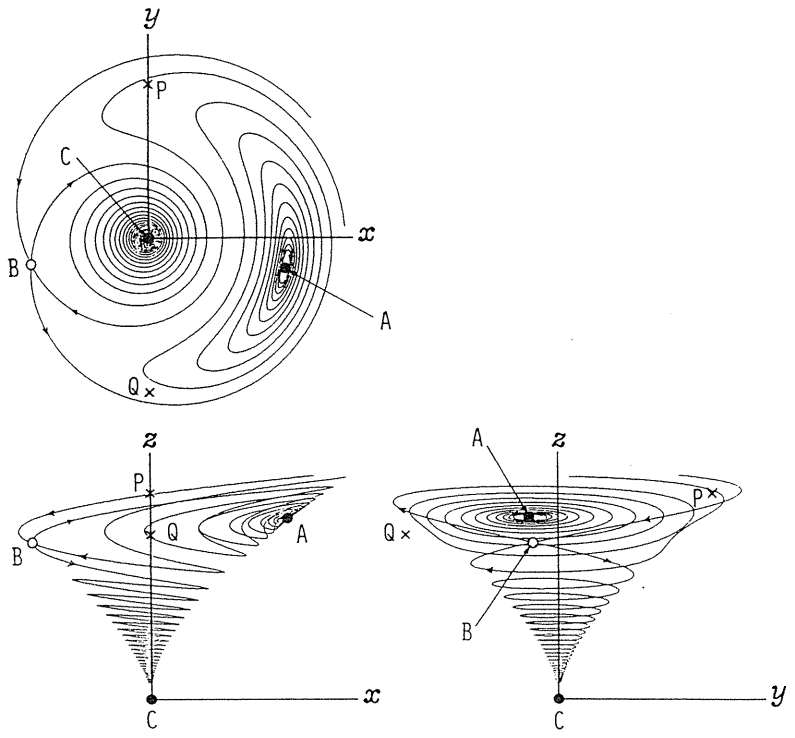

(a) Orthogonal projections of the trajectories passing through the saddle point B

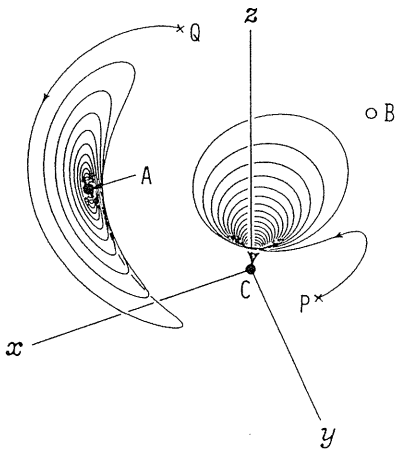

(b) Perspective projections of the trajectories starting from ordinary points P and Q

Fig. 5.6. Trajectories in the phase space (ω = constant)

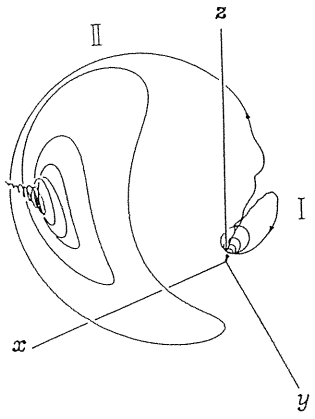

Fig. 5.7. Trajectories in the phase space corresponding to the nonstationary response during acceleration

plane. The phase space at $\omega = 2.80$ is shown as an example in Fig. 5.6. Because there exist two stable solutions (including a trivial solution) and one unstable solution at this rotating speed as shown in Fig. 5.2, three singular points A, B, and C appear in the phase space. In Fig. 5.6, the symbol ● is a singular point representing a stable stationary solution and the symbol ○ is one representing an unstable stationary solution. Among the trajectories in this phase space, only those passing through the unstable singular point are shown by fine full lines in Fig. 5.6(a). There are six such trajectories, but three of them almost overlap and seen to be one trajectory. In the two-dimensional phase plane used in the case of 1/2-order subharmonic oscillation, the trajectories passing through the unstable singular point become separatorices which divide the phase plane into two types of zone. The representative points in each zone move towards the stable singular point in the same zone. In the three-dimensional phase space, there exist curves surfaces corresponding to separatorices in the two dimensional phase plane. The trajectories shown in Fig. 5.6(a) are the intersection lines of these curved surfaces. The representative point on such trajectories moves to the directions designated by arrows as time passes. From these lines, we can imagine how the representative point moves from a given point in the phase space. In Fig. 5.6(b), the trajectories from the ordinary points P and Q (symbol ×) are drawn as an example.

5. 4. 2. Trajectories during acceleration passing through the critical speed

When the rotor passes the critical speed with a constant acceleration ($\ddot{\Psi}=\lambda$), the singular points A and B in Fig. 5.6 move in the phase space and the representative point expressing a nonstationary solution pursues one of stable singular points A (moving) and C. Such a trajectory can be drawn from the data obtained by the FFT-procedure mentioned previously. As an example, two trajectories are drawn in Fig. 5.7 — trajectory I for a passable case and II for a non-passable case. Here we discuss a case where the rotor is accelerated from a speed lower than the critical speed. There are three regions of $\dot{\Psi}$ that determine the number and type of the singular points. For $\dot{\Psi}$ in the region below point A_1 in Fig. 5.3, there is a stable singular point at the origin (a trivial solution); for $\dot{\Psi}$ between A_1 and A_2, there are an unstable singular point at the origin and a stable one away from the origin; and for $\dot{\Psi}$ above A_2, there are

three singular point — a stable one at the origin, and a stable one and an unstable one away from the origin, as shown in Fig. 5.6. When the rotor is accelerated from a rotating speed in the first region where only the harmonic oscillation $[+\omega]$ appears, the representative point expressing a nonstationary solution of the summed-and-differential harmonic oscillation stays very close to the origin in the beginning, and it starts to separate as soon as $\dot{\Psi}$ passes the rotating speed A_1. The distance of the representative point from the origin at the rotating speed A_1 corresponds to the initial disturbance for nonstationary solutions. The velocity with which the solution separates from the origin is determined by the relative position of the representative point with respect to the origin (that is, the magnitude and the direction of the initial disturbance). When $\dot{\Psi}$ passes the rotating speed A_2, the number of singular points becomes three as shown in Fig. 5.6, and the representative point start to approach one of the two stable singular points. The relative position of the representative point with respect to these singular points determines which stable singular point it will approach. In a passable case, the representative point approaches the origin C, and in a non-passable case, it approaches the stable singular point A. The relative position of the representative point with respect to the origin at the rotating speed A_1, depends on the initial angular position of Ψ_0 and the initial rotating speed ω_s. Therefore, the maximum amplitude $(r'_b)_{max}$ changes due to Ψ_0 and ω_s as shown in Fig. 5.4.

The relations between the maximum and minimum values of $(r'_b)_{max}$ and the angular acceleration λ, shown in Figs. 5.4 and 5.5, are different from that of the 1/2-order subharmonic oscillation, although the shapes of the resonance curves are similar. In the case of 1/2-order subharmonic oscillation, the trajectories of nonstationary oscillations are expressed in the two-dimensional phase plane. At a rotating speed between A_1 and A_2 in Fig. 5.3, the stationary trivial solution is unstable and is expressed by a saddle point at the origin in the phase plane. When the initial angular position Ψ_0 varies from 0° to 360°, the representative point at the rotating speed A_1 draws a closed roop containing the origin. As the rotating speed is increased beyond A_1, the representative point's location on this loop will determine its future trajectory and it will take one of the following courses: (a) approach the origin with decreasing velocity; (b) move towards the origin and then move away from it; (c) move away from the origin with an increasing velocity. In case (a), for example, the representative point is on a separatrix and the maximum amplitude during acceleration becomes almost 0. As a whole, the maximum amplitude during acceleration varies from almost 0 (case (a)) to a certain finite value (case (b) and (c)). This variation range is not influenced by λ because the location of the above-mentioned loop at A_1 does not differ much by λ. However, the region in which the representative point is attracted to the origin appear after the rotating speed passes the point A_2, and this region expands more rapidly as λ increases. Therefore in the range of large λ, the representative point is enclosed in this region and the upper bound decreases monotonously as λ increases.

On the other hand, in the case of summed-and-differential harmonic oscillation, the trajectory of a nonstationary solution is expressed in a three-dimensional phase space. When the initial angular position Ψ_0 varies from 0° to 360°, the representative point at the rotating speed A_1 draws a closed loop near the origin. However, because the representative points on the loop do not always have the cases (a), the maximum amplitude varies between a finite value and a finite or an infinite one. In addition, because the location of the loop changes in the phase space depending on the angular acceleration λ and on the initial rotating speed ω_s, the upper and lower bound of $(r'_b)_{max}$ vary complicatedly as shown in Figs. 5.4(a) and 5.5.

The representative point moves very slowly near the unstable singular point at the origin (the trivial solution) in phase plane and in phase space. When the rotor passes the point A_1 in Fig. 5.3 during acceleration, the representative point is located very near the origin. There-

fore, it moves very slowly near the origin and it seems that the response remains near the unstable trivial solution for a while in the response diagram. This period corresponds to penetration.

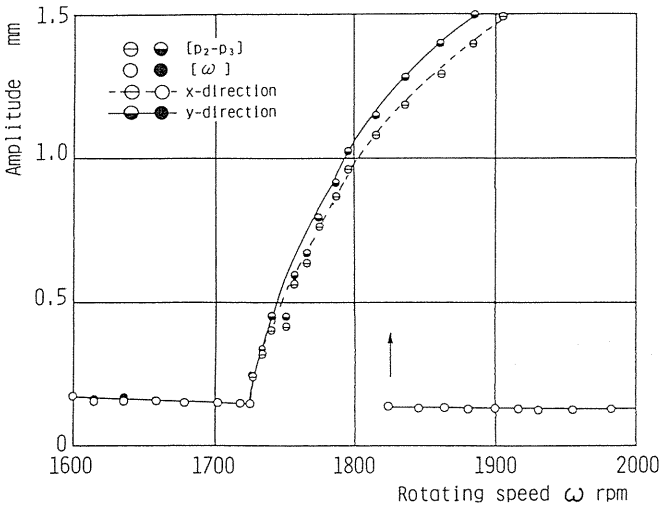

Fig. 5.8. Steady-state resonance curve of the summed-and-differential harmonic oscillation (experimental result)

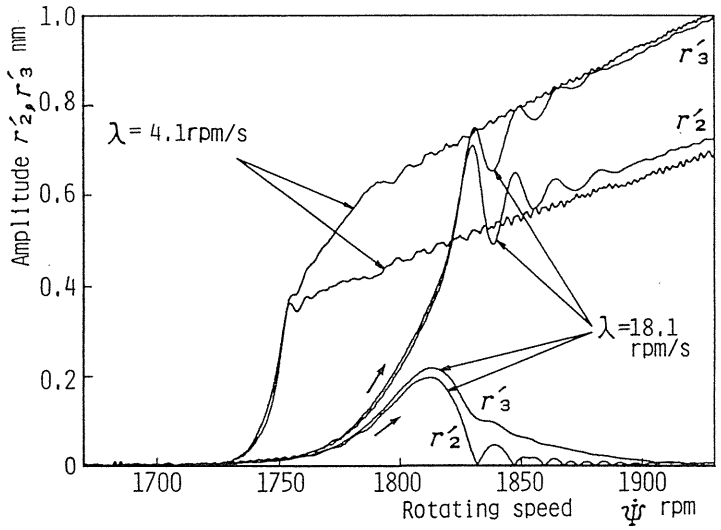

Fig. 5.9. Amplitude variations of the summed-and-differential harmonic oscillation during acceleration (experimental results): a case with a very slow acceleration and cases with the same acceleration but with different initial angular positions

5. 5. *Experimental apparatus and experimental results*

5. 5. 1. *Experimental apparatus*

The experimental apparatus and the measurement system are the same as that in the previous chapter (Fig. 4.9). But the dimensions of shaft and disk are different from them. The dimensions of the rotor were as follows: the diameter was 300 mm, the thickness was 14 mm, the mass was 7.78 kg. The dimensions of the shaft were as follows: the diameter was 12 mm, and the length was 700 mm. The rotor was mounted at a position 175 mm above the lower end.

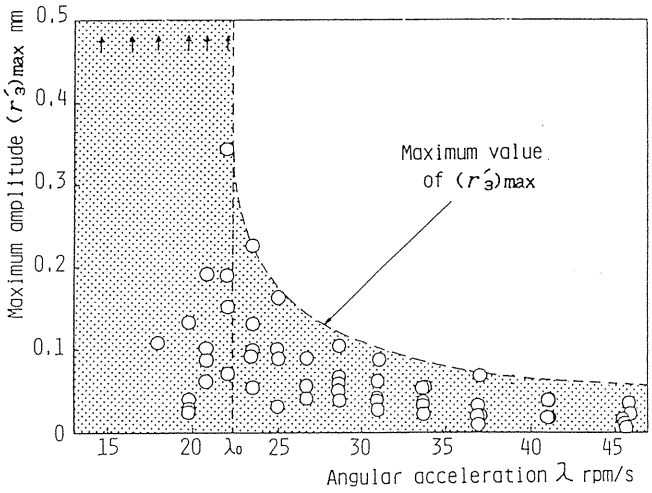

Fig. 5.10. Influence of the angular acceleration on the maximum amplitude (experimental results, acceleration)

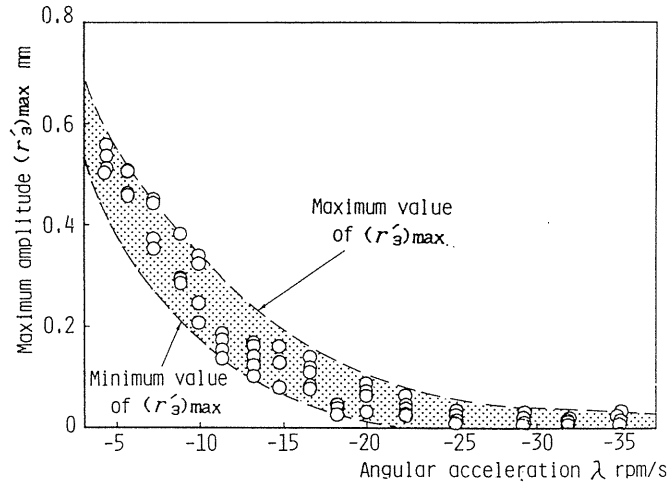

Fig. 5.11. Influence of the angular acceleration on the maximum amplitude (experimental results, deceleration)

5. 5. 2. *Experimental results*

A resonance curve of the summed-and-differential harmonic oscillation which appeared in the neighborhood of the rotating speed $\omega \fallingdotseq p_2 - p_3$ is shown in Fig. 5.8. The symbol ○, ⊖ and ⊖, ● represent amplitudes in the x- and y-directions, respectively. The abscissa represents rotating speed (rpm) and the ordinate represents total amplitude (mm), that is, the sum of the amplitude of the harmonic oscillation and that of the summed-and-differential harmonic oscillation. The arrow indicates a jump phenomenon. The steady-state trivial solution is unstable at about 1730 ~ 1820 rpm.

Figure 5.9 shows experimental results on amplitude variation curves during acceleration through a critical speed. It shows the amplitude variation curves of each component near the frequencies p_2 and p_3. These curves were obtained by the FFT-procedure used in the theoretical analysis. A passable case and a non-passable case are shown for the same angular acceleration $\lambda = 18.1$ rpm/s, and initial rotating speed $\omega_s = 1500$ rpm. (The initial position Ψ_0 are different in these two cases). In addition to show a stable resonance curve of a stationary oscillation, we measured the amplitude variation curve with a very low acceleration ($\lambda =$ 4.1 rpm/s was the lowest acceleration that this apparatus could attain. And this curve represents stable resonance curve approximately).

Next, we examined the influence of angular acceleration on the maximum amplitude. In our experiments it was impossible to set or measure the initial angular position Ψ_0, and therefore it was set at random between 0° ~ 360°. We observed nonstationary response by repeating the experiment many times under the same condition of assembly, acceleration and initial angular velocity. The apparatus had about ±0.1 % error in the rotating speed (for example, there is about ±2 rpm error at $\omega_s = 1500$ rpm).

Figure 5.10 shows the relationship between the angular acceleration λ and the maximum amplitude $(r_3')_{max}$ in the case of acceleration. The symbol $(r_3')_{max}$ represents the maximum amplitude of the vibration component with frequency near p_3. This corresponds to $(r_b')_{max}$ in the theoretical analysis. In this figure, an arrow indicates a non-passable case in which the amplitude increased along the resonance curve. The broken line is the envelope of maximum amplitudes. Therefore, the maximum amplitude $(r_3')_{max}$ are contained within the shaded zone. We could not verify the existence of several maxima and minima of the shaded zone, such as those shown in Fig. 5.4(a), due to the above-mentioned apparatus error in the adjustment of the initial rotating speed ω_s. But, as expected from the discussion in Section 5.3.2, the experimental results are similar to those of the 1/2-order subharmonic oscillation. That is, when the angular acceleration was larger than a certain critical value λ_0 ($\fallingdotseq$ 22 rpm/s), the rotor could always pass the critical speed; and if λ was less than λ_0, both a passable case and non-passable case appeared.

Figure 5.11 shows the relationship between λ and $(r_3')_{max}$ in the case of deceleration. The experimental result agrees qualitatively with the theoretical result in Fig. 5.5. The zone in which $(r_3')_{max}$ exists has the shape of a band.

5. 6. *Conclusions*

Regarding the nonstationary phenomena of a summed-and-differential harmonic oscillation in a rotating shaft system with nonlinear spring characteristics, the following results are obtained.

(1) The maximum amplitude $(r_b')_{max}$ during acceleration or deceleration through the critical speed depends not only on the angular acceleration λ but also on the initial angular position Ψ_0 and the initial rotating speed ω_s.

(2) Unlike the case of 1/2-order subharmonic oscillation, when the initial angular position Ψ_0 varies from 0° to 360°, there exist an upper bound and a lower bound to the maximum

amplitude $(r'_b)_{max}$, and the value of $(r'_b)_{max}$ varies within these two bounds. These values don't decrease monotonously as the angular acceleration λ increases.

(3) In the case of acceleration ($\lambda > 0$), there exist several regions of angular acceleration λ, in which the rotor can always pass with finite amplitude, under the angular acceleration with which the rotor cannot pass for some values of Ψ_0 (nonpassable region).

(4) In the case of deceleration ($\lambda < 0$), the rotor can always pass the critical speed with any value of angular acceleration λ. But the maximum amplitude $(r'_b)_{max}$ has an upper and a lower bound, unlike the case of the 1/2-order subharmonic oscillation.

(5) In the experiments of acceleration, the upper bound of the maximum amplitude $(r'_b)_{max}$ decreases monotonously as λ increases and the existence of the critical value λ_0 is ascertained. In deceleration, there exist an upper bound and a lower bound for $(r'_b)_{max}$.

(6) The discrepancy between the simulation results and the experimental results in acceleration can be explained by noting that a slight fluctuation in the initial rotating speed ω_s has a big influence on the maximum amplitude.

Chapter 6 A critical speed of a 1/3-Order subharmonic oscillation[61]

6. 1. Introduction

It is known that nonlinear oscillations, such as subharmonic oscillations and summed-and-differential harmonic oscillations, appear in hydraulic turbine generators[62] and steam turbine generators[63]. Recently, it was reported that subharmonic oscillations of order 1/2, 1/3 and higher occurred in aircraft gas-turbine engines[64)-66)] and space shuttle high-pressure fuel turbo pumps[67)-69)], due to angular clearances in the bearings. For example, in aircraft engines whose rotating speeds are changed frequently, it is very important to clarify the nonstationary vibration characteristics during acceleration through critical speeds.

As reported in many papers mentioned above, many types of subharmonic oscillation can appear in rotating machines. In the previous chapters, we treated nonlinear oscillations due to unsymmetrical nonlinearity. In this paper, firstly, we discuss a 1/3-order subharmonic oscillation of forward precession due to symmetrical nonlinearity. Its resonance curve does not bifurcate from that of a trivial solution and exists separately. As the shape of this resonance curve is completely different from the shape of a 1/2-order subharmonic oscillation, it is expected that its nonstationary characteristics are different from those reported previously.

Secondly, we investigate nonstationary characteristics of the other kinds of subharmonic oscillations, such as 1/2-order and 1/3-order subharmonic oscillations of backward precession. Then we compare the characteristics of all kinds of oscillations due to the second and third power terms of coordinates.

6. 2. Equations of Motion and Steady-State Oscillations

In the theoretical analysis, we treat the inclination oscillation of a rotor which is mounted at the center of an elastic shaft. The equation of motion is the same as that treated in chapters 4 and 5.

$$\begin{aligned}
&\ddot{\theta}_x + i_p\dot{\Psi}\theta_y + i_p\Psi\dot{\theta}_y + c\dot{\theta}_x + \theta_x + N_{\theta x} = (1 - i_p)\tau(\Psi^2\cos\Psi + \dot{\Psi}\sin\Psi)\\
&\ddot{\theta}_y - i_p\dot{\Psi}\theta_x - i_p\Psi\dot{\theta}_x + c\dot{\theta}_y + \theta_y + N_{\theta y} = (1 - i_p)\tau(\Psi^2\sin\Psi - \dot{\Psi}\cos\Psi)
\end{aligned} \tag{6.1}$$

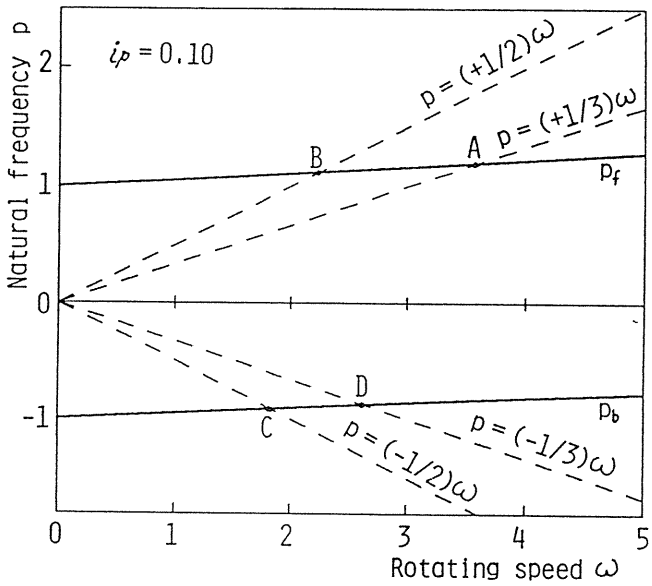

Fig. 6.1. $p - \omega$ diagram

We discuss the case of constant rotating speed. If the initial angular position of τ at $t = 0$ is Ψ_0, then the angle Ψ is given as follows:

$$\Psi = \omega t + \Psi_0 , \quad \dot{\Psi} = \omega , \quad \ddot{\Psi} = 0 \tag{6.2}$$

Figure 6.1 shows a natural frequency p as a function of the rotating speed ω for the case $i_p = 0.10$. The point of intersection A of curve p_f and straight line $p = +(1/3)\omega$ gives the resonance point of a 1/3-order subharmonic oscillation of a forward precession. In the following, we use the symbol $[+(1/3)\omega]$ to represent this kind of oscillation. The sign + indicates a forward precession. The points C and D denote the resonance points of the subharmonic oscillations $[-(1/2)\omega]$ and $[-(1/3)\omega]$, repectively. The signs − indicates a backward precession.

The solution in the neighborhood of the resonance point B is assumed to be approximately as follows:

$$\begin{aligned} \theta_x &= R\cos\theta_f + P\cos\theta_\omega + \varepsilon\{a\cos\theta_f + b\sin\theta_f + \cdots\} \\ \theta_y &= R\sin\theta_f + P\cos\theta_\omega + \varepsilon\{a'\cos\theta_f + b'\sin\theta_f + \cdots\} \end{aligned} \tag{6.3}$$

where $\theta_f = 1/3 \cdot \omega t + \delta_f$ and $\theta_\omega = \omega t + \beta$.

For the steady-state solution $P = P_0$ and $\beta = \beta_0$ for the harmonic component, we use the following approximate solution within an accuracy of order ε^0.

$$\beta_0 = \pi , \quad P_0 = -F/G \tag{6.4}$$

where $G = 1 + i_p\omega^2 + \omega^2$.

The steady-state solutions $R = R_0$, $\delta_f = \delta_{f0}$ for the subharmonic oscillation $[+(1/3)\omega]$ in the accuracy of $O(\varepsilon)$ are given by the following equations:

$$\begin{aligned} &[(c\omega/3)^2 + \{G_f + 4\beta^{(0)}(2P_0^2 + R_0^2)\}^2]R_0^2 = (3\beta^{(2)}P_0R_0^2)^2 \qquad \text{(i)} \\ &\text{or } R_0 = 0 \qquad \text{(ii)} \end{aligned} \tag{6.5}$$

where $G_f = 1 + i_p\omega(1/3 \cdot \omega) - (1/3 \cdot \omega)^2$. It is shown in the previous report[12] that, among various kinds of nonlinear components in polar coordinate expression, only the isotropic component $N(0)$ (coefficient $\beta^{(0)}$) and the anisotropic component $N(2)$ (coefficient $\beta^{(2)}$) whose magnitude of potential distribution changes 2 time while the shaft whirls once around the origin have an influence on this type of oscillation. Although the resonance curve given by Eq. (6.5) has a comparatively large quantitative error, it is possible to improve the accuracy by considering a vibration component of backward precession $[-(1/3)\omega]$ in the analysis. Figure 6.2(a) and Fig. 3 show modified resonance curves obtained by such analysis. These curves are obtained in the system with a hard spring type (that is, a system with $\beta^{(0)} > 0$). The parameters have the values shown in the figures. The coefficients of nonlinear terms are zero except for $\beta^{(0)}$ and $\beta^{(2)}$ which have an influence on the resonance curves within an accuracy of ε. The solid and broken lines represent stable and unstable solutions, respectively. Unlike the cases of the 1/2-order subharmonic oscillation and the summed-and-differential harmonic oscillation, the resonance curve is separated from the trivial solution which is stable in every rotating speed.

6. 3. Nonstationary Response during Acceleration through a Critical Speed

We discuss the case in which the rotor is accelerated at a constant rate. The following relationship holds with respect to the angular position of the unbalance.

$$\ddot{\Psi} = \lambda\,, \quad \dot{\Psi} = \lambda t + \omega_s\,, \quad \Psi = (1/2)\lambda t^2 + \omega_s t + \Psi_0 \tag{6.6}$$

6. 3. 1. Method of analysis

If we adopt a steady-state solution as an initial value in the same way as in the previous reports, the rotor can pass the critical speed without the occurrence of a subharmonic oscillation for any value of acceleration. This is because a stable trivial solution exists for any rotating speed in the case of a 1/3-order subharmonic oscillation. Generally speaking, the rotor can pass a critical of a 1/3-order subharmonic oscillation much more easily than it can pass that of the 1/2-order subharmonic oscillation.

However, it may happen in the practical operation of rotating machinery that the rotor enters a resonance speed region with some residual vibration which was generated when the rotor passed another resonance point. In such a case, there is a possibility that the amplitude jumps to a resonance curve with nonzero amplitude. For this reason, we discuss nonstationary oscillation taking the initial disturbance into consideration. Among many types of initial disturbances, we consider one due to a constant amplitude deviation from a harmonic solution at the start of acceleration.

As many vibration components with various frequencies coexist in the obtained time history, we cannot determine the amplitude variation of nonstationary subharmonic oscillation directly from the numerical data. Therefore we use the same data processing procedure used in the previous chapters. Figure 6.2(a) is an amplitude variation curve before the complex-FFT signal processing and Fig. 6.2(b) is an spectrum distribution.

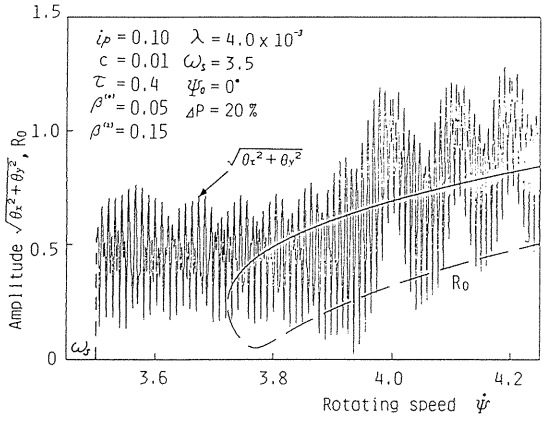

(a) Resonance curves and an amplitude variation curve in a nonstationary oscillation

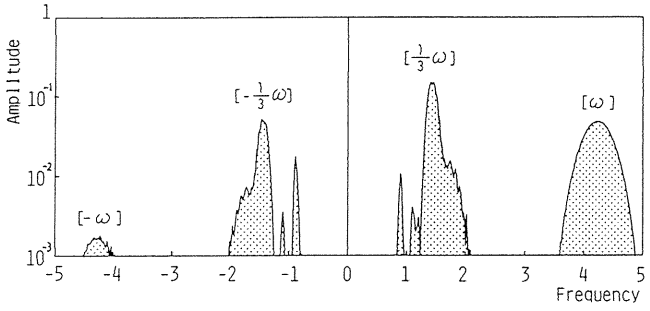

(b) Spectrum distribution

Fig. 6.2. Complex-FFT signal processing

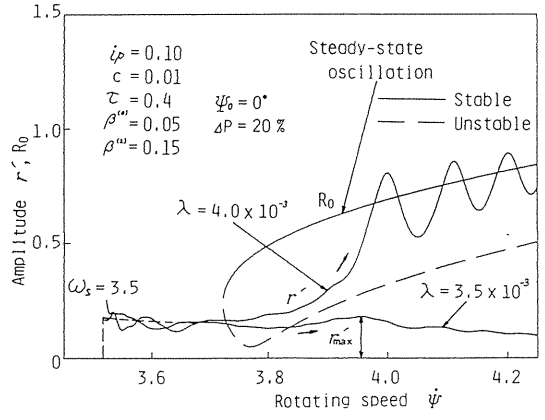

Fig. 6.3. Resonance curves and an amplitude variation curve in a nonstationary oscillation (after signal processing)

6. 3. 2. Maximum amplitude during acceleration through a critical speed of a 1/3-order subharmonic oscillation.

Figure 6.3 shows amplitude variation curves for two different cases of acceleration. We see that a subharmonic oscillation may possibly appear during acceleration if an initial disturbance is given at the start. As mentioned above, such an amplitude variation curve contains some error due to data processing in the neighborhood of the initial velocity ω_s. As in the case of a 1/2-order subharmonic oscillation and summed-and-differential harmonic oscillation reported previously[10),11)], two types of amplitude variation curves are obtained. One is the case (a non-passable case) in which an amplitude increases along the resonance curve to the large-amplitude region, and the other is the case (a passable case) in which the amplitude converges to the stable trivial solution after once increasing toward a resonance curve with nonzero amplitude. In the passable case, we can determine the maximum amplitude r'_{max}, as shown in the figure. In the following, we designate the nonpassable case by $r'_{max} = \infty$ for convenience. In this example, although the same initial disturbance is given, the case with smaller acceleration is passable and the case with larger acceleration is nonpassable.

Figure 6.4 shows effects of some parameters. In these figures, the initial angular velocity ω_s is selected at $\omega_s = 3.50$ and the initial disturbance is given as an amplitude deviation ΔP which is 20 % of the amplitude of steady-state harmonic solution at ω_s. In order to avoid errors due to division by time window, we determined the maximum value in the range $\omega > 3.6$. Only the cases of acceleration are shown because the amplitude of nonstationary oscillation does not increase infinitely along the resonance curve in the case of deceleration.

Figure 6.4(a) shows the relationship between an angular acceleration λ and the maximum amplitude r'_{max} for various initial angular positions of unbalance Ψ_0. It is known from the dash-dotted line for $\Psi_0 = 0°$ and the solid line for $\Psi_0 = 60°$ that the variation of r'_{max} for λ is complex, and a passable case and a nonpassable case appear repeatedly as λ increases. And such curve depends remarkably on the initial angular position Ψ_0.

Figure 4(b) shows an effect of Ψ_0 on r'_{max} for various angular acceleration values λ. For the acceleration $\lambda = 2.1 \times 10^{-3}$, a nonpassable case appears for some ranges of Ψ_0. However, there exists an acceleration for which the rotor can pass the resonance point for every angular position Ψ_0 not only in the higher speed side ($\lambda = 9.8 \times 10^{-3}$) but also in the lower speed side ($\lambda = 1.8 \times 10^{-3}$). When the angle changes from 0° to 360° with a constant acceleration, r'_{max} changes two times periodically. As r'_{max} depends on Ψ_0, we obtain the maximum

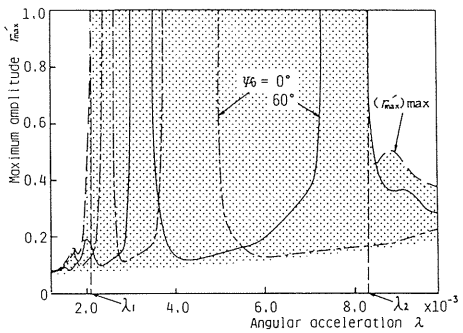

(a) Influence of angular acceleration

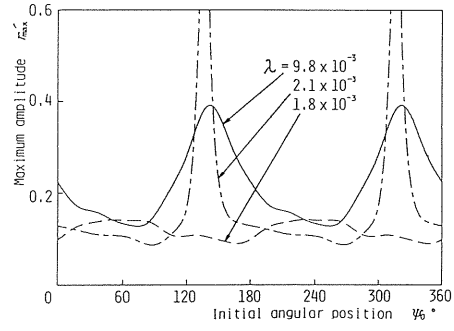

(b) Influence of initial angular positions Ψ_0 of unbalance

Fig. 6.4. Variation of maximum amplitude r'_{max}

value of r'_{max} and denote it by a broken line in Fig. 4(a). Therefore, the maximum value may exist in the shadowed region under the broken line if we consider the variations of λ and Ψ_0. The lower part of this figure is not shaded because we cannot determine the maximum amplitude when it is less than the initial disturbance. As the frequency of free vibration is close to the frequency of the subharmonic oscillation under investigation, we cannot separate them by such signal processing. The values of acceleration which the broken line approaches asymptotically are denoted by λ_1 and λ_2 ($\lambda_1 < \lambda_2$). When λ takes a value between these two critical values, a nonpassable case appears depending on Ψ_0. In the higher acceleration range ($\lambda_2 < \lambda$) or in the lower acceleration range ($\lambda_1 < \lambda$), the rotor can pass the critical speed with a finite amplitude for any value of Ψ_0.

6. 4. *An explanation of the phenomena by a phase plane*

As seen in the previous chapter, a 1/3-order subharmonic oscillation may occur due to an initial disturbance although a stable trivial solution exists at any rotating speed. However, the rotor can pass the critical speed for any initial angular position Ψ_0 of unbalance if the acceleration is larger than the critical value λ_2 or smaller than the critical speed λ_1 (see Fig. 6.4(a)). Such a characteristic is different from those in the cases of a 1/2-order subharmonic oscillation and a summed-and-differential harmonic oscillation, where the rotor can pass the critical speed for any initial angular position Ψ_0 only when the acceleration exceeds a certain critical value.

In this section, we shall explain such characteristics, using a phase plane.

6. 4. 1. *Trajectory of a transient oscillation when the rotating speed is constant ($\dot{\Psi} = \omega =$ constant)*

First, we consider the case in which the shaft is rotating with a constant angular velocity $\dot{\Psi} = \omega$. We transform an amplitude R and a phase δ_f into new variables u and v by the following relationships:

$$u = R\cos\delta_f, \quad v = R\sin\delta_f \tag{6.10}$$

Then, a rectangular coordinate system $0 - uv$ is defined by these variables u, v. In the following, we call this phase plane the uv-plane. This plane represents the subharmonic oscillation observed on the plane rotating with the angular velocity $1/3 \cdot \omega$. Strictly speaking, the trajectory should be discussed in a phase space constituted by the four coordinate axes u, $\dot{u}$, v, and $\dot{v}$. However, as $\dot{u}$ and $\dot{v}$ are expressed approximately as functions of u and v if the velocities $\dot{u}$ and $\dot{v}$ are small, we can discuss in this two-dimensional uv-plane. In this phase plane, the steady-state solution of a 1/3-order subharmonic oscillation is represented by a point whose coordinates are given as follows:

$$u_0 = R_0\cos\delta_{f0}, \quad v_0 = R_0\sin\delta_{f0} \tag{6.11}$$

If the arbitrary point in this plane is given as an initial value, the solution approaches some singular point corresponding to a stable steady-state solution in the course of time. If plural stable steady-state solutions exist, they depend on the initial position and the initial velocity to which the trajectory converges. Figure 6.5 shows the uv-plane at $\omega = 3.85$. (In this figure, a nonstationary phase plane called the $u'v'$-plane, which will be defined later, is also shown in duplicate). Three unstable steady-state solutions (Saddle point) exist and are shown by the symbol O. Four trajectories pass each saddle point as shown by solid lines. The

arrows designate the direction of movement of a representative point. Among these trajectories, those which have a direction toward the saddle point divide the uv-plane into several regions. They are called separatrices. We can imagine a trajectory of a transient solution approximately on such a phase plane by referring to the distribution of singular points and trajectories passing through the saddle points. For example, a solution moves along a trajectory which passes a saddle point and converges to a stable singular point in the same region. The solution in the region with no shade converges to the origin which corresponds to a stable trivial solution (a stable spiral point). In the other three shaded regions, a solution converges to the stable singular point (which is located outside the figure) in respective regions.

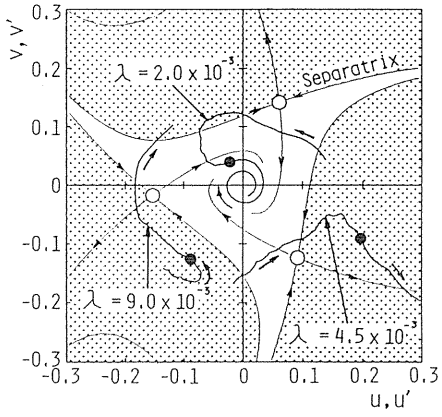

Fig. 6.5. Trajectories on $u'v'$-plane and uv-plane

6. 4. 2. Trajectory of a nonstationary oscillation when the rotating speed is changed with constant angular acceleration (Ψ = constant).

In this section, we observe a nonstationary oscillation during acceleration in the $u'v'$-plane which is rotating with an angular velocity $\dot{\Psi}/3$ ($\ddot{\Psi}$ = constant) and compare the trajectory with separatrices in a uv-plane corresponding to a certain instantaneous rotating speed.

In time histories on θ_x and θ_y, the components corresponding to the frequency $\dot{\Psi}/3$ are represented by θ_{x1} and θ_{y1}. These components are transformed from the coordinates θ_{x1} and θ_{y1} fixed in space to the coordinates u' and v' rotating with acceleration by the following relationships:

$$\begin{aligned} u' &= \theta_{x1}\cos(\Psi/3) - \theta_{y1}\sin(\Psi/3) \\ v' &= \theta_{x1}\sin(\Psi/3) + \theta_{y1}\cos(\Psi/3) \end{aligned} \tag{6.12}$$

The components θ_{x1} and θ_{y1} are separated from θ_x and θ_y by the above-mentioned complex-FFT method and then transformed into u' and v' by Eq. (6.12).

The trajectories are shown in Fig. 6.5. As shown in Fig. 6.4(a), the maximum amplitude of the 1/3-order subharmonic oscillation r'_{max} during acceleration through the resonance

point changes in a complex way. In this figure, three trajectories for different λ with the same initial angular position $\Psi_0 = 0°$ are shown. These trajectories are drawn for $\dot{\Psi} = 3.60 \sim 4.15$. The position representing the solution when $\omega = 3.85$ is shown by the symbol ●. The trajectory converges to the origin when $\lambda = 2.0 \times 10^{-3}$ and it extends to a stable singular point corresponding a large amplitude steady-state solution when $\lambda = 4.5 \times 10^{-3}$. In the case of $\lambda = 9.0 \times 10^{-3}$, if the numerical integration is continued further, it becomes clear that the trajectory converges to the origin. The shapes of separatrices change in the $u'v'$-plane as $\dot{\Psi}$ increases. Using this figure, we can explain why the rotor can pass the resonance region with finite amplitude in the cases of large and small acceleration ranges as follows: The region with no shade expands as the angular velocity increases. Therefore, if the angular acceleration is very large, this region with no shade expands at a rate faster than the growth rate of the solution, and consequently, the solution comes to be included in this region in which every solution converges to the origin (for example, the case of $\lambda = 9.0 \times 10^{-3}$). If the acceleration is not so large, the trajectory grows rapidly and is not included in this region. The trajectory converges to the stable solution with large amplitude in the shaded region ($\lambda = 4.5 \times 10^{-3}$). If the acceleration is very small ($\lambda = 2.0 \times 10^{-3}$), the residual free vibration is damped out and becomes small when saddle points appear. It is enclosed in the unshaded region from the start.

6. 5. *Other Subharmonic Oscillations*

Besides the subharmonic and summed-and-differential harmonic oscillations in chapters 4 and 5, and the subharmonic oscillation discussed in this chapter, a 1/2-order subharmonic oscillation of backward precession $[-(1/2)\omega]$ and a 1/3-order subharmonic oscillation of backward precession $[-(1/3)\omega]$ may appear in such a system. The shapes of the resonance curves of these oscillations are similar to those for some of the oscillations which have already been discussed. In this chapter, we summarize the results of these oscillations and compare their characteristics.

6. 5. 1. *A 1/2-order subharmonic oscillation of backward precession*

The amplitude of steady-state oscillation is given by the following equations:

$$\begin{aligned} &\{G_b + 4\beta^{(0)}(R_0^2 + 2P^2)\}^2 + (c\omega/2)^2 = 36\varepsilon^{(3)2}P^2 \\ &\text{or } R_0 = 0 \end{aligned} \tag{6.13}$$

where $G_b = 1 + i_p\omega(-\omega/2) - (-\omega/2)^2$. The shape of the resonance curve is the same as that of the 1/2-order subharmonic oscillation $[+(1/2)\omega]$. However, the effective nonlinear components in polar coordinate expression are of a different kind. Contrary to the case of oscillation $[+(1/2)\omega]$ which is under the influence of the coefficients $\beta^{(0)}$ and $\varepsilon^{(1)}$, the coefficients $\beta^{(0)}$ and $\varepsilon^{(3)}$ influence this oscillation $[-(1/2)\omega]$. The relationship between the angular acceleration λ and the maximum amplitude r'_{max} is the same as that of the oscillation $[+(1/2)\omega]$. However, the effect of the initial angular position Ψ_0 upon r'_{max} is different. While Ψ_0 changes from 0° to 360°, r'_{max} changes 3 times periodically in the oscillation $[-(1/2)\omega]$, as shown in Fig. 6.6, although it changes once in the oscillation $[+(1/2)\omega]$.

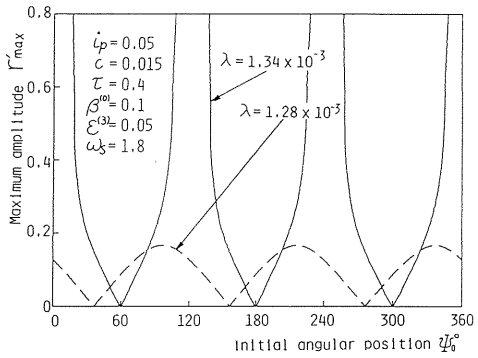

Fig. 6.6. Influence of the initial angular position Ψ_0 on the maximum amplitude r'_{max} (A $-1/2$ order subharmonic oscillation)

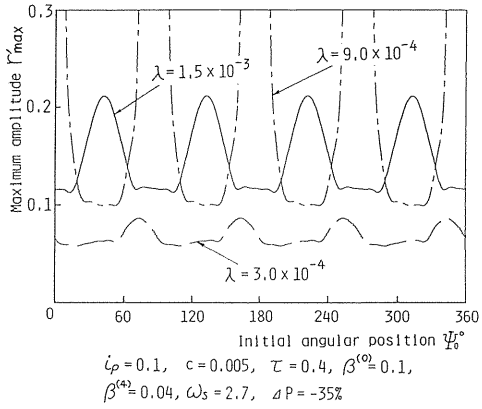

Fig. 6.7. Influence of the initial angular position Ψ_0 on the maximum amplitude r'_{max} (A $-1/3$ order subharmonic oscillation)

6. 5. 2. *A 1/3-order subharmonic oscillation of backward precession*

The amplitudes of steady-state oscillation are given by the following equations:

$$[(c\omega/3)^2 + \{G'_b + 4\beta^{(0)}(2P^2 + R_0^2)\}^2]R_0^2 = (12\beta^{(4)}PR_0^2)^2$$
$$\text{or} \quad R_0 = 0 \tag{6.14}$$

where $G'_b = 1 + i_p\omega(-\omega/3) - (-\omega/3)^2$. The shape of this resonance curve is the same as that of the oscillation $[+(1/3)\omega]$. While the coefficients $\beta^{(0)}$ and $\beta^{(2)}$ influence the oscillation $[+(1/3)\omega]$, the coefficients $\beta^{(0)}$ and $\beta^{(4)}$ have influence on this oscillation. Although the characteristics of these oscillations are similar, the relationships between Ψ_0 and r'_{max} are different. The maximum amplitude r'_{max} changes 4 times periodically in the case of this oscillation $[-(1/3)\omega]$, while the angle Ψ_0 changes from 0° to 360°.

Table 6.1. Comparison of nonstationary characteristics passing through critical speeds of harmonic, subharmonic, and summed-and-differential harmonic oscillations

Kinds of Oscillation	[+ω]	[+1/2ω]	[-1/2ω]	[+1/3ω]	[-1/3ω]	[pf - pb]
Influential Nonlinear Components	$\beta^{(0)}$ only	$\beta^{(0)}$, $\varepsilon^{(1)}$	$\beta^{(0)}$, $\varepsilon^{(3)}$	$\beta^{(0)}$, $\beta^{(2)}$	$\beta^{(0)}$, $\beta^{(4)}$	$\beta^{(0)}$, $\varepsilon^{(1)}$
Variation Range of r'_{max} due to changes of parameters (with λ = Const.)	One definite value	0 ~ A* or 0 ~ ∞	0 ~ A or 0 ~ ∞	0 ~ A or 0 ~ ∞	0 ~ A or 0 ~ ∞	A ~ B* or A ~ ∞
Variation of $(r'_{max})_{max}$ for λ	Decrease monotonously	Decrease monotonously	Decrease monotonously	Increase in slow acceleration range Decrease in fast acceleration range	Increase in slow acceleration range Decrease in fast acceleration range	Not monotonous
Periodicity of r'_{max} for Ψ_0	None	Once	Three times	Twice	Four times	once
Range of λ where the rotor cannot pass for a certain Ψ_0	$\lambda < \lambda_0$	$\lambda < \lambda_0$	$\lambda < \lambda_0$	$\lambda_1 < \lambda < \lambda_2$	$\lambda_1 < \lambda < \lambda_2$	$\lambda < \lambda_0$

* A, B : Finite values

6. 5. 3. *Comparison of the results*

The results of all kinds of subharmonic oscillations, a summed-and-differential harmonic oscillation $[p_f - p_b]$, and a harmonic oscillation at the major critical speed are summarized in Table 6.1.

From this table, we see that the periodicity in the relationship between the maximum amplitude r'_{max} and the initial angular position Ψ_0 corresponds to the periodicity of the nonlinear coefficients. When Ψ_0 changes from 0° to 360°, r'_{max} changes once in the oscillation $[+(1/2)\omega]$ caused by $\varepsilon^{(1)}$, once in the summed-and-differential harmonic oscillation caused by $\varepsilon^{(1)}$, two times in the oscillation $[+(1/3)\omega]$ caused by $\beta^{(2)}$, three times in the oscillation $[-(1/2)\omega]$ caused by $\varepsilon^{(3)}$, and four times in the oscillation $[-(1/3)\omega]$ caused by $\beta^{(4)}$. The reason for this result is that the symmetry of the phase plane is determined by the potential distribution.

6. 6. *Conclusions*

Concerning the nonstationary characteristics of a rotating shaft during acceleration through a critical speed of a 1/3-order subharmonic oscillation of forward precession, the following results are obtained.

(1) The maximum amplitude r'_{max} depends not only on angular acceleration λ but also on initial angular position Ψ_0 of the unbalance and the initial disturbance.

(2) For the passage with a finite amplitude, there exist two critical values of acceleration λ_1 and λ_2. With an angular acceleration between these values ($\lambda_1 < \lambda < \lambda_2$), the rotor cannot pass the critical speed for some values of Ψ_0.

(3) The reason for the existence of the two critical values λ_1 and λ_2 is explained as follows: In the case in which the angular acceleration is very small, the 1/3-order subharmonic component in the residual vibration due to disturbance is damped sufficiently when the angular acceleration reaches the critical speed. The representative point is located in the attractive region of a stable spiral at the origin. In the case in which the angular acceleration is very large, the attractive region of the stable spiral expands faster than the growth of the trajectory and finally the solution comes to be included in this attractive region.

(4) From the comparison with the cases of a major critical speed, subharmonic oscillations

$[+(1/2)\omega]$, $[-(1/2)\omega]$, $[-(1/3)\omega]$, and a summed-and-differential harmonic oscillation $[p_f - p_b]$, it becomes clear that the periodicity of the maximum amplitude r'_{max} for the angular position Ψ_0 is related to the periodicity of nonlinear components in polar coordinate expression.

References

1) Dimentberg, F.M., Flexural Vibrations of Rotating Shafts, Butterworths, London, (1961).
2) Fernlund, I., Running through the Critical Speed of a Rotor, Scandinavian University Books, (1963).
3) Kononenko, V.O., Vibrating Systems with a Limmited Power Supply, Iliffe Books, (1969).
4) Evan-Iwanowski, R.M., Resonance Oscillations in Mechanical Systems, Elsevier Scientific Pub. Co. New York, 1976.
5) Evan-Iwanowski, R.M., "Nonstationary Vibration of Mechanical Systems", Applied Mechanics Reviews, 22 (1969), 213.
6) Iwatubo, T., "Vibration of Rotors through Critical Speeds", The Shock and Vibration Digest, 8-2 (1976), 89.
7) Yanabe, S., "Vibration of a Shaft Passing through a Critical Speed", Study of Machinery, 29-10, 1191. (in Japanese).
8) Yanabe, S., "Vibration of a Shaft Passing through a Critical Speed (A Case of Constant Acceleration)", Text of Course, No.483, Jpn. Soc. Mech. Eng. (1979), 51, (in Japanese).
9) Matsuura, K. "On the Vibration of a Rotating Machinery Passing through a Critical Speed (A Case with an Influence of Vibration Response to the Driving Sourse)", Text of Course, No.483, Jpn. Soc. Mech. Eng. (1979), 61. (in Japanese).
10) Lewis, F.M., "Vibration during Acceleration through a Critical Speed", J. Appl. Mech., Trans ASME, 54 (1932), 253.
11) Poschl, T., "Das Anlaufen eines einfachen Schwingers", Ing-Arch., 4-1, (1933), 98.
12) Baker, J.G., "Mathamatica-machine Determination of the Vibration of an Accelerated Unbalanced Rotor", J. Appl. Mech., Trans. ASME, 61-9, (1939), A-145.
13) Yamada, H. and Tsumura, T., "Vibration Analysis of a Rotor with Acceleration", Trans. Jpn. Soc. Mech. Eng. 17-64 (1951), 115. (in Japanese).
14) Dornig, A. "Transients in Simple Undamped Oscillators Under Inertial Disturbances", Trans. ASME, Ser. E, 26-2 (1956), 217.
15) Fearn, R.L. and Millsaps, K., "Constant Acceleration of an Undamped Simple Vibrator Through Resonance", J. Roy. Aeron. Soc. 71 (1967), 567.
16) Shimoyama, Y., and Yamamoto, T., "A Study on the shaft passing through a Critical Speed Region", Trans. Jpn. Soc. Mech. Eng., 15-50 (1949), 1-113.
17) Qazi, A.S. and MacFarlane, "The Controlled Transition of a Rotating Shaft Through its Critical Speed", Int. J. Contr. 6-4 (1967-9), 301.
18) Yanabe, S. and Tamura, A. "Vibration of a Shaft Passing through a Critical Speed (1st Report, Experiments and Numerical Solutions)", Bull. JSME, vol.14, No.76 (1971), 1050.
19) Yanabe, S. and Tamura, A. "Vibration of a Shaft Passing through a Critical Speed (2nd Report, Approximate Equations)", Bull. JSME, vol.15, No.89 (1972), 1365.
20) Yanabe, S. "Vibration of a Shaft Passing through a Critical Speed (3rd Report, Approximate Solutions II)", Bull. JSME, vol.17, No.107 (1974), 569.
21) Mitropol'skii, Yu.A, (1965). Problems of the Asymptopic Theory of Non-stationary Vibrations (English translation), D. Davey & Co., New York, 1965.
22) Yanabe, S. "Vibration of a Shaft Passing through a Critical Speed (4th Report, Effect of Gyroscopic moment)", Bull. JSME, vol.23, No.180 (1980), 945.

23) Nonami, K. and Miyashita, M. "Problem of Rotor Passing Through Critical Speed with Gyroscopic Effect (Analysis by Asymptotic Method and Experiments)", Bull. JSME, vol.21 No.151 (1978), 56.
24) Nonami, K. and Miyashita, M. "Problem of Rotor Passing Through Critical Speed with Gyroscopic Effect (2nd Report, Generating of Self-excited Vibration Caused by Internal Damping)", Bull. JSME, vol.22, No.169 (1979), 911.
25) Koretysski, I. (1979). "Study on Nonstationary Vibrations of Rotor Systems with Semirigid Spindles", Proc. 5th World Congress on Thesry of Machines and mechanisms, ASME. (1979), 203.
26) Nonami, K., and Miyashita, M., "Problem of Rotor Passing Through Critical Speed with Gyroscopic Effect (3rd Report, Case of Rotating Shaft on Flexible Support)", Bull. JSME, vol.23, No.186 (1980), 2104.
27) Yanabe, S., Kikuchi, K. and Kobayashi, A., "Vibration of a Shaft Passing through Several Critical Speeds", Bull. JSME, vol.22 No.164 (1979), 156.
28) Nonami, K., "Response in Passing through Critical Speed of Arbitrarity Distributed Flexible Rotor System (Partl, Case without Gyroscopic Effect)", Bull. JSME, vol.26, No.217 (1983), 1198.
29) Nonami, K., "Response in Passing through Critical Speed of Arbitrarity Distributed Flexible Rotor System (Part 2, Case with Gyroscopic Effect)", Bull. JSME, vol.26, No.217 (1983), 1205.
30) Yanabe, S., "Nonstationary Vibration during Acceleration through two Critical Speeds (Without Damping)", Bull. JSME, vol.24, No.188 (1981), 405.
31) Yanabe, S., "Nonstationary Vibration during Acceleration through two Critical Speeds (Maximum Amplitudes and Their Rotational Speeds)", Bull. JSME, vol.24, No.196 (1981), 1820.
32) McCann, G.D. and Bennett, R.R. (1949), "Vibration of Multifrequency Systems During Acceleration Through Critical Speeds, J. Appl. Mech., 16-4 (1949), 375.
33) Iwata, Y. and Nonami, K., "Vibration Control of Rotating Shaft with Self-Optimizing Support System", Bull. JSME, vol.27, No.228 (1984), 1306.
34) Aiba, S., "On the Vibration of a Rotating Shaft Passing through the Critical Speed", Bull. JSME, vol.19, No.128 (1976), 95.
35) Aiba, S., "Vibration of a Rotating Shaft Passing through a Critical Speed (2nd Report, The Effect of Viscus Damping)", Trans. JSME, 43-370, (1977-6), 2131, (in Japanese).
36) Kotera, T., "Analysis of Vibration of Flexible Rotor by Integral Equation (3rd Report)", Trans. JSME, 37-297, (1971-5), 941, (in Japanese).
37) Ots, H., Ishida, Y., Kato, Y., and Kondo, H., "Experiments on the Nonstationary Oscillation of an unsymmetrical Shaft", Trans. Jpn. Soc. Mech. Eng., 53-490, C(1987), 1160. (in Japanese).
38) Matsuura, K., "A Study of Vibration and Velocity Characteristics of an Accelerated Unbalanced Rotor", Trans. JSME, vol.37, No.302 (1971), 1854, (in Japanese).
39) Matsuura, K., "A Study of Vibration and Velocity Characteristics of an Accelerated Unbalanced Rotor (4th Report)", Prepr. of. JSME, No.740-3 (1974-4), 167, (in Japanese).
40) Matsuura, K., "A Study of Vibration and Velocity Characteristics of an Accelerated Unbalanced Rotor (1st Report, Stationary Solutions of Motion)", Bull. JSME, vol.18, No.125 (1975), 1226.
41) Matsuura, K., "A Method for Estimating the Condition That a Rotor Can Pass through Resonance", Bull. JSME, vol.23, No.179 (1980), 749.
42) Matsuura, K., "A Study on a Rotor Passing through a Resonance", Bull. JSME, vol.23, No.179 (1980), 749.
46) Gasch, R., Markert, R. and Pfutzner, H. (1979), "Acceleration of Unbalanced Flexible Rotors through the Critical Speeds.", J. Sound Vib, 63-3 (1979), 393.
47) Kawai, R., Iwatsubo, T. and Kanki, H., "Transient Vibrations of Asymmetric Rotor at Critical Speeds with Limited Power", Trans. JSME, 35-280 (1969-12), 2325, (in Japanese).
48) Iwatsubo, T., Kawai, R. and Kanki, H., "Transient Vibrations of Asymmetric Rotor at Critical Speeds with Limited Power (Part 2, Effect of Phase Angle of Eccentricity)", Trans. JSME, 40-335, (1974-7), 1908, (in Japanese).

49) Kotera, T., "Vibration of Flexible Rotor Driven by Limited Torque through Its Critical Speed", Bull. JSME, vol.17, No.108 (1974), 686.
50) Agrawal, B.N. and Evan-Iwanowski (1973). "Resonances in Nonstationary, Nonlinear, Multidegree-of-Freedom Systems", AIAA J. 11-7 (1973), 907.
51) Yamamoto, T. and Ishida, Y., Theoretical Discussion on Vibration of a Rotating Shaft with Nonlinear Spring Characteristics, Ingenieur-Archiv, Band 46, Heft 2 (1977), p.125.
52) Yamamoto, T. "Mechanical Vibration", Asakura (1964), 202. (in Japanese)
53) Ishida, Y., Ikeda, T. and Yamamoto, T., "Transient Vibration of a Rotating Shaft with Nonlinear Spring Characteristics during Acceleration through a Major Critical Speed", JSME Int. J. vol.30, No.261 (1987), 458.
54) Yamamoto, T. and Hayashi, S., "On the Response Curves and the Stability of Summed-and-Differential Harmonic Oscillations", Bull. JSME, vol.6, No.23 (1963), pp.420-429.
55) Yamamoto, T. Ishida, Y. and Kawasumi, J., "Oscillations of Rotating Shaft with Symmetrical Nonlinear Spring Characteristics", Bull. JSME, vol.18, No.123 (1975), 965.
56) Ishida, Y., Ikeda, T., Yamamoto, T., Murakami, S. (1989b). "Nonstationary Vibration of a Rotating Shaft with Nonlinear Spring Characteristics During Acceleration Through a Critical Speed (A Critical Speed of 1/2-Order Subharmonic Oscillation)", JSME Int. J., Ser. III 32-4 (1989), 575.
57) Ishida, Y., Ikeda, T. and Yamamoto, T., "Effects of Quartic Nonlinear Restoring Forces on 1/2-Order Subharmonic and Summed-and-Differential Harmonic Oscillations of a Rotating Shaft (Variations of Resonance Curves and Occurrence of Unstable Vibrations)", Bull. JSME, vol.29, No.258 (1986), p.4326.
58) Ishida, Y., and Ikeda, T., "The 1/2-Order Subharmonic and Summed-and-Differential Harmonic Oscillations in a Nonlinear Rectilinear Vibratory System (The variations of Resonance Curves and the Occurrence of Unstable Vibration due to Quartic Nonlinear Terms)", Trans. Jpn. Soc. Mec. Eng., (in Japanese), vol.52, No.486, C(1987), 269.
59) ibid. (5), 80.
60) Ishida, Y., Ikeda, T., Yamamoto, T., Murakami, S. "Nonstationary Vibration of a Rotating Shaft with Nonlinear Spring Characteristics During Acceleration Through a Critical Speed (A Critical Speed of a Summed-and-Differential Harmonic Oscillation)", Nonlinear Dynamics 1(1990), 341.
61) Ishida, Y., Yamamoto, T. and Murakami, S., Nonstationary Vibration of a Rotating Shaft with Nonlinear Characteristics during Acceleration through a Critical Speed (A Critical Speed of a 1/3-Order Subharmonic Oscillation), JSME Int. J. vol., No. (19),
62) Benko, G.B. and Holmen, E.K., Parametric Resonances in Umbrella-Type Generating Units, Proc. Inst. Mech. Eng., vol.181, Pt.3A (1966-67), 39.
63) Nakane, H., Kokubo, R., Iida, S. and Takeshita, K., 1/2-Order Subharmonic Resonance of Rotating Shaft Supported by Sliding Journal Bearings, Mitsubishi Heavy Industries Ltd. Tech. Rev., (1968), 1.
64) Ehrich, F.F., Subharmonic Vibration of Rotors in Bearing Clearance, ASME paper, No.66-MD-1 (1966).
65) Ehrich, F.F., High Order Subharmonic Response of High Speed Rotos in Bearing Clearance, Trans. ASME, J. Vib., Acoust. Stress Reliab. Des., vol.110 (1988), No. , 9.
66) Ehrich, F.F., A State-of-the-Art Survey in Rotordynamics — Non-Linear and Self-Excited Vibration Phenomena, 2nd Int Symp. Transport Phenomena, Dynamics, Des. Rotat. Machinery. (1988), No. , 1.
67) Childs, D.W., Fractional-Frequency Rotor Motion Due to Nonsymmetric Clearance Effects, Trans. ASME, vol.104 (1982), 533.
68) Beatty, R.F., Differentiating Rotor Response Due to Radial Rubbing, Trans. ASME, J. Vib., Acoust. Stress Reliab. Des., vol.107 (1985), No. , 151.
69) Kim, Y.B. and Noah, S.T., Steady-State Analysis of a Nonlinear Rotor-Housing System, ASME paper, No.90-GT-328 (1990).